Doctoral Dissertation

Basin and petroleum system modeling of the northern Mannar Basin, offshore Sri Lanka

（スリランカ沖北部マナー堆積盆地の堆積盆石油システムモデリング）

Dissanayake Mudiyanselage Upul Ajantha Kumara Premarathne

Division of Earth and Planetary System Science
Department of Natural History Sciences
Graduate School of Science
Hokkaido University

2015 年 12 月

“Essentially all models are wrong, but some are useful”

George E.P. Box

TABLE OF CONTENT PAGE

LIST OF FIGURES PAGE

CHAPTER 1

CHAPTER 2

CHAPTER 3

LIST OF FIGURES PAGE

LIST OF TABLES PAGES

CHAPTER 2

CHAPTER 3

ABSTRACT

The Gulf of Mannar is located between the southeastern coast of India and the western coastline of Sri Lanka. The Sri Lankan sector of the gulf, which is commonly referred to as the Mannar Basin, extends over around 45000 km^2 in water depths of 20 m to more than 3000 m. The northern part of the Mannar Basin has Holocene to probably Late Jurassic or older sediment. The sediment thickness ranges from 4 km in shallow water depths in the northern part of the Mannar Basin to more than 6 km in the deep water depths towards the south of the basin. The basin has rift structure. The rifting started probably in late Aptian and ended at the end of the Cretaceous. During rifting, the Sri Lankan landmass has rotated counter clockwise direction, acting the north part of the island as a pivot. As a result, the crustal extension has taken place in such a way that the degree of extension has progressively increased from north to south of the Gulf of Mannar. There has been several episodes of basin wide basaltic lava flows during the Maastrichtian. The basin entered a thermal sag phase from the Palaeocene. In the latter stage of the thermal sag phase, the basin has undergone compressional tectonics giving rise to the formation of anticlinal closures. The Mannar Basin is an exploration frontier with only the Pearl-1 well, which was drilled in shallow water depths in 1981. Cairn Lanka Private Limited (CLPL), the recipient of an exploration licence from the Sri Lankan Government for an exploration block in the northern part of the Mannar Basin, drilled three exploration wells during August-December 2011. Two of these wells, Dorado and Barracuda, penetrated natural gas bearing sandstone, which confirmed the occurrence of an active petroleum system in the Gulf of Mannar. However, the geology, geological history and petroleum system of this exploration frontier is poorly understood. The objective of this research is to understand these aspects of the basin. Drill cuttings from recent wells, data from the Pearl-1 well and seismic data were used in this study.

The results of the preliminary analyses of drill cuttings show that they have been heavily contaminated with diesel based drilling fluid. These samples are not suitable for biomarker studies and Rock Eval pyrolysis. Pulverised cutting samples used for elemental analysis to determine total organic carbon (TOC) were washed with methanol and dichloromethane in 2:1, 1:1 and 0:1 volume ratios three times in an ultrasonication bath each time for 15 minutes to remove drilling oil. Maturity data and hydrocarbon source character of sediments indicate that none of the wells drilled in the Mannar Basin have penetrated its potential source rocks, which could be Early Cretaceous and older sedimentary rocks. Therefore, further study of drill cuttings could not give an insight into the petroleum system of the Mannar Basin. For

this reasion, the focus of the study was shifted to two dimensional (2D) basin and petroleum system modeling. SIGMA-2D basin modeling software of Japanese Oil, Gas and Metals National Corporation (JOGMEC) was used to simulate the integrated hydrocarbon generation, migration and accumulation in the northern part of the Mannar Basin.

Modeling results suggest that the geothermal gradient in the northern Mannar Basin is 24.4 ^{o}C/km. The present day heat flows in the Mannar Basin vary from 33 to 40 mW/m^{2}. The present-day heat flows in the northern Mannar Basin are relatively lower than that in the adjacent Indian waters. The heat flow history of the Mannar Basin was predicted, assuming that the Mannar Basin has the heat flow history of a typical rift basin. The maximum heat flows at the Pearl-1 and Dorado-North well locations at the end of rifting have been around 68.2 and 71.1 mW/m^{2}, respectively. The Campanian to present sediment in the northern Mannar Basin, which has been derived from vascular land plants, is rich in type III and IV kerogen and has poor hydrocarbon source potential. If the Santonian to Cenomanian sediment has good source potential it could have expelled relatively small quantity of oil and natural gas. The productivity of this stratigraphic interval increases towards the southern part of the Mannar Basin. Due to no well penetration, the source character of the Early Cretaceous to older sediment, the potential hydrocarbon source rocks in the Mannar Basin, is unknown. In the event of the Early Cretaceous to older sediment having good hydrocarbon source potential, oil and gas could have been expelled mainly during the Late Cretaceous, which is followed by a couple of minor expulsion phases in the Palaeogene and Neogene. The time lag between oil generation and expulsion is around 5 Ma. Oil cracking starts at 120-140 ^{o}C. Even if deeply buried sediment in the Mannar Basin has poor hydrocarbon source potential of around 0.5% TOC content and only Type III kerogen they can still give rise to economically feasible gas deposits. Potential source rocks in the Mannar Basin could have an average TOC content of at least 1% and 10-15% contribution from Type II kerogen. In this case, economically feasible oil and gas deposits could occur mainly in Cretaceous sandstone. Potential hydrocarbon traps in the Mannar Basin include tilted/rotated fault blocks, anticlinal closures, channel fills and stratigraphic pitchouts. Igneous rocks interbedded with sandstone may also act as hydrocarbon traps and seals. Both vertical and lateral drainage system might have occurred in the Mannar Basin.

1. INTRODUCTION

1.1. Outline geology of Sri Lanka

Nine-tenths of Sri Lanka are composed of upper-amphibolite to granulite facies Precambrian metamorphic rocks in three lithotectonic units (Cooray, 1984:1994; Kröner *et al*., 1987; 2003; Fig. 1.1). The remaining one-tenth, located mainly in the northern, north-western and north-eastern coastal areas, is covered with sedimentary rocks, principally Quaternary sands ("red earth"; Cooray, 1984), Miocene limestones, and Late Jurassic siliciclastic rocks that crop out in the Tabbowa, Aadigama and Pallama grabens (Fig. 1.1). In Tabbowa, the Late Jurassic includes arkosic sandstones, siltstones, and mudstones (Money and Cooray, 1966), and carbonaceous shales interbedded with coal seams are present among other lithologies in Pallama (Raveendrasinghe *et al*., 2013). Sediment thickness in the Tabbowa and Pallama grabens is 1.2-1.5 km and 0.9-1.2 km, respectively (Tantrigoda and Geekiyanage, 1991).

1.2. History of hydrocarbon exploration in Sri Lanka

Oil exploration in Sri Lanka commenced with Canada's Hunting Survey Company Limited carrying out an aeromagnetic survey in the Sri Lankan sector of the Cauvery Basin in 1957. Compaigne General de Geophysicque of France shot the first seismic survey in Sri Lanka in 1967. During 1972-1975, three exploration wells, Pesalai-1, 2 & 3, were drilled in the Mannar Island, located northeast of Sri Lanka around 225 km north of Colombo (Fig. 1.2). Several stratigraphic intervals of these wells had traces of natural gas. Encouraged by gas shows in Pesalai wells, different consortia drilled four more exploration wells, Palk Bay-1 & Delft-1 in 1976 and Pedro-1 & Pearl-1 in 1981 in northwestern shallow waters in Sri Lanka (Fig. 1.2). Since any of these wells did not encounter economically viable hydrocarbon deposits, they were plugged and abandoned as dry holes.

The Gulf of Mannar, an exploration frontier located between the western coastline of Sri Lanka and the eastern coastline of India, is separated from the Cauvery Basin to the north by Rama-Sethu (Fig. 1.2). The Gulf of Mannar is one of the least studied basins in the region. The Sri Lankan sector of the Gulf of Mannar, which is called the Mannar Basin, extends over of around 45000 km^2 in water depths varying from 20 m to more than 3000 m. Around 3000 km^2 in the northern part of the Mannar Basin lies in shallow water depths (< 400m). Pearl-1 drilled in 1981 by Cities Services Limited was the first and the only exploration well drilled in the Mannar Basin until 2011. Although oil exploration in Sri Lanka was active from early 1970s to 1981, little further exploration took place during 1981-2000.

Quaternary sand ("red earth") deposited on Miocene limestone

Fossil flora in Late Jurassic sediments from Tabbowa graben (After Edirisooriya and Dharmagunawardhane, 2013)

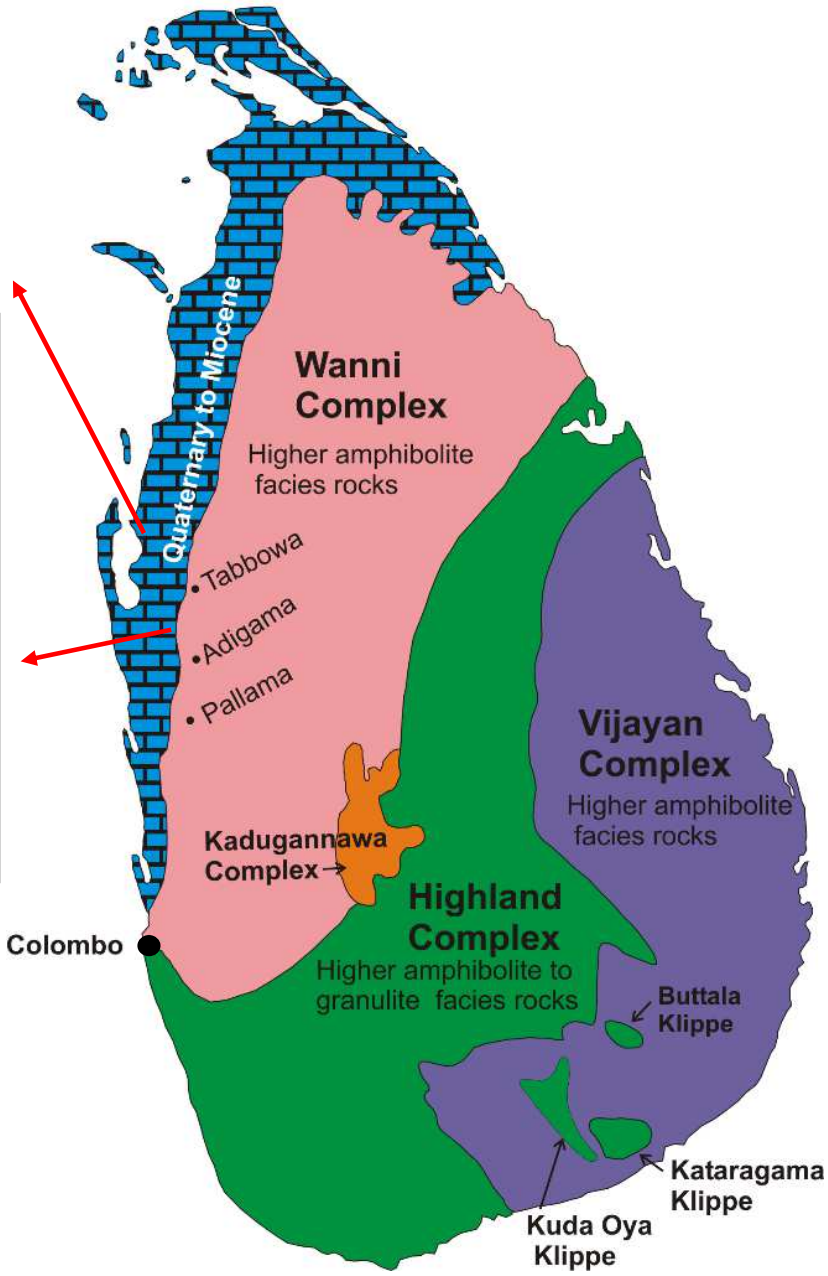

Fig. 1.1. Outline geology of Sri Lanka (After Kroner *et al*., 1987)

After a hiatus, Tomlinson Geophysical Services Inc. (TGS), a Norwegian geophysical company in 2001 shot 1050 km of two-dimensional (2D) marine seismic survey in the Mannar Basin. Interpretation of these data showed the Mannar Basin to have rift structure (Fig. 3.4) and other geological conditions favorable for accumulation of economically viable hydrocarbon deposits. Seismic data show that stratigraphic thickness of the Mannar Basin varies from around 4 km in shallow water depths to more than 6 km in deep water depths towards the south of the basin (Fig. 3.4b). In 2008, the Sri Lankan Government granted an exploration license for an exploration block in the northern Mannar Basin to Cairn Lanka Private Limited (CLPL). CLPL drilled three exploration wells in the exploration block during August-December 2011. The first well, CLPL-Dorado-91H/1z (Dorado in Fig. 1.2), was drilled in a water depth of 1354 m up to a total depth of 3288 m. It penetrated natural gas bearing sandstones between the depths of 3044-3069 m. Dorado was the first exploration well drilled in Sri Lanka in 30 years and the first to discover hydrocarbons in Sri Lanka as well as in the Gulf of Mannar (Premarathne *et al*., 2013). The second exploration well, CLPL-Barracuda-1G/1 (Barracuda in Fig. 1.2), drilled 68 km off the western coastline of Sri Lanka in a water depth of 1509 m, also penetrated three natural gas bearing sandstones between the depths of 4067-4206 m. CLPL-Dorado-North-1-82K/1 (Dorado-North in Fig. 1.2), the third exploration well drilled approximately 2.5 km north of the Dorado well up to a total depth of 3622 m was plugged and abandoned as a dry hole in December 2011.

The discovery of natural gas in the Dorado and Barracuda wells in the Mannar Basin established the existence of an active petroleum system in the Gulf of Mannar (Mohapatra *et al*., 2012; Premarathne *et al*., 2013). However, petroleum system of this deep water frontier basin is poorly understood. The objective of this research is to understand the geology, geological history and the petroleum system of the Mannar Basin. Seismic data, analysis of drill cuttings from the Dorado, Dorado-North and Barracuda wells, data from the well completion report for the Pearl-1 well held at PRDS were used in this study.

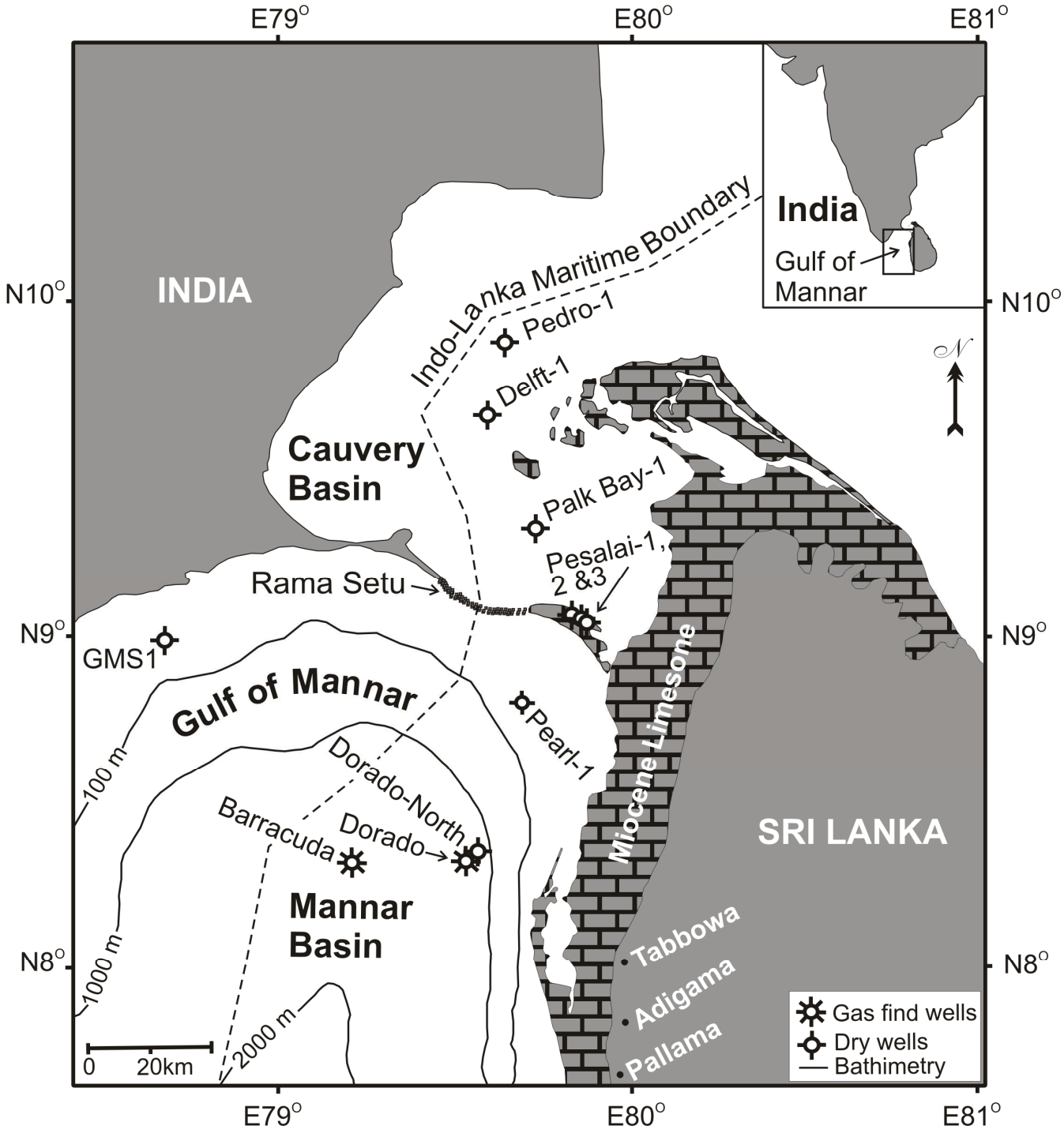

Fig. 1.2. The northern part of the Mannar Basin and exploration wells drilled in Sri Lanka. The location of the GMS1 well in the Indian shallow waters of the Gulf of Mannar was quoted from Rao *et al*. (2010).

1.3. Geological setting

The Gulf of Mannar is a failed rift (Curray, 1984), which evolved due to multiphase break up of Gondwana (Baillie *et al*., 2003; Fig. 1.3). Sea floor spreading between India and Antarctica and rifting of Indo-Lanka landmasses have been initiated in Early Cretaceous around 130 Ma (Lal *et al*., 2009). During rifting, counter clockwise rotation of Sri Lanka with respect India (Yoshida *et al*., 1992) is believed to have driven the crustal extension between Indo-Lanka landmasses. Thompson (1976) suggested that Sri Lanka's separation from India could be similar in fashion to Madagascar's separation from Africa. The counter-clockwise rotation of Sri Lanka has given rise to Cretaceous marine incursion into the Gulf of Mannar prior to similar events in northwestern offshore areas in Sri Lanka (Cantwell *et al*., 1978). This is supported by higher stratigraphic thickness in the Gulf of Mannar (Fig. 3.4b) than that in the northwestern offshore areas. Palaeo magnetic measurements from the Pesalai-1 well (Location: Fig. 1.2) suggest Sri Lanka's migration of some 2400 km from 16º S during the Paleogene to 8º N at present (Cantwell *et al*., 1978). This observation is in general agreement with the paleo geographic reconstructions of the Indo-Lanka landmasses by Torsvik *et al*. (2002; Fig. 1.3). Baillie *et al*. (2003) proposed that the Gulf of Mannar evolved during at least two periods of rifting. The first phase of rifting, the culmination of which is represented by the Albian unconformity, began during the beginning of seafloor in the Bay of Bengal (Baillie *et al*., 2003) due to separation of India and Antarctica. A Late Cretaceous unconformity marks the end of the second phase of rifting, which was initiated with the separation of Madagascar from India (Baillie *et al*., 2003). At the end of the Cretaceous period, the Gulf of Mannar has entered a thermal sag phase (Premarathne *et al*., 2015). The Gulf of Mannar has undergone compressional tectonics (De Silva, 2006), which has given rise to popup structures appear in seismic data (Fig. 3.4a).

Due to similarities in origin, geological structure, and stratigraphy, many researchers have proposed that the Mannar Basin is a sub basin of the Cauvery Basin to the north (Fig. 1.2), which produce both oil and gas (Baillie *et al*., 2003; Premarathne, 2008; Rana *et al*., 2008; Rao *et al*., 2010; Chandra *et al*., 1991; Chari *et al*., 1994). However, there are marked differences between the basins. The Indian sector of Cauvery Basin is dominated by NE-SW striking ridges and intervening depressions (Chandra *et al*., 1991), which may extend into Sri Lankan sector. However, the seismic data show that the Mannar Basin is devoid of such structures. In addition, igneous rocks are present in the Mannar Basin, but absent in the Cauvery Basin, while unconformities in the Cauvery Basin are associated with longer hiatuses than in the Gulf of Mannar.

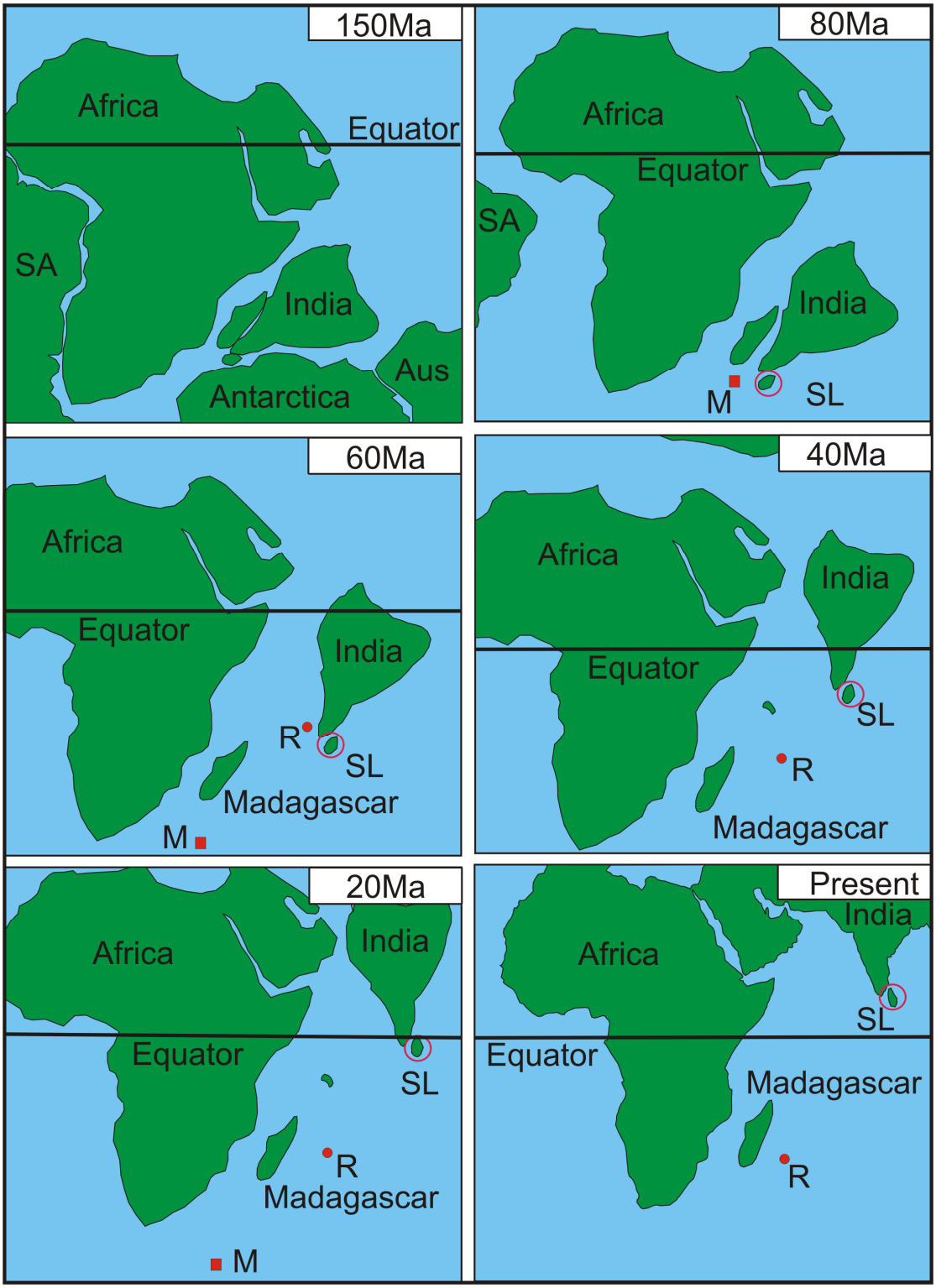

Fig. 1.3. Evolution of the Gulf of Mannar from the late Jurassic to present. Shifting of the geographic location of Sri Lanka and India from the Late Jurassic to present with respect to the Earth's equator is based on Torsvik *et al*. (2002). The letters "M" and "R" stand for Marion and Reunion hotspots, respectively, while SL and SA stands for Sri Lanka and South America, respectively. The red colored circle shows the location of Sri Lanka.

1.4. Stratigraphy

Seismic data from the Mannar Basin show a stratigraphic column more than 6 km thick underlain by the crystalline basement. No well drilled in the Mannar Basin has penetrated sediment older than the Late Cretaceous (Fig. 1.4). However, GMS1 well drilled in the Indian sector of the Gulf of Mannar (Location: Fig. 1.2) penetrated Late Albian shale between 3283 m and 3500 m (Rao *et al*., 2010). Pesalei wells located near the northern margin of the Mannar Basin also penetrated Albian sediments resting on the crystalline basement. The oldest sediment in the Gulf of Mannar could be the Late Jurassic or earlier. The Jurassic sediment encountered onshore areas of Sri Lanka and India suggest the possible occurrence of Jurassic sediments in the deeper part of the Mannar Basin. The Late Jurassic sediment crop out in the Tabbowa, Aadigama and Pallama grabbers in Sri Lanka (Wayland, 1920; Daraniyagala, 1939; Sitholey, 1942; 1944; Money and Cooray, 1966) and in southeastern coast of India (eg. Sastri *et al*., 1981). The Jurassic sediments is thought to have deposited prior to rifting in the Gulf of Mannar. Therefore, their occurrence in the gulf could be disseminated. Baillie *et al*., (2003) categorized the sedimentary rocks in the Mannar Basin into four tectonostratigraphic packages or megasequences. Accordingly, Albian and older sedimentary rocks in the gulf belongs to the first megasequence (MS-1 in Fig. 1.5). The Albian interval is bounded above by an unconformity in both the Cauvery and Mannar Basin (Rao *et al*., 2010; Fig. 1.5).

The Late Cretaceous sediments comprise a syn-rift megasequence (MS-2, Fig. 1.5; Baillie *et al*., 2003). The Dorado and Dorado-North wells terminated in the Campanian and Santonian stratigraphic sections, respectively (Fig. 1.4). Pearl-1 penetrated 750 m thick Maastrichtian to Santonian sandstone, which is separated from the overlying Palaeocene sediments by an unconformity (U/C-2 in Fig. 1.5), which has been encountered in wells drilled in the Cauvery Basin and the Krishna-Godavari Basin (Raju *et al*., 1994). The hiatus accompanying this unconformity is shorter in the Mannar Basin than in the Cauvery Basin (Fig. 1.5). Thus, the Late Cretaceous sediments in the Delft-1 well are overlain by Early Oligocene sediments, whereas those in the Palk Bay-1 well are overlain by the Early Eocene sediments.

Below the Late Cretaceous sedimentary rocks in the Pearl-1 well are about 57 m of Basalt composed mainly of medium to coarse grained olivine and Plagioclase and dated 76.8 ± 4.5 Ma based on the K-Ar. The Barracuda well recorded a roughly 760 m section between

the depths of 3480 and 4260 m, in which basalts are interbedded with the Maastrichtian sedimentary rocks (Fig. 1.4D). These igneous rocks are interpreted as basaltic lava, which occur over a wider areas of the basin (Premarathne *et al*., 2013). Dolerite dykes have been recorded in GMS1 well (Rao *et al*., 2008) and in five of six wells drilled in the Indian sector of the Gulf of Mannar (Rana *et al*., 2008), and have crystalline ages of 88 to 61 Ma (Rao *et al*., 2008) i.e. the late Cretaceous and early Palaeocene (Danian).

The origin of the igneous rocks remains incompletely understood. Biostratigraphic data, which indicate that a younger (76.8 ± 4.5 Ma/Campanian age) igneous rock is overlain by older (Coniacian-Turonian) sediments, suggest an intrusive origin of the igneous rocks encountered in the Pearl-1 well. If basalts encountered in the Barracuda well are to be lava flows their crystallization ages should vary between 66-72 Ma (see fig. 1.4D). This indicates the existence of both intrusive and extrusive rocks in the Gulf of Mannar. Baillie *et al*. (2003) suggested that the Late Cretaceous sediments belong to the second megasequence in the Gulf of Mannar.

The Paleogene and Neogene in the Mannar Basin are characterised by interbedded limestones, claystones, and sandstones. Unconformities such as the Late Eocene (U/C 3 in Fig. 1.5) could be the result of the Himalayan orogeny and associated uplift (Baillie *et al*., 2003). The late Oligocene and late Miocene unconformities (Fig. 1.5) may be eustatic in origin as these periods are marked by low eustatic sea levels (see Vail *et al*., 1977).

All wells drilled in the Mannar and Cauvery Basins encountered a thick succession of Miocene limestones (Figs. 1.4 & 1.5), which is >900 m thick in the Pearl-1 well. Thick Miocene limestones are exposed in the northern, northwestern and northeastern areas of Sri Lanka (horizontal bricks in Fig. 1.1). The Paleogene to Neogene interval in the Gulf of Mannar comprises the third megasequence (Baillie *et al*., 2003; Fig. 1.5).

The Pliocene and Quaternary sediment in the Gulf of Mannar is basically composed of unconsolidated sand. This section formed the fourth megasequence (Baillie *et al*., 2003; Fig. 1.5). Well rounded red coloured Quaternary sandstones (“red earth; Cooray, 1984) encounters in the north and north western coastal belt of Sri Lanka (Fig. 1.1).

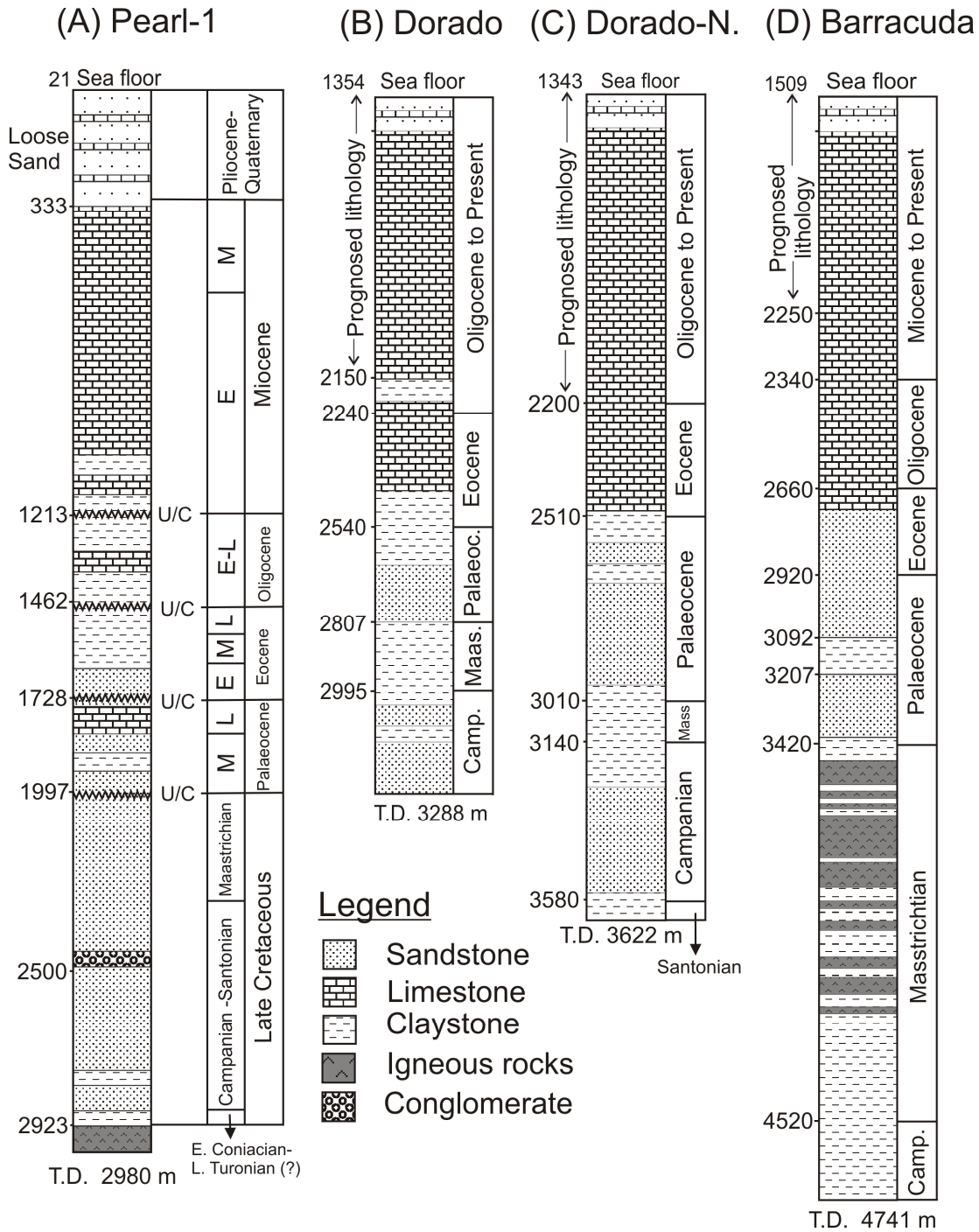

Fig. 1.4. Generalised stratigraphic sections of the wells drilled in the Mannar Basin. (A) Pearl-1 (B) Dorado (C) Dorado-North (modified after Ratnayake *et al*., 2014) and (D) Barracuda wells (modified after Premarathne *et al*., 2013; Ratnayake *et al*., 2014). Stratigraphy of the Pearl-1 well is based on information from unpublished reports held at PRDS; Formation ages are based on biostratigraphic data from the same report. Geologic ages of the formations for Dorado, are based on well correlation and seismic data interpretation. Oligo. = Oligocene, Paleoc. = Palaeocene, Maas. = Maastrichtian, Camp. = Campanian, E= Early, M = Middle, L = Late, U/C = unconformity and T.D. = total depth. The depth is in meters (m) below the mean seal level.

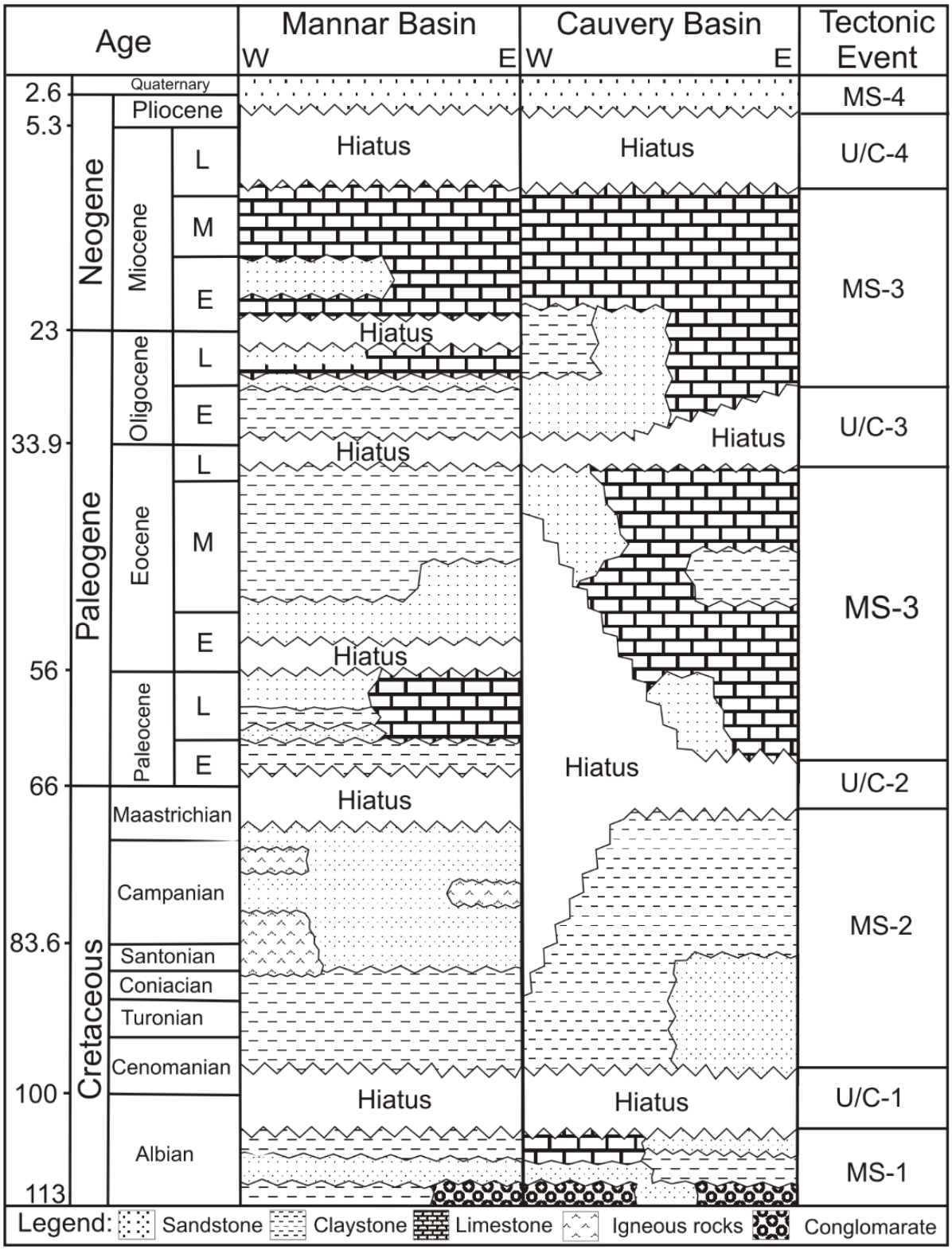

Fig 1.5. Chronostratigraphic comparison between the Mannar and Cauvery Basins. At least seven depositional sequences can be identified in the Mannar Basin. The tectonostratigraphic packages/megasequences (MS) proposed by Baillie *et al*. (2003) are also shown. U/C = unconformity. Time boundaries of lithological units are based on the Geological Time Scale v. 4.0 of the Geological Society of America.

2. PETROLEUM GEOLOGY AS SUGGESTED BY EXPLORATION WELLS

2.1. Samples and data

A memorandum of understanding (MOU) was signed with Sri Lanka's Petroleum Resources Development Secretariat (PRDS) to obtain samples and data for this research. Accordingly, a total of 635 unwashed drill cutting samples from the Dorado, Dorado-North, and Barracuda wells (Location: Fig. 1.2) were collected from the PRDS. Each sample contained around 35g of drill cuttings from a 10 m depth interval. Samples for the Dorado, Dorado-North, and Barracuda wells, were available from the depths of 2150, 2200 and 2140 m, respectively to the total depth of each well at 3228, 3620 and 4741 m, respectively (Appendix A). The samples were frozen dried for 20 hours prior to analytical preparations. Cutting samples contained oily substance, apparently drilling oil. Therefore, cutting samples were washed three times with hexane in an ultra-sonication bath each time for 15 minutes to remove drilling oil. Since cutting samples were not available for the Pearl-1 well, its unpublished well completion report was collected from the PRDS.

Fig. 2.1. A drill cutting sample from the Barracuda well washed with hexane. The sample is calcareous claystone from the depths of 4710-4720m.

2.2. Analytical methods

2.2.1. GC and GC-MS analysis

10 g of frozen dried drill cutting samples were washed with 30 mL hexane three times under ultrasonication each time for 15 minutes to remove drilling oil. The samples were kept inside a fume cupboard for around 24 hours before pulverizing them using an agate mortar. Bitumen in pulverized (~75µm) drill cutting samples was extracted by ultrasonication (3 × 15 minutes) with a mixture of dichloromethane and methanol (v/v 1:3, 1:1, and 1:0, respectively). Aliphatic and aromatic compounds in the extract were fractionated using silica-gel column chromatography. Each fraction was analyzed using *Hewlett Packard (HP) 6890 G*as Chromatography (GC) and *HP 5973 G*as Chromatography and Mass Spectrometry (GC-MS: Fig. 2.2) with fused silica DB-5HT (30 m × 0.25 mm J &W) column with a splitless injection system and a flame ionization detector (FID). Carrier gas (1.5 ml min^{-1}) was helium. The oven temperature was programmed for 2 minutes at 40 ºC, increased from 40 to 300 ^{o}C at 4 ^{o}C per minute and finally held for 20 minutes at 300 ^{o}C.

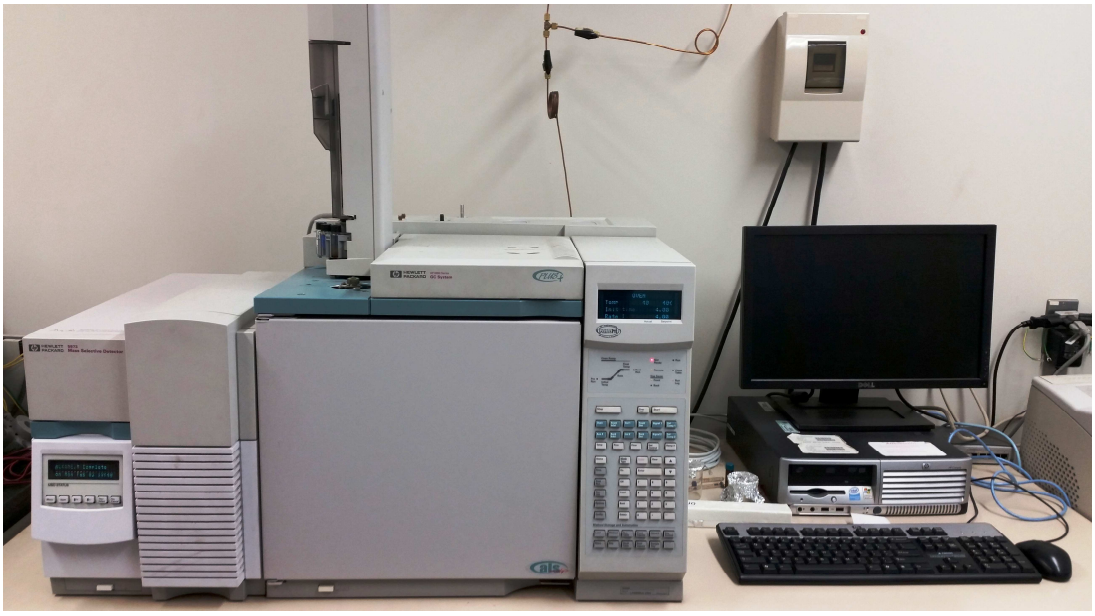

Fig. 2.2. *HP 5973* Gas chromatography and mass spectrometry (*GC-MS*) instrument.

2.2.2. Elemental analysis

This study focused on the analysis of sediments from the Dorado well and calcareous claystone between the depths of 4260 to 4740 m in the Barracuda well. Each sample was frozen dried for 20 hours before being pulverised using an agate mortar. Since initial geochemical analysis of cutting samples from the Dorado, Dorado-North, and Barracuda

wells show the cuttings to have been contaminated significantly with drilling oil (Fig. 2.6), the pulverised cutting samples were washed with 30 mL mixture of methanol and dichloromethane in 2:1, 1:1 and 0:1 volume ratios in an ultrasonic bath, each time for 15 minutes to remove drilling oil. 3.7-4.3 mg from each dried sample was weighed into an Ag capsule, to which a few drops of 1N HCl was added and kept at 160^{o}C over night to remove inorganic carbon. Then, 6 mg of vanadium (V) oxide (V_2O_5) powder was placed in the Ag capsule. It was then enclosed in a Sn capsule before moulding it into a tiny cube. Each sample was analysed using *Euro EA 3000* CHNS elemental analyser (Fig. 2.3). The combustion temperature inside the furnace was around 1020 ºC. L-cystine was used as the standard. Regression analysis was employed for quantitative analysis. Elemental concentration was determined on a dry-weight basis. The errors of the analyses were ±3% for TOC.

Washing of pulverised cutting samples with methanol and dichloromethane in an ultra-sonication bath is thought to remove a significant quantity of bitumen (Bit), which is extractable using polar and nonpolar organic solvents. Bitumen to total organic carbon ratio (Bit/TOC) varies from zero in shallow sediments to ~0.25 at peak oil generation (Peters *et al*., 2007). Miles (1994) on the other hand inferred that greater than 0.2 Bit/TOC ratios for oil-prone sediments suggest contamination. The Bit/TOC ratio of sediment in the oil window decreases with further burial due to conversion of bitumen to volatile hydrocarbon (Peters *et al*., 2007). Therefore, it is generally assumed that the removal of the bitumen fraction does not significantly affect the measured total organic carbon (TOC) content of a sample excluding oil-prone sediments in the oil window.

Fig. 2.3. Euro EA 3000 CHNS-elemental analyser.

2.2.3. Vitrinite reflectance

The standard method of acid maceration for kerogen separation was used for 20–30 g cutting samples from the Dorado, Dorado-North, and Barracuda wells. Only fine-grained sediments with higher total organic carbon content (~1.0 wt.% or higher) were selected for acid maceration. Coaly fragments in acid-macerated sediments were extracted with a zinc bromide ($ZnBr_2$) solution with a density of 1.55 g/cm^3. Coaly fragments mounted on epoxy plugs were polished with progressively finer alumina dust followed by 3, 1 and 0.25 µm diamond paste, respectively. The reflectance of vitrinite was measured using a Nikon Eclipse-LV-100-ND microscope (Fig. 2.4) with a stabilised halogen light source and photonic multichannel analyser (PMA12, Hamamatsu Photonics Co.). Vitrinite reflectance (VR) was measured for a spot size of 20 µm diameter at a wavelength of 542.8 nm by comparison with standard values of polished glasses (Fig. 2.5), which have 0.55%, 0.79%, 1.08%, and 1.53% reflectance in oil, respectively. The reflectance of 30–40 individual vitrinite grains was measured for mean VR. Marceral composition analysis and fluorescence microscopy were undertaken on bulk kerogen. Kerogen fluorescence was examined under ultraviolet (UV) light using a Nikon Optiphot-2 microscope with Hg lamp and UV filter set.

Fig. 2.4. Nikon Eclipse-LV-100-ND microscope

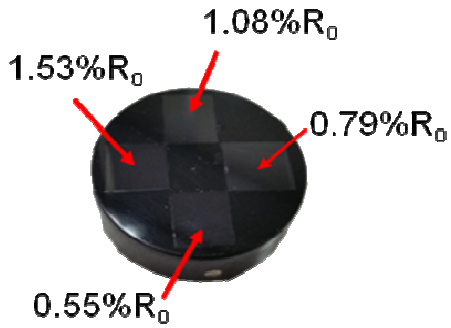

Fig. 2.5. Polished glass standard with different R_o values

2.3. RESULTS AND DISCUSSION

2.3.1. Composition of bitumen extract

GC-MS chromatograms for saturate fraction (F_1) of drilling oil contains C_{10}-C_{20} hydrocarbons (Fig. 2.6A), which is more or less similar to the composition of diesel that typically contains C_8-C_{21} hydrocarbons (Collins, 2007). GC-MS chromatogram for bitumen extracts of cutting samples, predominantly contain C_{10}-C_{20} compounds (Fig. 2.6B). This indicates that the samples contain a significant amount of drilling oil despite washing of the cuttings with hexane three times in an ultrasonication bath, each time for 15 minutes prior to pulverization. The relative abundance of drilling oil is so high that long chain alkanes having C_{21} or higher carbon number compounds in the extract, which generally elute after 40 minutes of retention time, are masked (Fig. 2.6B). These chromatograms are not conducive for biomarker studies because the relative abundance of different biomarkers (eg. pristane, phytane etc.) might have been affected by similar compounds in drilling oil giving rise to erroneous inferences especially of depositional environment, thermal maturity etc.

2.3.2. Hydrocarbon source character

With the exception of a couple of thin stratigraphic intervals, the total organic carbon (TOC) content of most sediments in the Pearl-1 well is less than 0.5% (Table 2.1 and Fig. 2.7). The cross plot of the hydrogen index against the oxygen index (Fig. 2.8) indicates that sediments from this well mostly contain Type III kerogen with inertinite in the Late Cretaceous section.

Peters (1986) defined Rock-Eval $S_2 > 5$ mg HC/g rock as an indication of good source potential. Accordingly, the Late Cretaceous section in the Pearl-1 well, which yields $S_2 < 5$ mg HC/g rock (Table 2.1), indicates poor source potential. Sediments with Type III kerogen, HI = 50–200 mg HC/g rock and $S_2/S_3 = 1–5$, indicate, among other factors, source potential for natural gas (Peters and Cassa, 1994). Accordingly, most Paleogene sediments from the Pearl-1 well seem to have source rock potential for natural gas. The TOC content of argillaceous sediments from the Dorado well varies from 0.5% to greater than 1%, while calcareous claystone between the depths of 4260 and 4741 m in the Barracuda well varies mainly from 1 to 2% (Fig. 2.9 or Appendix B). Kerogen in rock samples from the two wells show no fluoresce under ultraviolet (UV) light (Fig. 2.11).

(A)

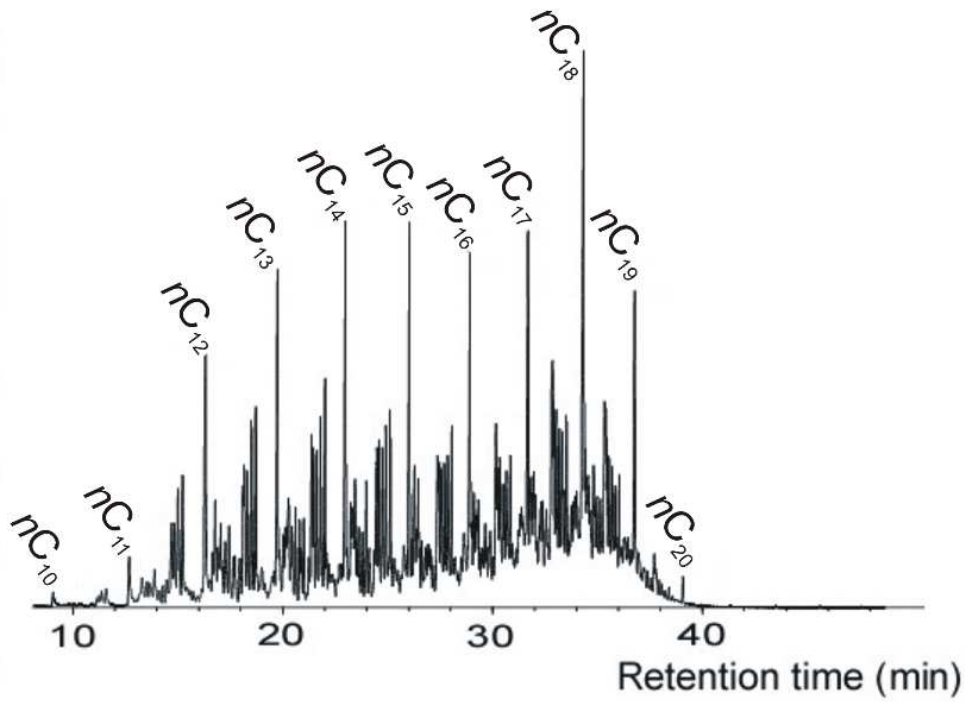

(B)

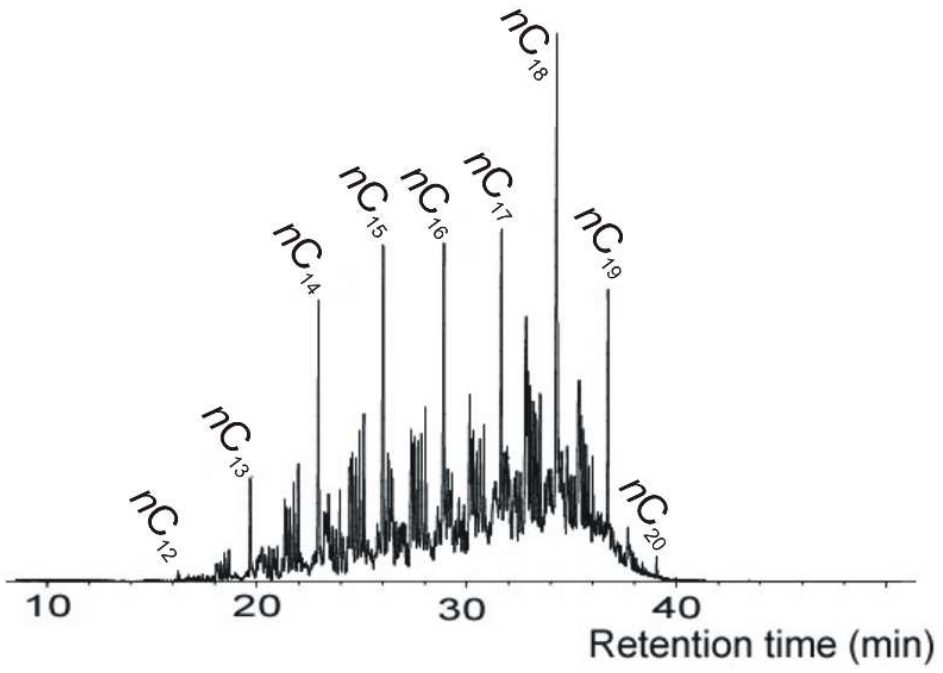

Fig. 2.6. GC-MS chromatograms of (A) drilling oil and (B) bitumen extract of pulverised drill cuttings from the depths of 3610-3620 m in the Dorado-North well.

Marceral composition analyses show predominance of vitrinite, detrovitrinite, and fusinite in sediments from the Dorado well and most samples from the depths of 4260-4741 m in the Barracuda are rich in fusinite and poor in other maceral (Figs. 2.11 and 2.12).

1-2% TOC indicates good hydrocarbon source potential (Peter and Cassa, 1994). Sediments from the Dorado well are rich in organic carbon but mainly have Type III kerogen. Therefore, these sediments may have source potential for natural gas. Though calcareous claystone between the depths of 4260–4741 m in the Barracuda well are rich in organic carbon, they have poor hydrocarbon source potential due to the higher inertinite content and lack of petroleum generative kerogen. Organic matter in sediments penetrated by the wells in the Mannar Basin has derived mainly from vascular land plants with little or no contribution from marine microorganisms.

Table 2.1. TOC and Rock-Eval pyrolysis data extracted from the well completion report for the Pearl-1 well. S_1 and S_2 are in mg HC/ g rock. S_3 is in mg CO_2/ g rock. HI = Hydrogen Index in mg HC/g TOC, OI= Oxygen Index in mg CO_2/g TOC), PI= Production Index (S_1/S_1+S_2).

Depth (m)	TOC (% wt.)	S_1	S_2	S_3	HI	OI	PI	S2/S3	T_{max} (^oC)
560	0.26	0.004	0.22	1.05	85.8	405.0	0.018	0.21	415.8
870	0.36	0.004	0.69	1.10	190.8	306.1	0.006	0.62	415.8
1,017	0.36	0.004	0.70	0.61	194.4	170.0	0.006	1.14	415.8
1,131	0.69	0.005	1.99	1.34	288.7	193.6	0.003	1.49	242.2
1,185	0.58	0.003	1.21	1.15	209.1	197.9	0.002	1.06	420
1,197	0.88	0.017	2.46	1.34	279.0	152.6	0.007	1.83	424
1,209	1.00	0.009	2.71	0.93	271.3	92.8	0.003	2.92	426
1,317	0.58	0.003	0.51	0.87	87.9	150.2	0.006	0.59	417
1,354	0.48	0.001	0.23	0.66	47.7	137.5	0.004	0.35	414
1,386	0.68	0.022	0.57	0.65	83.8	95.9	0.037	0.87	419
1,401	1.05	0.037	1.10	1.23	104.9	116.9	0.033	0.90	422
1,416	0.66	0.021	0.53	0.59	80.5	89.2	0.038	0.90	423
1,424	2.36	0.013	3.46	0.91	146.6	38.7	0.004	3.79	432
1,436	0.23	0.03	0.16	1.16	69.6	505.7	0.158	0.14	425
1,442	0.26	0.03	-	0.98	-	377.7	1.000	-	-
1,582	0.62	0.003	0.58	0.70	93.5	112.1	0.005	0.83	424
2,002	0.58	0.005	0.13	1.95	21.6	336.2	0.038	0.06	422
2,590	0.79	-	0.46	0.29	58.2	36.7	-	1.59	420
2,649	0.54	-	0.19	0.24	35.2	43.5	-	0.81	414
2,740	2.55	0.002	1.11	0.33	43.3	12.9	0.002	3.35	448
2,890	0.56	0.001	0.23	0.36	41.1	63.4	0.004	0.65	425
2,908	0.69	-	0.36	0.40	52.2	58.0	0.000	0.90	445
2,920	0.78	0.18	0.24	0.39	30.8	50.0	0.429	0.62	454

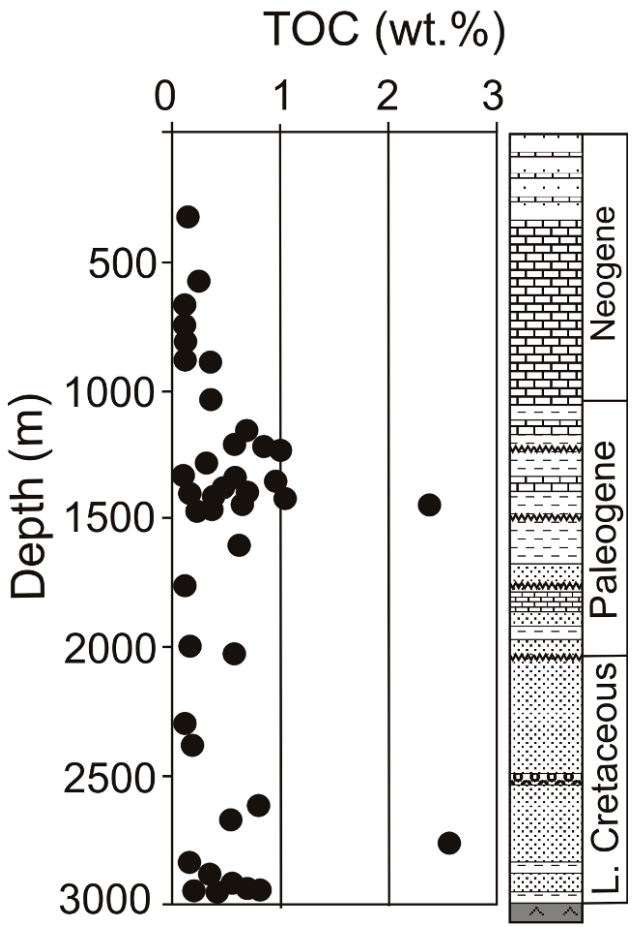

Fig. 2.7. Total organic carbon (TOC) content of sediments from the Pearl-1-well.

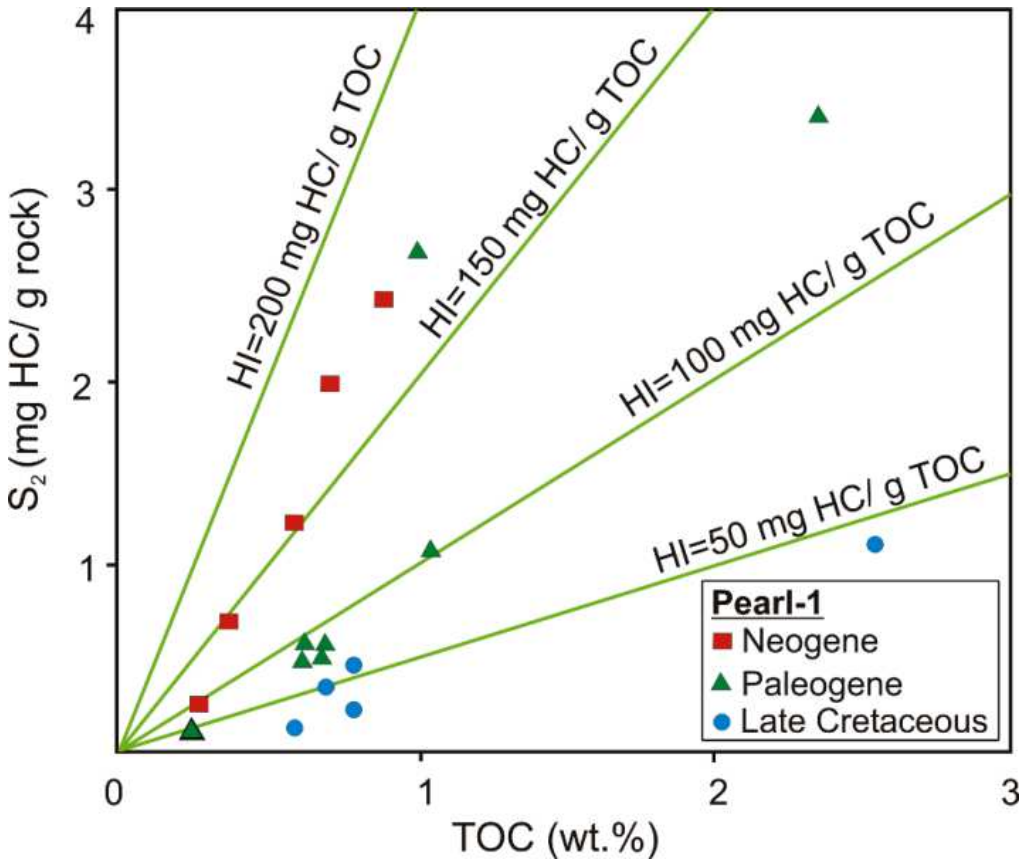

Fig. 2.8. Cross plot of Rock Eval S_2 versus TOC for the Pearl-1 well.

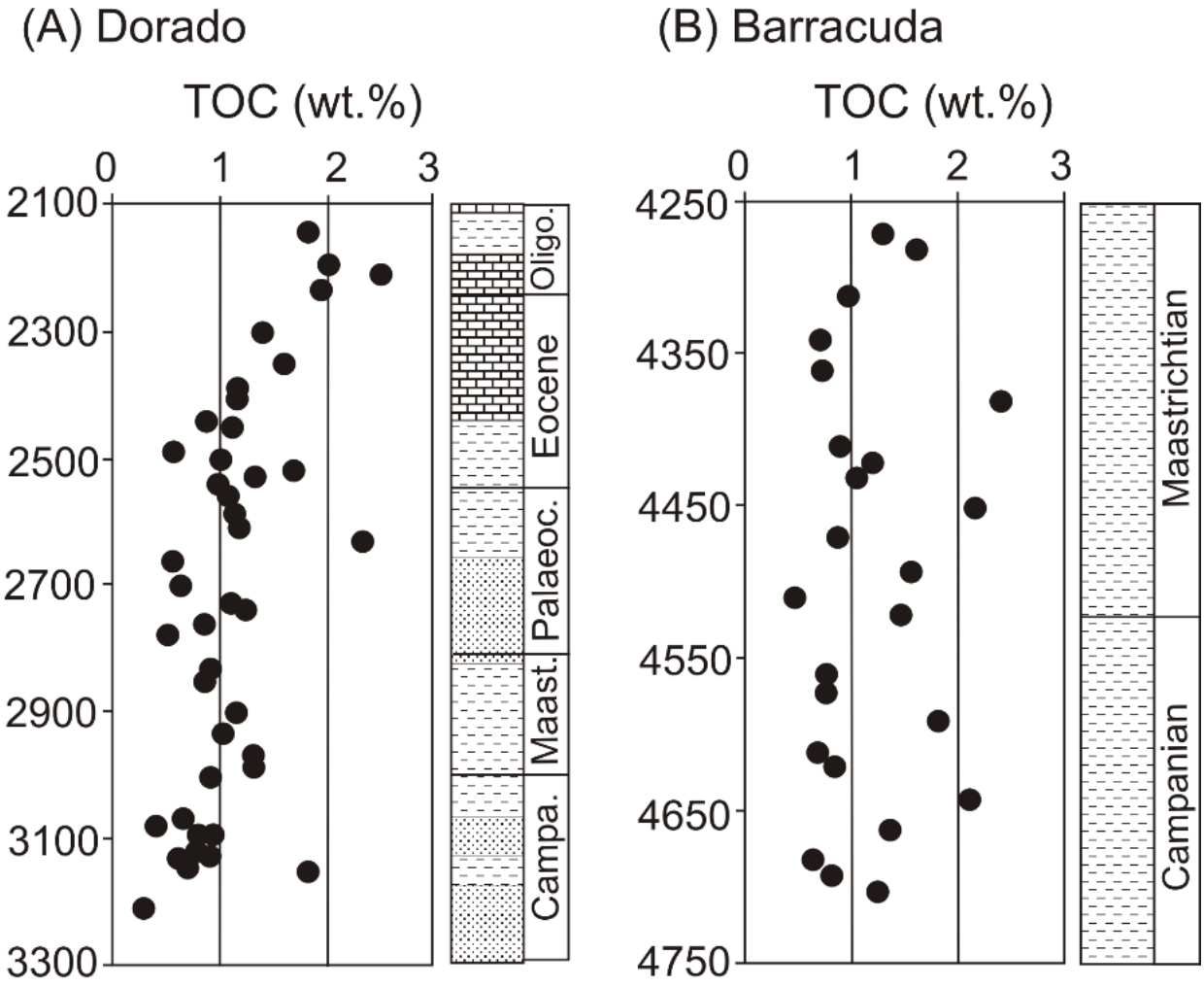

Fig. 2.9. Total organic carbon (TOC) content of (A) Dorado well and (B) calcareous claystones between the depths of 4260- 4741 m in the Barracuda well. Camp., Maast., Palaeoc., Oligo., stand for Campanian, Maastrichtian, Palaeocene and Oligocene, respectively. Depths are in meters (m) below mean sea level (MSL). Legend for the litholohic columns are the same as that in Fig. 1.4.

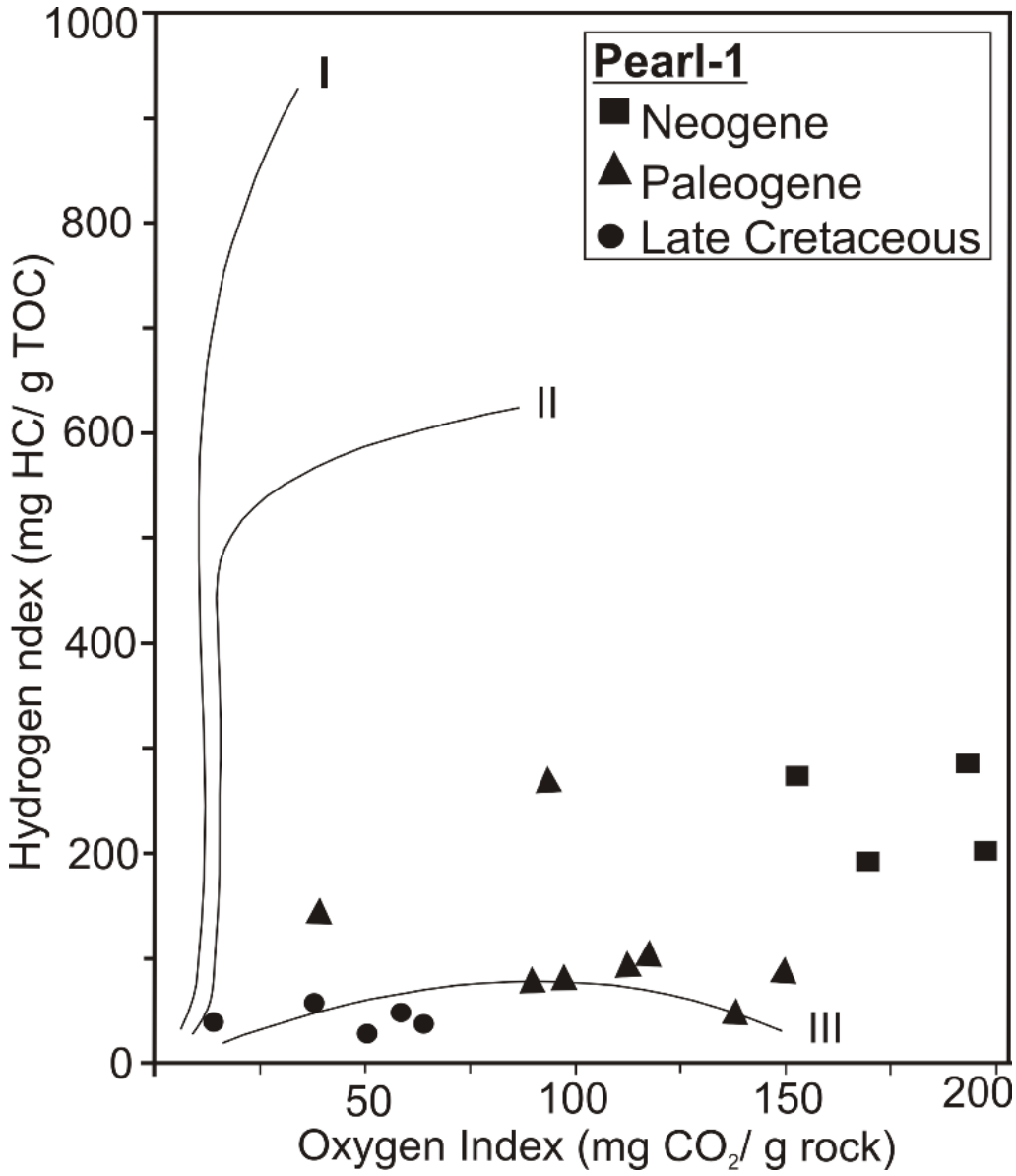

Fig. 2.10. Hydrogen Index (HI) versus Oxygen Index (OI) for Pearl-1 well. Organic maturation pathways (curves) of Types I, II, and III kerogen is based on Espitalié *et al*. (1977).

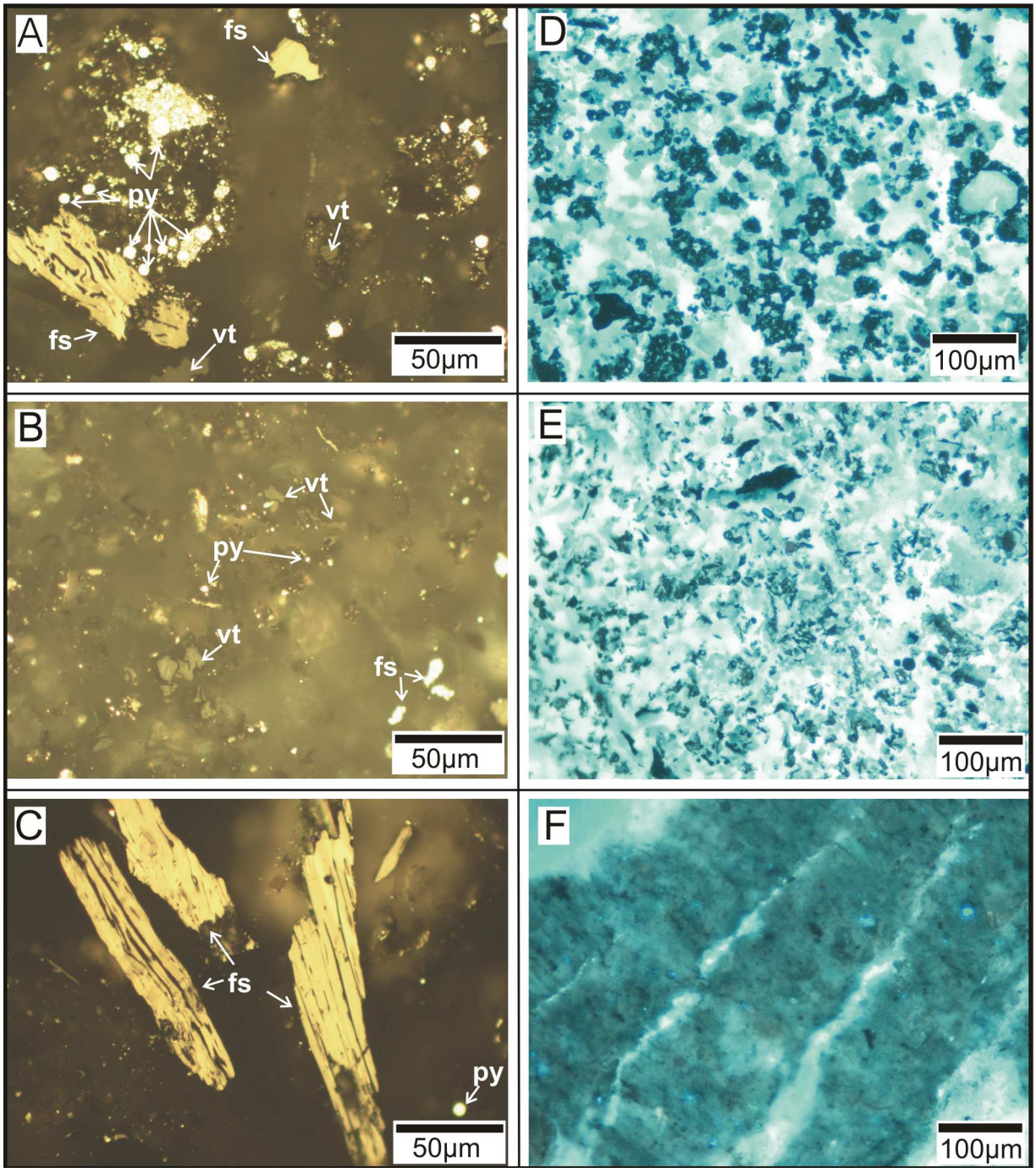

Fig. 2.11. Photomicrographs of kerogen under reflected white light in fine grained sediments between the depths of (A) 3140-3150 m in the Dorado well, (B) 4510-4520 m in the Barracuda well and (C) 4610-4620 m in the Barracuda well. Fluorescence microscopy under UV light of kerogen in fine grained sediment between the depths of (D) 3120-3130 m in the Dorado well, (E) 3140-3150 m in the Dorado well and (F) 4340-4350 m in the Barracuda well. fs, vt, and py stand for fusinite, vitrinite and pyrite, respectively.

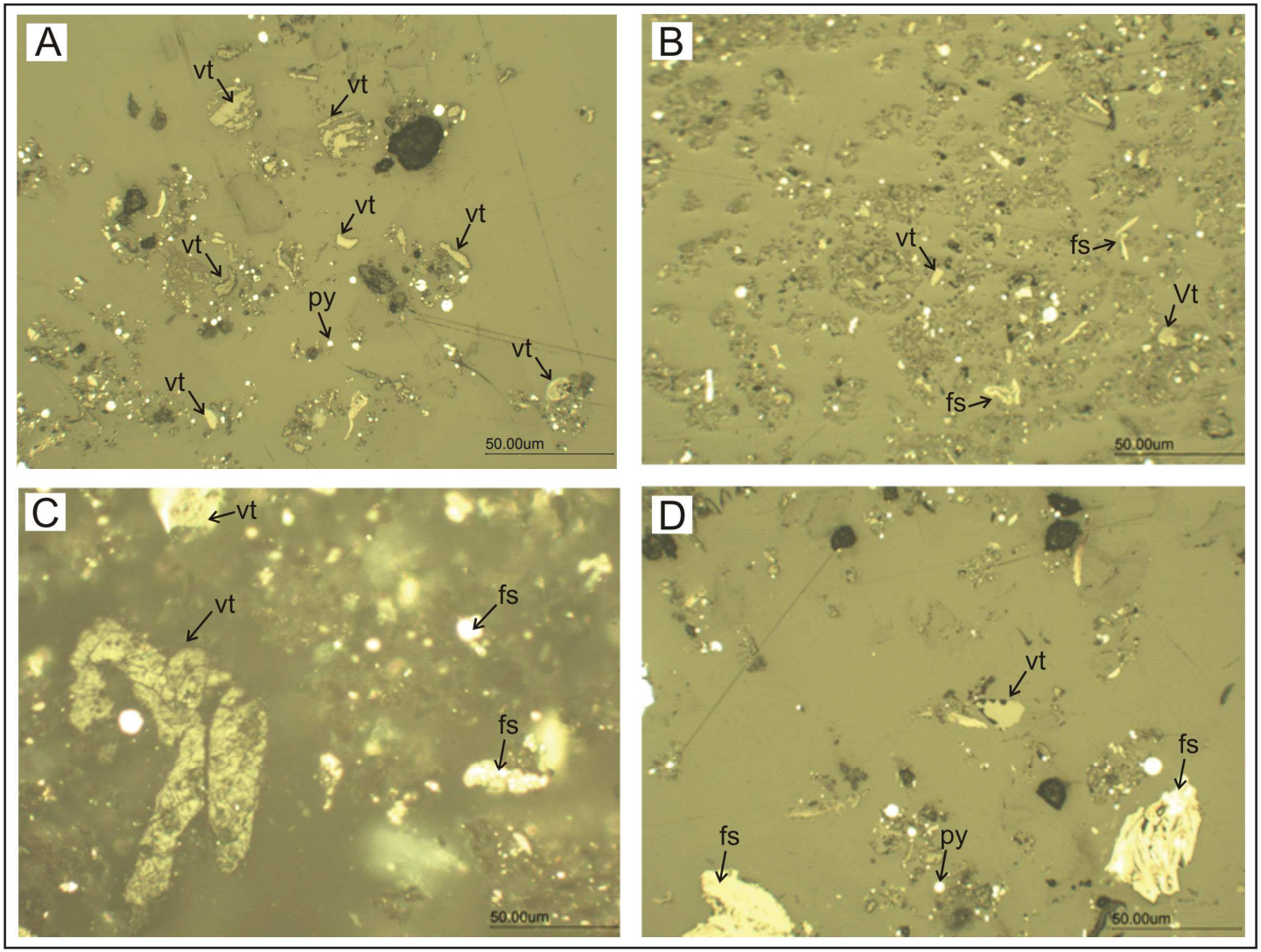

Fig. 2.12. Photomicrographs of vitrinite (vt) extracted from fine grained clastic sediment from the (A) Dorado well between the depths of 2930-2940 m (B) Dorado-North well between the depths of 3210- 3220 m and (C) & (D) Barracuda well between the depth of 4420- 4430 m and 4710- 4720 m, respectively. Photos were taken under reflected white light in oil. fs = fusinite and py = pyrite.

2.3.3. Thermal maturity

Vitrinite reflectance data is not available for the Pearl-1 well. Alternatively, Rock Eval T_{max} data, which is available for the Pearl-1 well (Table 2.1), could be used as a maturity indicator. Peters and Cassa (1994) reported that T_{max} of 435- 470 ^{o}C indicate the oil window. Three out of four samples from the last 200 m of the Pearl-1 well recorded T_{max} values of more than 440°C (Fig. 2.11 & Table 2.1), which correspond to the oil window. The sample from the depth of 2920 m had T_{max} of 454 °C and a production index (PI) of 0.43, suggesting oil generation in this sediment (Table 2.1). In addition, the T_{max} data suggest entering of sediment in the Pearl-1 well into the oil window at the depth of around 2700 m. Anomalously low T_{max} values (<425 °C) observed at the deeper part of the well (Table 2.1 and Fig. 2.11) could be due to mixing of rock fragments from shallower levels of the well during drilling. Rao *et al*. (2010) reported that Late Albian sediments between the depths of 3283 and 3500 m in the GMS-1 well (location: Fig. 1.2) have T_{max} of 473 °C, indicating entering of the sediment into the gas window. This observation basically agrees with the maturity trend in Figure 2.12. Overall, it indicates that the Santonian sediment in the Pearl-1 well has thermally matured and oil generation has started. However, most of the sediment penetrated by the Pearl-1 well below this depth is sandstone (Fig. 1.4A) and therefore, relatively thin claystone layers below the oil window could not have produced any commercial quantity of oil.

Sediment in the Dorado, Dorado-North, and Barracuda wells has entered the oil window (VR $\geq$ 0.6 %R_o; Petersen, 2002) at the depths of 3654, 3643, and 3809 m below mean sea level (bMSL), respectively, while the gas window (VR $\geq$ 1.35%R_o; Petres and Cassa, 1994) at the depths of 5154, 5143, 5409 m bMSL, respectively (Fig. 2.14).

The data suggest that sediments penetrated by the Dorado and Dorado-North wells are thermally immature. However, calcareous claystone below igneous rocks the Barracuda well (Fig. 1.4D) are thermally matured. However, the sediment in this section (4318-4741 m bMSL), which have a poor hydrocarbon source potential may not have produced any significant quantity of hydrocarbon.

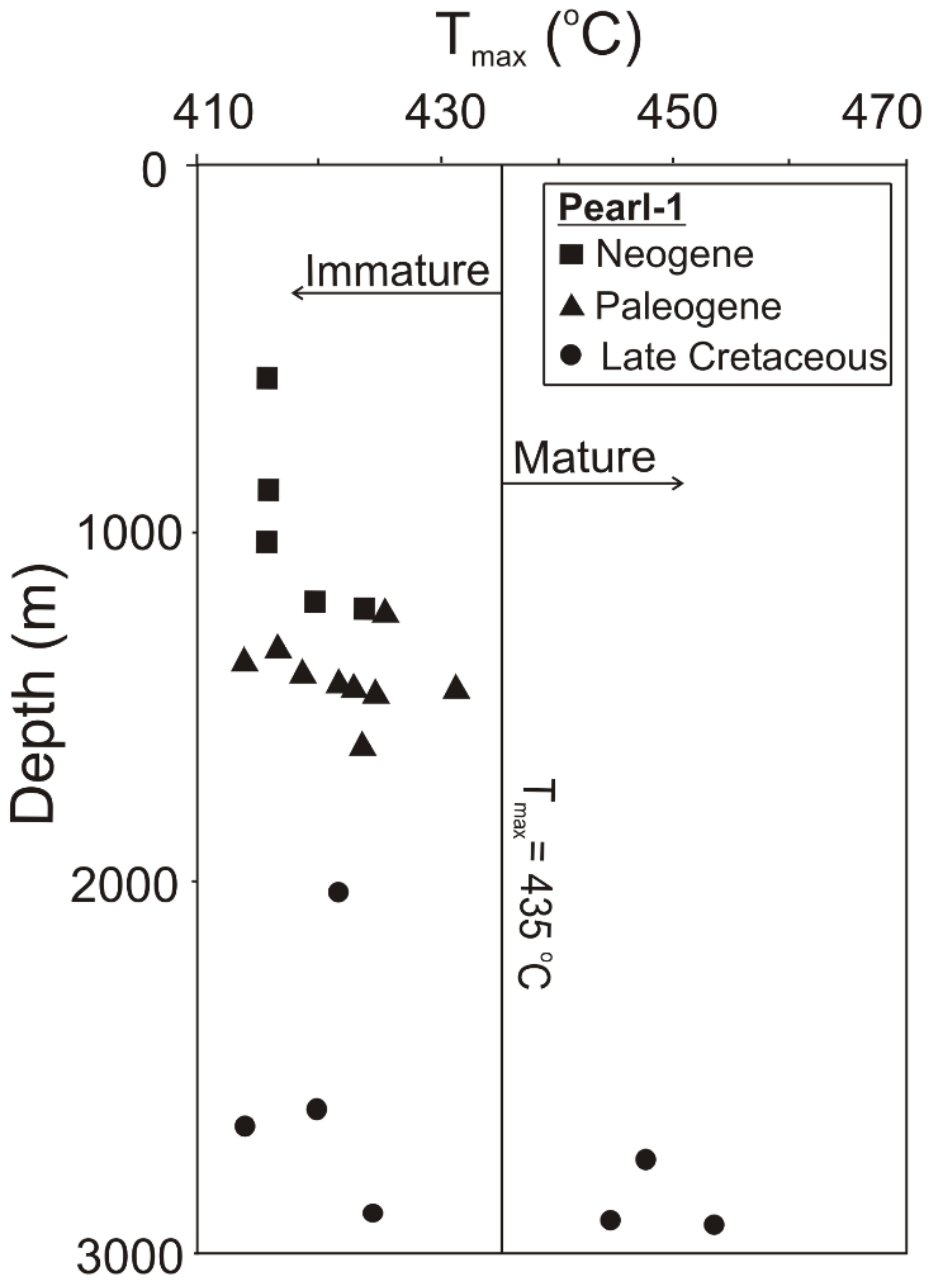

Fig. 2.13. Plot of Rock Eval T_{max} versus depth for Pearl-1 well. The boundary line for the oil window, where T_{max} = 435 ^{o}C is based on Peters and Cassa (1994).

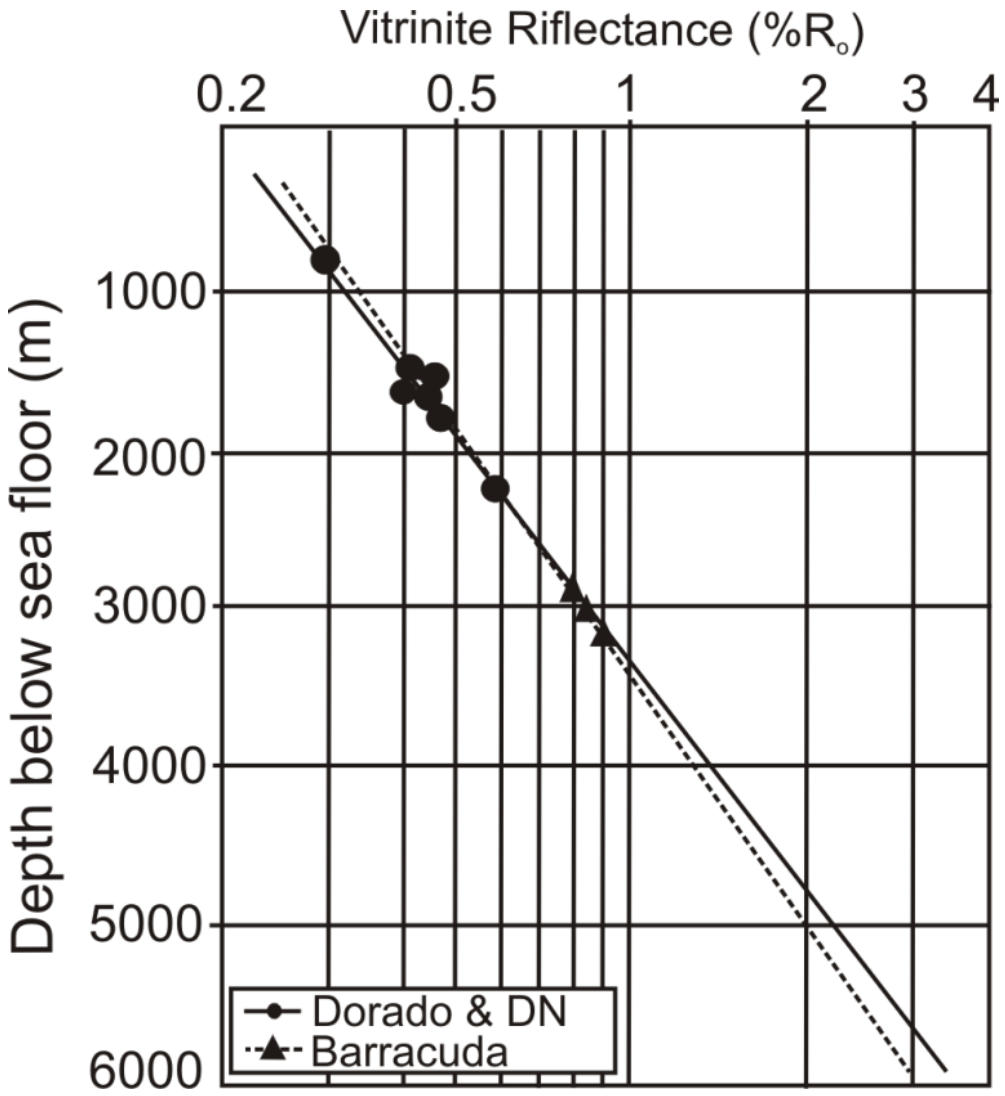

Fig. 2.14. Kerogen maturation profiles for Dorado, Dorado-North and Barracuda wells. Vitrinite reflectance (VR) is in percent reflectance of white light in oil (%R_o). Since the Dorado and Dorado-North (DN) wells are located in close proximity, VR data from them were combined to calculate a single regression line. Depths are in meters below seafloor. Water depths at the Dorado, Dorado-North and Barracuda wells are 1354, 1343, 1509 m, respectively. Most samples below igneous rocks in the Barracuda well are poor in vitrinite.

2.4. Interim inferences

GC and GC-MS analysis of bitumen extract of pulverised fine grained cutting samples indicate that most of the cutting samples, especially those from the deeper part of each well, are highly contaminated with diesel based drilling oil. Organic solvents such as hexane, dichloromethane and methanol cannot be used to remove drilling oil contamination to an acceptable level so that the results from biomarker analyses are reliable.

Thermal maturity and source character data suggest that wells drilled in the Mannar Basin might not have penetrated its potential source rocks. Hence, it is doubtful as to whether further analysis of drill cuttings would help fulfil the objectives of this research. No well drilled in the Mannar Basin has encountered oil or condensates. In this case, no opportunity to study biomarkers in oil or condensates, which otherwise would have been used to understand the type of source rocks and their thermal maturity at the time of oil/condensate expulsion. Though natural gas has been encountered in the Dorado and Barracuda wells, gas samples were not available for this study. Therefore, basin modeling technique is the best option available to fulfil the objectives of this search.

3. BASIN AND PETROLEUM SYSTEM MODELING

3.1. What is modeling?

Basin and petroleum system modeling (BPSM) is an iterative process (Al-Hajeri *et al*., 2009). It can simulate a basin's burial and thermal history, source maturation and hydrocarbon generation, expulsion, migration and trapping. BPSM is frequently used to draw valuable inferences on frontier basins with a limited data set such as the Mannar Basin. Its application is becoming increasingly common with the development of faster computers and increasing data storage facilities.

3.2. Modeling software

SIGMA-2D basin modeling software (version 6) of Japanese Oil, Gas and Metals National Cooperation (JOGMEC) was used in this study. The software could simulate the basin's burial and thermal history and hydrocarbon generation, expulsion, migration and accumulation in a two-dimensional (2D) cross section. Under geological modeling, the software reconstructs the burial and thermal history of a 2D cross section by using lithology distribution, rock physical properties and boundary conditions such as ocean bottom temperature, present and palaeo heat flows and depositional water depths and sea level changes. The software use SIMPLE-R_o (Suzuki *et al*., 1993) to calculate the vitrinite reflectance (VR). Computed maturity data together with TOC, kerogen composition and kinetic models for different types of kerogen converting into hydrocarbon are used to simulate hydrocarbon generation under generation modeling. Finally, under migration and accumulation modeling the software simulates hydrocarbon expulsion, migration and accumulation. Relative permeability of oil, water and gas in shale is used to determine the hydrocarbon expulsion threshold. Secondary hydrocarbon migration is also based on relative permeability of oil, water and gas in sandstone and carbonate rocks. Relative permeability is an extension of the Darcy's law on multiphase fluid (water, oil and gas) flow. The software also takes into account hydro fracturing and phase behavior of fluids such as dissolution of gas in oil. Fig. 3.1 summaries the main steps involved in numerical simulation of basin modeling. More information on SIGMA-2D software performing BPSM is available in Okui *et al.* (1996); Okui (1998).

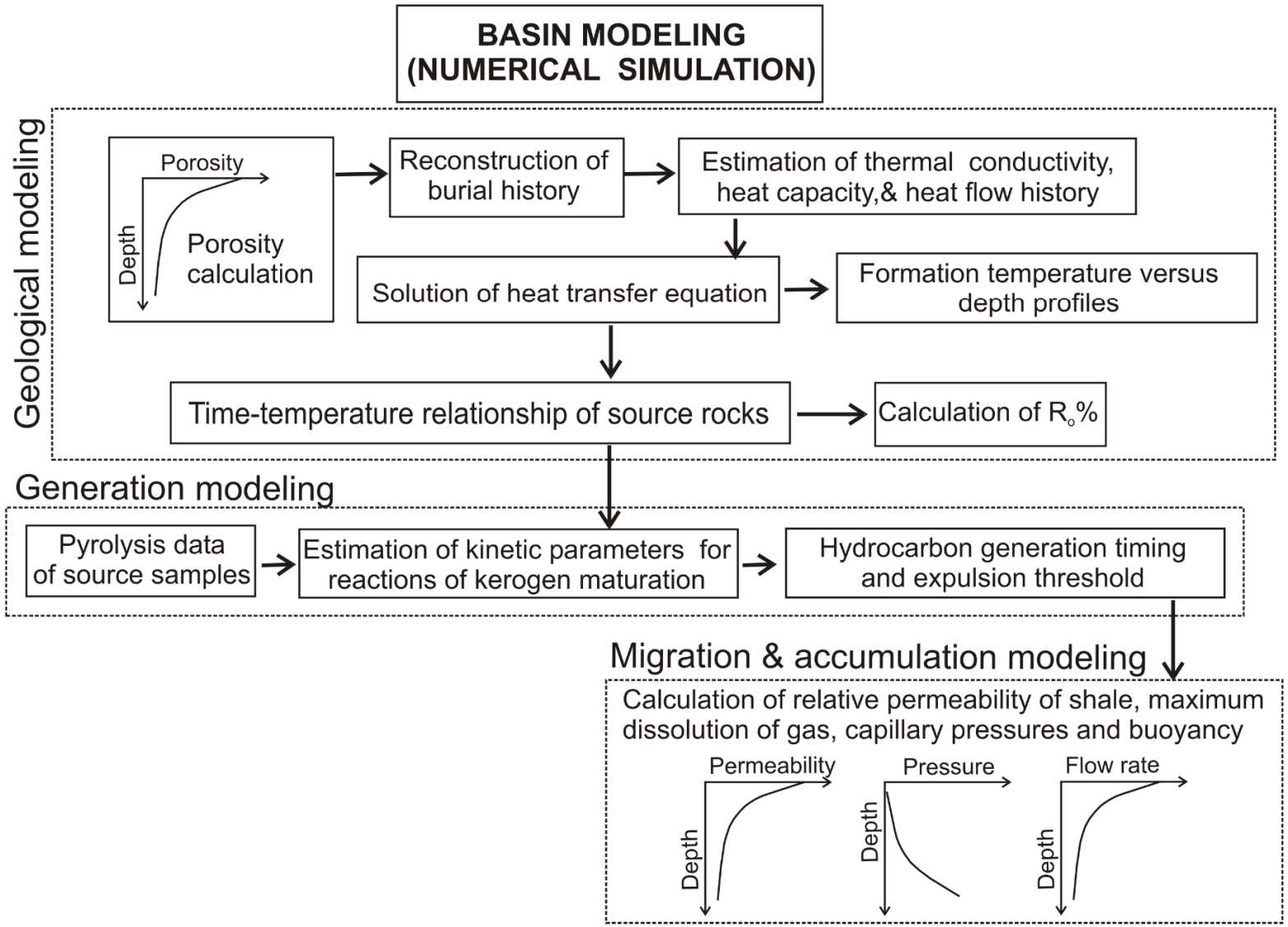

Fig. 3.1. Flow chart for forward modeling (modified after Makhous and Galushkin, 2005).

3.3. Workstation

Completion of numerical simulation of BPSM needs processing a large volume of data, which take relatively a longer lime. Therefore, a workstation with a higher processing speed is necessary in BPSM to save time. Dell Precision Tower 7810 workstation with Intel Xenon quad core processor and 8 GB random access memory (RAM) was used in this study (Fig. 3.2).

Fig. 3.2. Dell Precision Tower 7810 workstation.

3.4. Data required for modeling

Basin and petroleum system modeling requires a various input data, including the distribution of lithology, rock physical properties and their relation with burial depths and boundary conditions. Most sensitive rock physical properties in modeling include porosity, permeability, thermal conductivity and heat capacity. The boundary conditions include present and paleo heat flows, ocean bottom temperature and depositional water depths and sea levels. In addition, tectonic history of the basin, which gives rise to unconformities (erosional thickness), and faults, source character (TOC & kerogen type), kinetic model for hydrocarbon generation, condition of hydrocarbon expulsion and migration has to be entered as data.

3.5. RESULTS AND DISCUSSION

3.5.1. Simulation condition

3.5.1.1. Lithology distribution

Distribution of lithology means spatial distribution of potential reservoirs, seals and source rocks. Seismic attributes, well stratigraphy, and regional geology were used to determine the lithological distribution along the X-X' section (Fig.3.3), which is a part of the SL-01-04 seismic line acquired by TGS as part of the 2001 seismic survey. The Pearl-1 and Dorado-North wells fall in this section. In addition a pseudo well named the pseudo Mannar Deep was assumed at the end of the X-X' section (Fig. 3.4). The time-depth relationship for depth conversion of the seismic profile was derived from the Pearl-1 well. As for the regional geology, well stratigraphy reported for adjacent basins such as the Indian sector of the Gulf of Mannar (eg. Rana *et al*., 2008; Rao *et al*., 2010), the Cauvery Basin (eg. Cantwell *et al*., 1978; Sastri *et al*., 1981; Chandra *et al*., 1991; Ramana *et al*., 1995) and the Late Jurassic sediments deposited in Tabbowa, Aadigama and Pallama grabens onshore Sri Lanka (eg. Wayland, 1920; Deraniyagala, 1939; Sitholey, 1942; 1944; Money and Cooray, 1966; Tantrigoda and Geekiyanage, 1991; Raveendrasinghe *et al*., 2013 were used. Determination of rock percentages from seismic data were based on seismic stratigraphy (eg. Vail *et al*., 1977), sequence stratigraphic principles (eg. Sloss, 1963; Mitchum 1977; Payton, 1977) and correlations between seismic facies to reflection attributes (eg. Stoker *et al*., 1997; Futalan *et al*. 2012; Zeng, 2013). Figure 3.4a shows the interpreted lithology distribution along the depth converted X-X' section. Seven horizons/ reflectors, sea floor and the tops of Neogene, Paleocene, Late Cretaceous, Early Cretaceous, Jurassic, and the basement, were interpreted (Fig. 3.4). Based on the tectonic history and stratigraphy described in chapter 1, the age of sediment immediately above the crystalline basement of the Mannar Basin was assumed to be around 174 Ma.

Figure 3.5 shows the recreated stratigraphic section in the SIGMA-2D software. Here, interpreted horizons were further divided into 27 formations, which together with 37 columns, divides the section into mosaic of cells (Fig. 3.5). The higher number of cells in the section the more accurate and realistic the accumulation modeling. Rock percentage of each formation in three stratigraphic columns (from sea floor to the basement) at Pearl-1, Dorado-North and pseudo Mannar-Deep well locations are listed in Table 3.1.

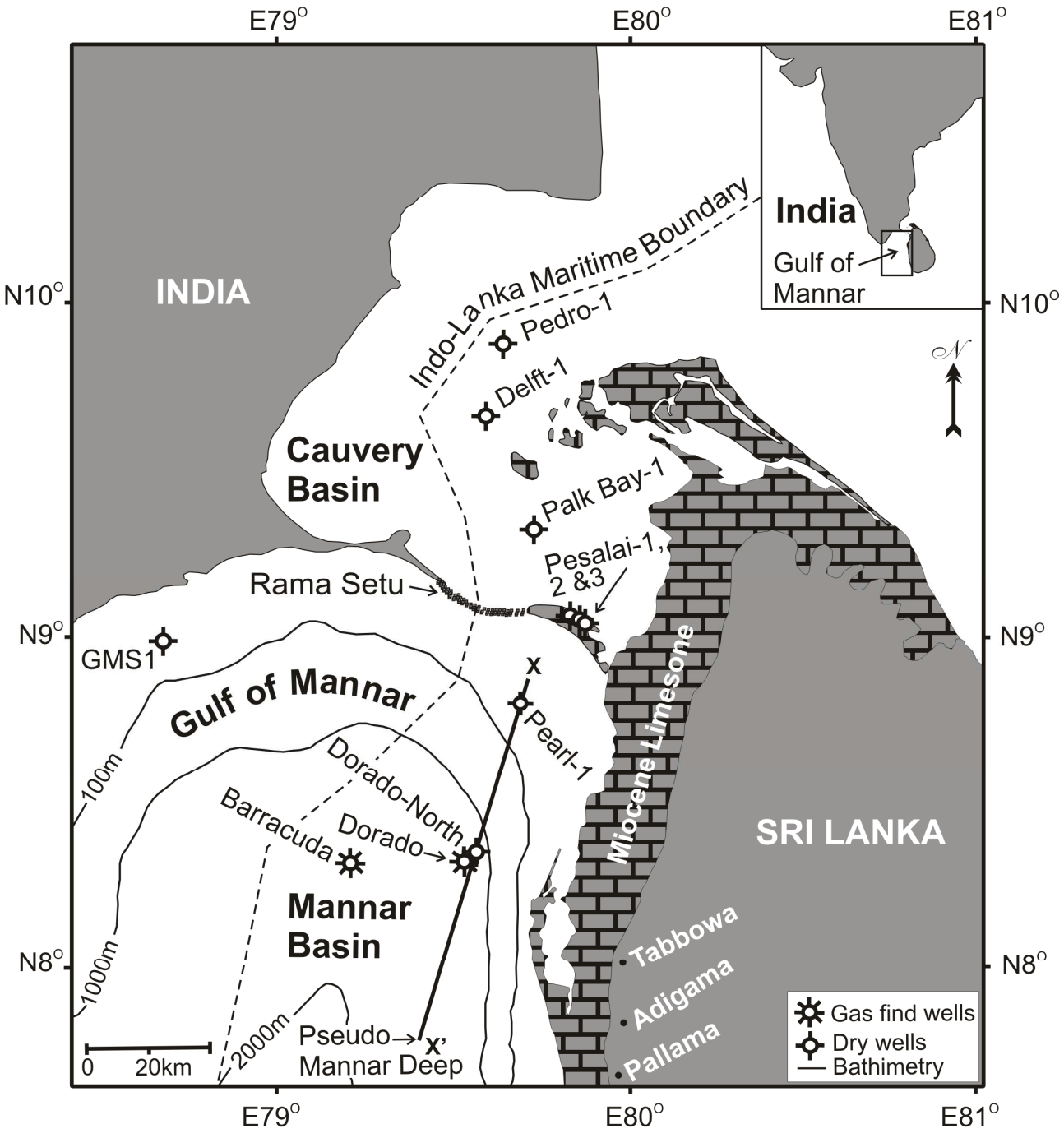

Fig. 3.3. Location of a part of SL-01-04 seismic line (X-X') in the northern part of the Mannar Basin.

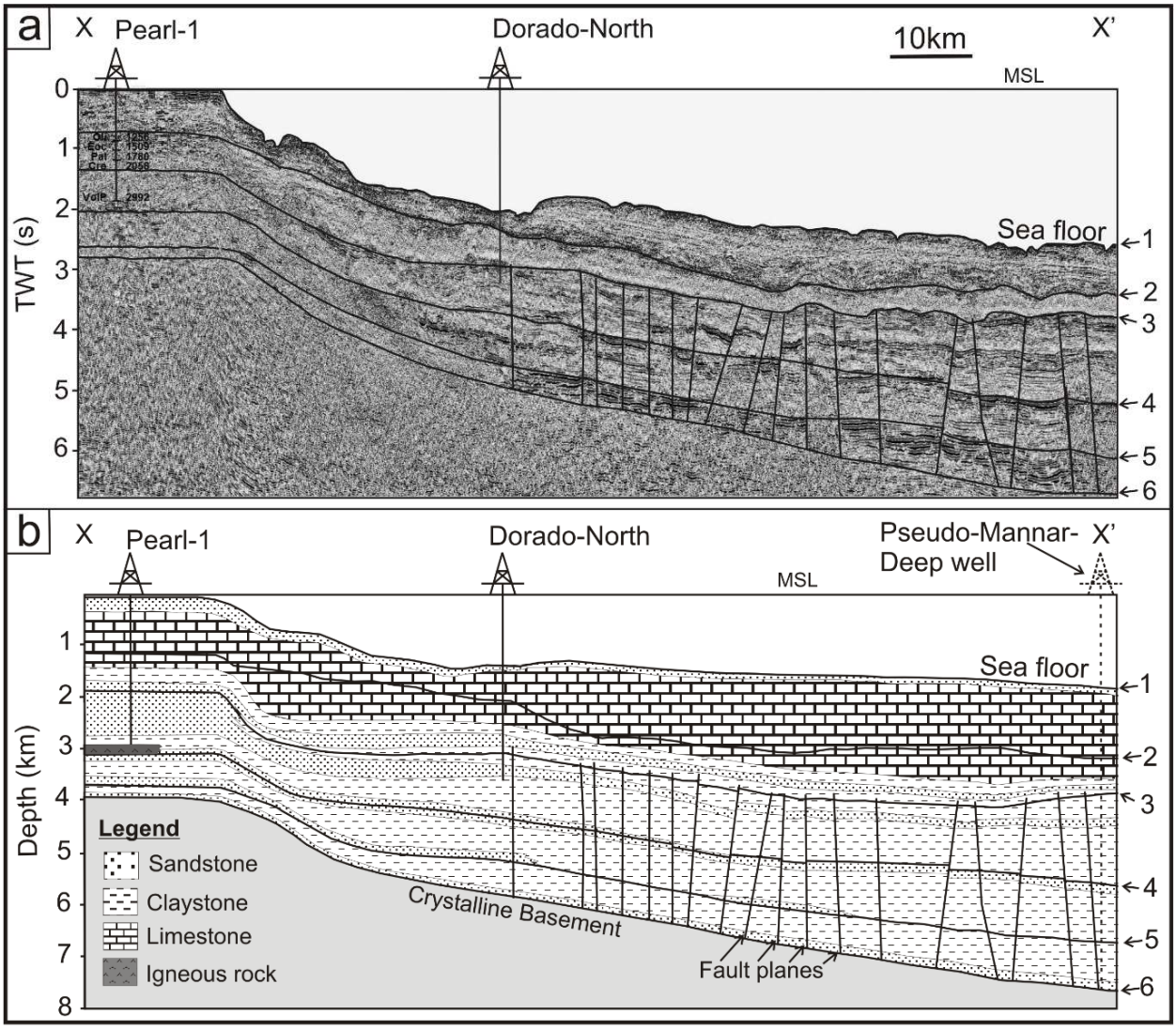

Fig.3.4. (A) The seismic profile across the northern part of the Mannar Basin. The location of the cross section is shown in figure 3.3. The depth is in two way travel time (TWT) in seconds. (B) Generalised lithology distribution interpreted along the X-X' section based on well data, regional geology and seismic attributes. Trajectories of the Pearl-1 and Dorado-North wells are also depicted. No. 1 indicates the sea floor reflector, while Nos. 2 to 6 indicate tops of the Paleogene, late Cretaceous, early Cretaceous, Jurassic and crystalline basement, respectively. MSL = mean sea level.

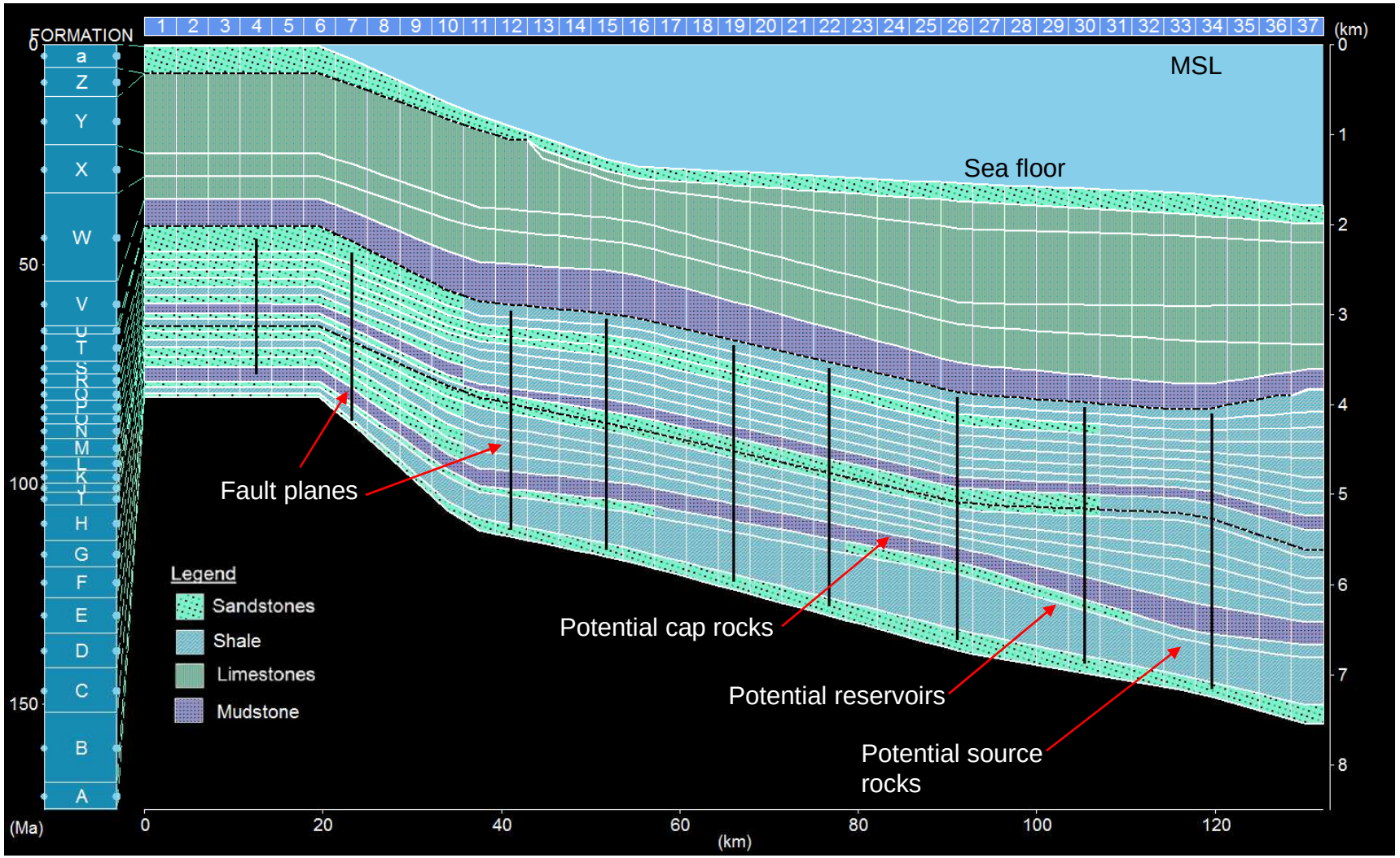

Fig. 3.5. Recreated stratigraphic section in SIGMA 2D modeling system. The figure shows different formations and relative positioning of source, reservoir and cap rocks.

Table 3.1. Lithologic compositions of wells used for calculation of present-day heat flows. Lithologic compositions of Pearl-1 and Dorado-North were derived from well reports and seismic data, and the lithologic composition of the pseudo Mannar-Deep well was entirely derived from well correlation and seismic data. The well locations are shown in Figs. 3.3. & 3.4. Depth is in meters (m) below sea floor. Water depths at the Pearl-1, Dorado-North, and pseudo Mannar-Deep well locations are 20, 1343, and 1800 m, respectively. SS = sandstone, CL = claystone, and LS = limestone.

Pearl-1				**Dorado-North**				**Pseudo-Mannar-Deep**			
Depth (m)	**SS (%)**	**CL (%)**	**LS (%)**	**Depth (m)**	**SS (%)**	**CL (%)**	**LS (%)**	**Depth (m)**	**SS (%)**	**CL (%)**	**LS (%)**
0 - 330	90	0	10	0 - 90	100			0-80	90	0	10
330 - 1070	0	0	100	90 - 720	0	0	100	80 - 1830	30	0	70
1070 - 1130	0	100	0	720 - 790	0	100	0	1830 - 2090	50	50	0
1130 - 1150	0	0	100	790 - 1140	0	0	100	2090 - 2430	0	100	0
1150 - 1310	0	100	0	1140 - 1250	15	80	5	2430 - 2840	15	70	15
1310 - 1400	0	0	100	1250 - 1290	90	5	5	3840 - 3954	100	0	0
1400 - 1670	0	100	0	1290 -1340	5	90	5	2610 - 2810	0	100	0
1670 - 1790	100	0	0	1340 -1630	70	30	0	2810 - 3120	15	70	15
1790 - 1880	0	0	100	1630 -1910	10	90	0	3120 - 3800	0	100	0
1880 - 1910	100	0	0	1910 - 2230	80	20	0	3800 - 4000	100	0	0
1910 - 1980	0	100	0	2230 - 2850	15	70	15	4000 - 4565	20	80	0
1980 - 2840	100	0	0	2850 - 2990	100	0	0	4565 - 4870	0	100	0
2840 - 2900	0	100	0	2990 - 3650	20	80	0	4870 - 5391	50	50	0
2900 - 2970	100	0	0	3650 - 3820	100	0	0	5391- 5565	100	0	0
2980 - 3000	0	100	0	3820 - 4090	50	50	0				
3000 - 3310	100	0	0	4090 - 4360	100	0	0				
3310 - 3420	0	100	0								
3420 - 3520	100	0	0								
3520 - 3660	0	100	0								
3660 - 3760	100	0	0								
3760 - 3840	0	100	0								
3840 - 4000	100	0	0								

3.5.1.2. Rock physical properties

Equations 1, 3, and 5 show the method used by the SIGMA-2D software to calculate the resultant porosity, thermal conductivity and permeability of a lithology mixture using the input data (Eqs. 2, 4 & 6).

$$\phi = \sum \phi_i a_i \quad (1)$$

$$\phi_i = \int (P_e) \quad (2)$$

Where; ϕ is the porosity of the lithology mixture, ϕ_i and a_i are the porosity and volume fraction of each rock type (e.g., sandstone, shale, limestone etc.), respectively. P_e is the effective pressure, which is the difference between the lithostatic and pore pressure. The software uses a geometric mean model to calculate the permeability and thermal conductivity of a lithologic mixture.

$$\lambda = \Pi \lambda_i^{a_i} \quad (3)$$

$$\lambda_i = \int (P_e, T) \quad (4)$$

where; λ is the thermal conductivity of the lithology mixture, λ_i and a_i are the thermal conductivity and volume fraction of each rock type, respectively. T = temperature.

$$k = \Pi k_i^{a_i} \quad (5)$$

$$k_i = \int (\phi_i) \quad (6)$$

Where; k is the permeability of the rock aggregate, k_i and a_i are the permeability and volume fraction of each rock type, respectively.

The software does not estimate the porosity versus effective pressure (Eq. 2), the thermal conductivity versus effective pressure and temperature (Eq. 4), permeability versus porosity (Eq. 6), or heat capacity versus temperature. These have to be input into the modeling system as data. The methods for selecting or deriving each of these relationships of rock physical properties are described below.

3.5.1.2.1. Porosity

Athy (1930) proposed a simple depth–porosity function (Eq. 7), which is based only on the surface (initial) porosity (ϕ_o) and a compaction parameter (c) of a particular sedimentary rock type. Athy's law (Athy, 1930) formulated with hydrostatic depth (Eq. 8),

which is described in detail by Hantschel and Kauerauf, (2009), was used to derive the porosity versus effective pressure relationship for sandstone, shale, and limestone used in this study. Sclater and Christie (1980) determined surface porosity (ϕ_o) and a compaction parameter (c) for sandstone, shale, and chalk in the North Sea Basin. Mannar and North Sea basins have more or less similar rift basin architecture. Therefore, the ϕ_o and c data derived by Sclater and Christie (1980) were used for this study. Figure 3.6 shows the porosity versus effective pressure derived for sandstone, shale and limestone used in this study.

$$\phi_z = \phi_o e^{-cz} \quad (7)$$

Where; ϕ_o = surface porosity, c = compaction parameter, z =depth

$$\sigma'_z(\phi) = (\Delta\rho g/c) - (\phi - \phi_o - \ln \phi/\phi_o) \quad (8)$$

where; $\sigma'_z(\phi)$ = effective pressure, $\Delta\rho$ = difference between rock matrix and pore fluid densities, g = acceleration due to gravity.

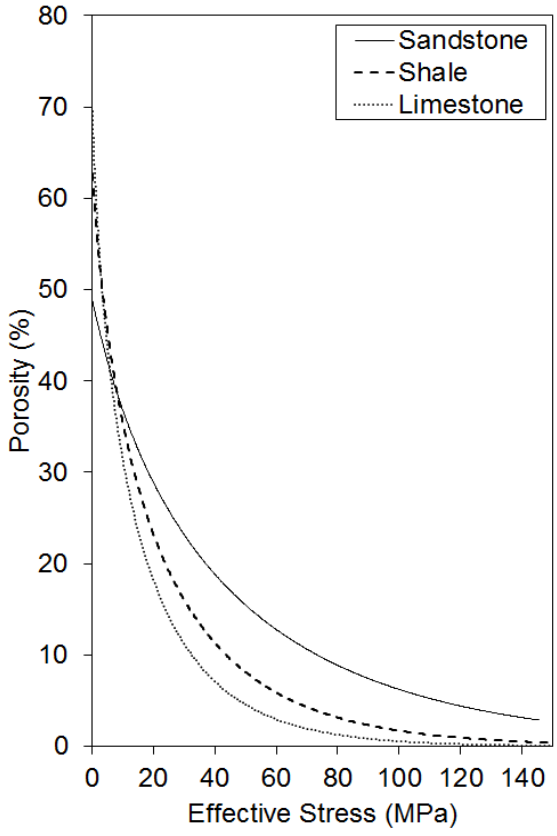

Fig. 3.6. Porosity versus effective pressure relationships for sandstone, shale, and limestone used for modeling. The surface porosity (ϕ_o) and compaction parameter (c) used for the derivation are: shale ϕ_o = 0.63; c = 0.051 km^{-1}, limestone ϕ_o = 0.7; c = 0.71 km^{-1} and sandstone ϕ_o = 0.49; c = 0.27 km^{-1} (after Sclater and Christie, 1980).

3.5.1.2.2. Permeability

Permeability is an important rock physical property in hydrocarbon migration and accumulation. It depends on interconnected pores or in other words the effective porosity. Potential hydrocarbon reservoirs (e.g. sandstones and limestones) should be porous and permeable for hydrocarbon accommodation. On the contrary, seals/ cap rocks (e.g., claystones, igneous rocks and anhydrites) should be impermeable to stop hydrocarbon being leaked out of the reservoir.

The most commonly used permeability relationship, the Kozeny-Carman relationship, was revised by Ungerer *et al*. (1990) for practical use in basin modeling (Hantschel and Kauerauf, 2009). However, the permeability determined by a more complex geometrical model deviates from that determined by the Kozeny-Carman formula (Doyen, 1988). Hantschel and Kauerauf (2009) reported porosity-permeability relationships for various lithologies derived by an alternative method, which result in piecewise linear functions of permeability in the log permeability versus porosity diagram. The permeability curves derived by Hantschel and Kauerauf (2009) generally agree with empirically derived porosity-permeability cross-plots for sandstones (e.g., Shenhav, 1971; Diederix, 1982; Wendt *et al*., 1986; Saner *et al*., 2006; Pellerin and Zinszner, 2007) and for carbonate rocks (e.g., Lucia, 1983; Turner, 1983; Pellerin and Zinszner, 2007; Lindgreen *et al*., 2012). Therefore, the permeability–porosity curves derived by Hantschel and Kauerauf (2009) for sandstone, limestones, and shale (Fig. 3.7) were used for this study.

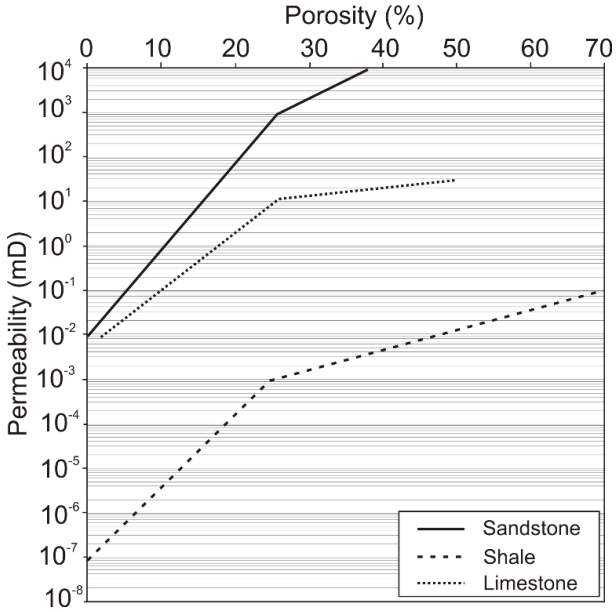

Fig. 3.7. Porosity versus permeability relationship for sandstone, shale and limestone (After Hantschel and Kauerauf, 2009).

3.5.1.2.3. Thermal conductivity

The thermal conductivity of rocks is dependent on temperature, porosity, composition, and properties of pore-filling fluids (Eppelbaum *et al*., 2014). Woodside and Messmer (1961) proposed a relationship (Eq. 9) to describe the dependency of the thermal conductivity of a monomineralic aggregate on its porosity and pore fluids (e.g., water). This relationship was used to determine the thermal conductivity versus porosity function of sandstone, shale, and limestone used in this study. Pores of all of these rock types were assumed to have been entirely filled with water. Based on mineralogical descriptions in unpublished reports on sandstones and limestones penetrated by wells drilled in the Cauvery and Mannar Basins, sandstones and limestones were assumed to be composed entirely of quartz and calcite, respectively. Horai (1971) reported the thermal conductivity of quartz, calcite, and water as 7.7, 3.6, and 0.6 W m^{-1} K^{-1}, respectively. Robertson (1988) discussed the changing thermal conductivity of shales with different scenarios of quartz fractions and solidities in detail. Accordingly, shale composed of 10% quartz and clay as the remainder has a thermal conductivity of 2.2 W m^{-1} K^{-1} at 100% solidity. Sekiguchi (1984) reported the thermal conductivity of shale to be 2.35 W m^{-1} K^{-1}, with the average value being 1.355 W m^{-1} K^{-1}, whereas Blackwell and Steele (1989) reported a value of 1.2 ± 0.1 W m^{-1} K^{-1}. Considering these observations, the matrix thermal conductivity of shale at 100% solidity was assumed to be 2.35 $Wm^{-1}K^{-1}$ in this study. Because, the thermal conductivity should be fed into the modeling system as a function of the effective pressure, the equation (Eq. 8) described earlier was used to convert porosity into corresponding effective pressure. Figure 3.8 shows the thermal conductivity versus effective pressure for sandstone, shale, and limestone calculated using this method.

Robertson (1988) discussed the temperature dependency of the thermal conductivity of rocks and rock forming minerals in detail. Lee and Deming (1998) evaluated the accuracy of methods proposed by Sekiguchi (1984), Chapman *et al*. (1984), Somerton (1992), Sass, *et al*. (1992), and Funnell *et al*. (1996) for temperature correction of the thermal conductivity of rocks and minerals. The dataset used by Lee and Deming (1998) included the thermal conductivity of minerals and igneous, metamorphic and sedimentary rocks at temperatures ranging from 0–500 °C. Based on accuracies benchmarked against the full dataset, Lee and Deming (1998) inferred that the method (Eq. 10) proposed by Sekiguchi (1984) gave the lowest mean absolute relative error. Therefore, the formula proposed by Sekiguchi (1984)

was used for temperature correction of the thermal conductivities of the three rock types. The thermal conductivities of rocks under effective pressures of 0, 20, 40, 60, 100 and 200 MPa and at 20 °C were used to generate a dataset for the temperature dependency of the thermal conductivity for sandstone, shale, and limestone at 0, 50, 100, 200, 300 and 500 °C (Table 3.2). However, maturity indicators suggest that even the deepest sediments in the Mannar Basin may not have reached 500 °C for any length of time.

$$\lambda_s = \lambda_w^{\phi}\, \lambda_g^{(1-\phi)} \qquad (9)$$

Where; λ_s , λ_w and λ_g are the thermal conductivities of mineral aggregate saturated with pore fluid, water, and mineral, respectively. ϕ = porosity of mineral aggregate.

$$\lambda_{(T)} = \lambda_m + \{(T_o T_m/T_m - T_o) * (\lambda_o - \lambda_m) * (1/T - 1/T_m)\} \qquad (10)$$

where; λ_o,= thermal conductivity in $Wm^{-1}K^{-1}$ at ambient conditions, T = temperature in Kelvin. Sekiguchi (1984) reported such that λ_m = 1.8418 and T_m= 1473 K.

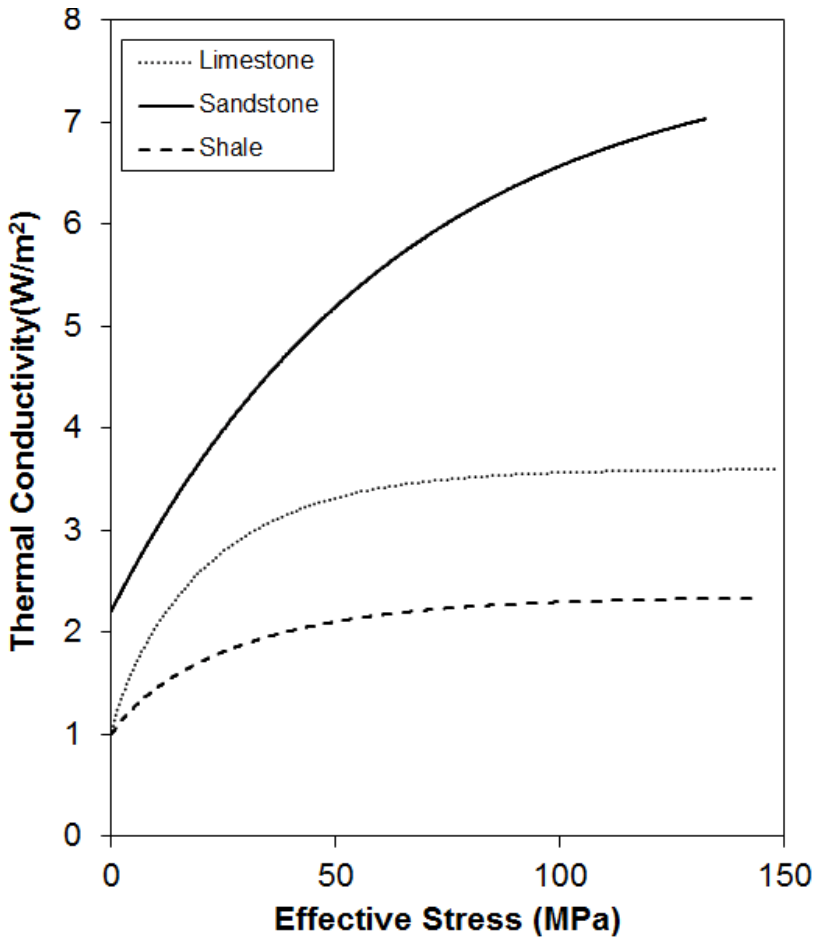

Fig. 3.8. Effective stress versus thermal conductivity for sandstone, shale and limestone.

Table 3.2. Temperature dependency of the thermal conductivity of sandstone, limestone, and shale for six different effective pressure conditions. Temp. = temperature.

Sandstone

Temp.	Thermal conductivity (W m^{-1} K^{-1}) at different effective stresses					
(^{o}C)	0 MPa	20 MPa	40 MPa	60 MPa	100 MPa	200 MPa
0	2.29	3.87	5.03	5.89	7	8.17
50	2.11	3.45	4.42	5.13	6.03	6.97
100	1.97	3.13	3.96	4.56	5.31	6.09
200	1.76	2.68	3.31	3.76	4.31	4.89
300	1.61	2.37	2.87	3.23	3.66	4.8
500	1.4	1.96	2.31	2.56	2.85	3.14

Limestone

Temp.	Thermal conductivity (W m^{-1} K^{-1}) at different effective stresses					
(^{o}C)	0 MPa	20 MPa	40 MPa	60 MPa	100 MPa	200 MPa
0	1.05	2.69	3.3	3.56	3.72	3.76
50	1.02	2.48	3	3.23	3.36	3.4
100	0.99	2.32	2.78	2.98	3.1	3.13
200	0.96	2.09	2.48	2.64	2.74	2.76
300	0.93	1.95	2.28	2.42	2.51	2.76
500	0.9	1.76	2.04	2.15	2.22	2.24

Shale

Temp.	Thermal conductivity (W m^{-1} K^{-1}) at different effective stresses					
(^{o}C)	0 MPa	20 MPa	40 MPa	60 MPa	100 MPa	200 MPa
0	1.01	1.74	2.05	2.21	2.34	2.4
50	0.99	1.68	1.97	2.12	2.24	2.29
100	0.98	1.64	1.91	2.02	2.17	2.21
200	0.96	1.58	1.83	1.96	2.06	2.11
300	0.95	1.54	1.78	1.9	2	2.16
500	0.93	1.49	1.71	1.82	1.92	1.96

3.5.1.2.4. Heat capacity

Robertson (1988) reported the average heat capacities of sandstone, limestone, and shale at 0 °C to be 0.93, 1.0 and 0.77 $mJkg^{-1}K^{-1}$, respectively, whereas Proselkov (1975) reported 0.84, 0.851, 0.795 $mJkg^{-1}K^{-1}$, respectively, for sandstone, limestone, and clayey siltstone in the Romashkino oil field in Russia. Based on laboratory measurements, Somerton (1992) reported the temperature dependency of the heat capacities of sedimentary rocks within a temperature range of 25–527 °C. Table 3.3 summarises the heat capacities of sandstone, limestone, and shale at 25, 50, 100, 200, 300, 400 and 500 °C, as reported by Somerton (1992). The observed and measured heat capacities for each rock type mentioned above seem to be roughly similar. Therefore, temperature corrections for the heat capacity of sandstone, limestone, and shale as reported by Somerton (1992) may be reasonably valid for similar lithologies in the Mannar Basin.

Table 3.3. Temperature dependence of heat capacity of sedimentary rocks (After Somerton, 1992)

Rock	Heat Capacity (in KJ kg^{-1} $^oC^{-1}$) at different temperatures						
Type	**25°C**	**50°C**	**100°C**	**200°C**	**300°C**	**400°C**	**500°C**
Sandstone	0.82	0.85	0.925	1.2	1.09	1.13	1.16
Shale	0.79	0.82	0.88	1	1.08	1.14	1.18
Limestone	0.84	0.86	0.93	1	1.06	1.12	1.18

3.5.1.3. Tectonic history

Upliftment, subduction, and rifting are the primary processes during the tectonic history of a rift basin. As described earlier, the Mannar Basin is a rift basin, which shows a rift structure in seismic profiles. The termination of the majority of faults in the basin at the top of the Late Cretaceous (Fig. 3.4a) indicates the cessation of rifting at the end of the Cretaceous period, around 66 Ma. The beginning of rifting in the Mannar Basin is thought to be associated with the onset of separation of Antarctica from India around 130 Ma (Lal *et al*., 2009). Based on these observations, fault plane trajectories were plotted from the basement to the top of the Late Cretaceous in the stratigraphic section used for modeling (Fig. 3.4).

Unconformities suggest upliftment, lower sea levels, or sediment starvation. Unconformities were assumed to indicate upliftment in the present study (Fig. 3.4a). Seismic profiles indicate the absence of major unconformities in the Mannar Basin. However,

biostratigraphic data from the Pearl-1 well indicate several unconformities (Fig. 1.4A). Among them, the Cretaceous–Palaeogene (K-Pg) boundary shows a significant hiatus (~3 Ma). The K–Pg is a regional hiatus observed on the Indian side of the Gulf of Mannar Basin (e.g., Rao *et al*., 2010), in the Cauvery Basin (e.g., Cantwell *et al*., 1978; Sastri *et al*., 1981), and in the Krishna-Godavari Basin in India (Raju *et al*., 1994). However, biostratigraphic data from the wells drilled in deep water depths in 2011 do not clearly indicate the presence of a significant hiatus at the K–Pg boundary. The presence of a hiatus at the top of the Albian was reported in shallow water depths on the Indian side of the Gulf of Mannar (e.g., Rao *et al*., 2010) and in the Cauvery Basin (e.g., Cantwell *et al*., 1978; Sastri *et al*., 1981). Baillie *et al*. (2003) reported that the Albian and K–Pg hiatuses represent break up unconformities related to the separations of Antarctica and Madagascar, respectively, from India. However, Lower Cretaceous sediments have not been penetrated by wells in the Mannar Basin. Therefore, the presence of the Albian unconformity is uncertain, particularly in areas with deep water depths. Biostratigraphy data from the Pearl-1 well indicate a hiatus at the Palaeocene-Eocene boundary, which is also observed in the shallow waters on the Indian side (e.g., Rao *et al*., 2010). This could be a regional event related to upliftment associated with the collision of India with the Eurasian plate in the early Eocene (Torsvik *et al*., 2002). However, the occurrence of the early Eocene unconformity in the areas with a deep water depth in the Mannar Basin is uncertain.

Erosional thicknesses of the Albian, K-Pg, and Eocene unconformities were taken into account for modeling due to their possible regional presence. The erosional thickness of the K–Pg unconformity in shallow water areas was estimated to be approximately 100 m based on the sedimentation rate and the occurrence of the hiatus mainly during the Palaeocene. However, there are insufficient data to estimate the hiatus of the K–Pg unconformity in the deep water areas, as well as the Albian and early Eocene unconformities. Nevertheless, taking into account their regional presence and the rates of sedimentation close to each event, their erosional thicknesses were assumed to be 100 m each. Taking into account possible deep water depths in the early Eocene, it was assumed that the early Eocene unconformity was not present in areas with a deep water depth in the Mannar Basin. Nevertheless, the erosional thicknesses of these unconformities are relatively small and they may not have a significant impact on overall thermal and burial history.

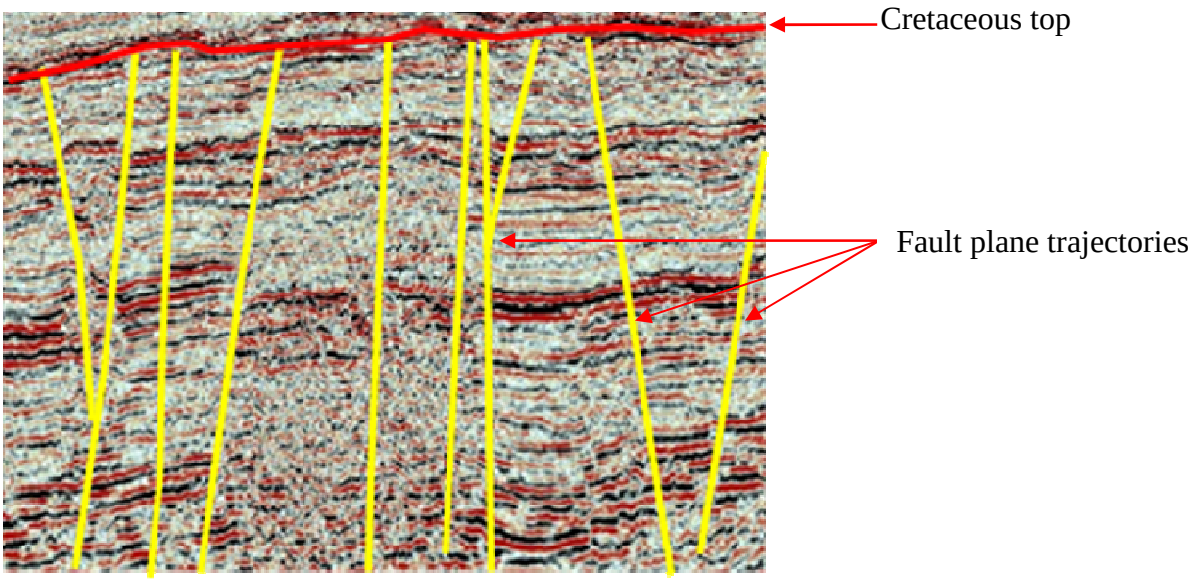

Fig. 3.9. Faults terminating at the top of the Cretaceous. Seismic profile is a part of SL-01-04 seismic line acquired in 2001 by TGS.

3.5.1.4. Surface/ ocean bottom temperature

Because heat flow depends on the surface and ocean bottom temperatures, it is an important physical parameter in the modeling of the heat flow history. The accuracy of the optimised heat flow history depends, among other factors, on the accuracy of the surface and ocean bottom temperatures. For an offshore basin such as the Mannar Basin, the ocean bottom temperature mainly depends on the water depth. Due to the thermocline, the ocean bottom temperature decreases rapidly below around 500 m water depth. In tropical waters, the ocean bottom temperature reaches as low as 5 °C at around 1000 m depth. In addition, the surface temperature and the ocean bottom temperature at relatively shallow water depths (< 500 m) are controlled by palaeolatitudinal position and global climatic trends such as the Palaeocene-Eocene thermal maximum (PETM).

The present-day ocean bottom temperature (OBT) in the shallow water areas of the Mannar Basin is around 26 °C. Taking into account more than 1000 m of water depth, the OBT in the areas with a deep water depth was assumed to be 5 °C. Past OBT can be determined from biostratigraphic data. According to Zakharov *et al.* (2009), the palaeotemperature of the southern Indian near-bottom shelf waters during the early Maastrichtian was around 21.2 °C, and temperatures during the Late Albian for the Cauvery Basin were in the range of 14.9–18.5 °C. The rifting had not yet started or had just begun in

the Albian (e.g., Lal *et al*., 2009). In addition, the eustatic sea level from the late Jurassic to Albian was comparatively low (e.g., Pitman, 1978; Fig. 3.11). The water depth in the Mannar Basin prior to the Albian, therefore, was likely to have been much less than at present. Based on these factors, the annual average surface temperatures during the Late Jurassic to Albian were assumed to be 17 °C. Due to the subsidence related to rifting and subsequent thermal sag phase and lithospheric flexure related to sediment load, the areas with a deep water depth in the northern Mannar Basin were assumed to have maintained more than 1000 m water depth from the middle Oligocene to present. Therefore, the ocean bottom temperatures in the areas with a deep water depth in the Mannar Basin are thought to have been around 5 °C in the latter part of the Palaeogene and in the Neogene. The latitudinal shift of the Mannar Basin from 16°S in the Cretaceous to its present location of 8°N (Cantwell *et al*., 1978; Fig. 1.3) and PETM were taken into account for the OBT estimation. The average OBTs assumed in the present study are shown in figure 3.10. The actual OBT in the Mannar Basin, especially in the shallow water areas, is much more complex than that shown in Fig. 10. OBT fluctuations due to the relatively short sea level cycles (e.g., Vail *et al*., 1977) and due to climatic changes such as glacial and interglacial periods were not taken into account in the present study.

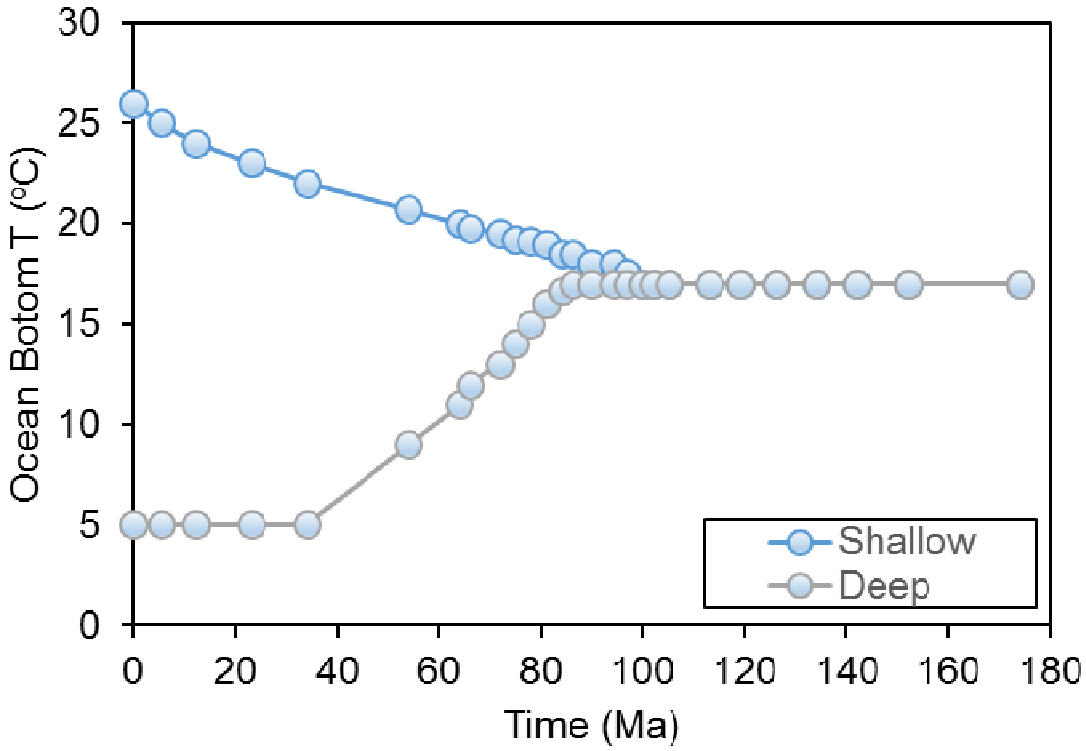

Fig. 3.10. Change in the ocean bottom temperatures in the Mannar Basin. "Deep" and "Shallow" in the legend stands for shallow (< 200 m) and deep (> 1000 m) water depths. T = Temperature

3.5.1.5. Sea level change

Based on sequence stratigraphic principle, different eustatic sea level curves have been suggested by Vail *et al*. (1977); Pitman (1978); Watts & Steckler (1979). Sea level curves by Vail *et al*. (1977) and Pitman, (1978) roughly agree. However, sea level changes reported by Watts & Steckler (1979) are abnormally low compared that by Vail *et al.* (1977) and Pitman, (1978). Sea level curve by Vail *et al*. (1977) is more detailed and include even relatively short-term cycles, which was difficult to take into account in modeling. In contrast, sea level change proposed by Pitman (1978) is more smooth (Fig. 3.11) and therefore used in this study.

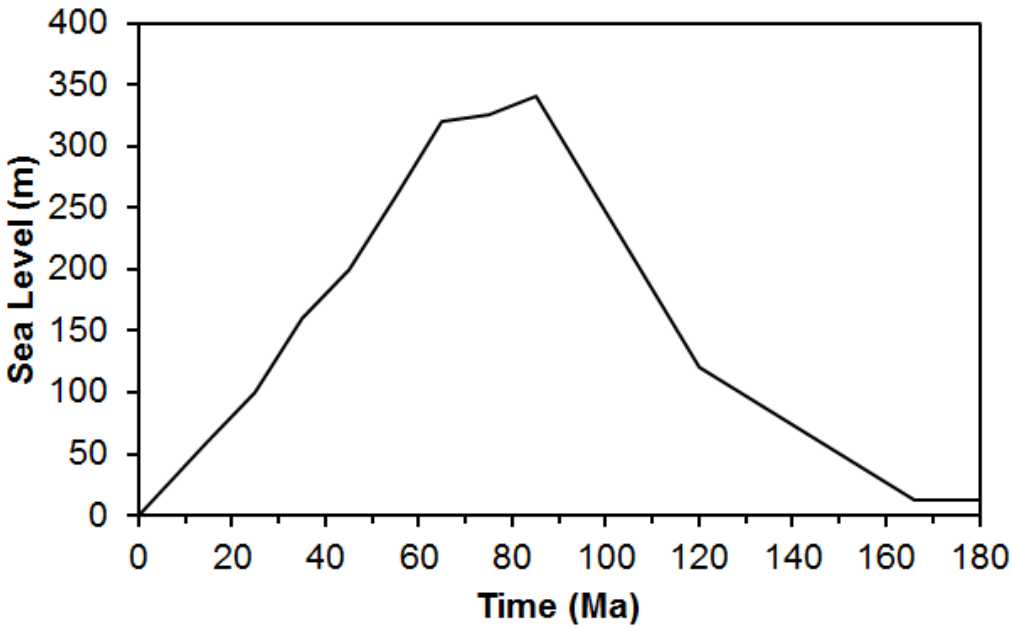

Fig. 3.11. Sea level change proposed by Pitman (1978).

3.5.1.6. Palaeo-depositional water depths

Palaeo bathymetry data for Pearl-1 well (Table. 3.4) in unpublished well completion report held at PRDS were used to estimate depositional water depths of sediments in shallow water depths in the Mannar Basin. The depositional water depths of sediments in deep water areas in the Mannar Basin were determined based on present day water depths and paleo sea levels proposed by Pitman (1978; Fig. 3.11).

Table 3.4. Palaeo depositional water depths at the Pearl-1 well location, estimated based on the biostratigrphic data from the Pearl-1 well.

Stratigraphic section	Depositional environment	Water depth (m)
Pleistocene to Recent	inner sub littoral environment	200
Late Miocene	inner sub littoral environment	200
Early Miocene	outer sub littoral environment	400
Late Oligocene	Upper bathyal	500
Early Oligocene	upper middle bathyal	600
Middle to Late Eocene	upper middle bathyal	600
Middle Eocene	upper middle bathyal	600
Early Eocene	Upper bathyal	500
Middle to Late Paleocene	outer sub littoral / upper bathyal	400
Late Cretaceous	Sub littoral/ upper bathyal	400

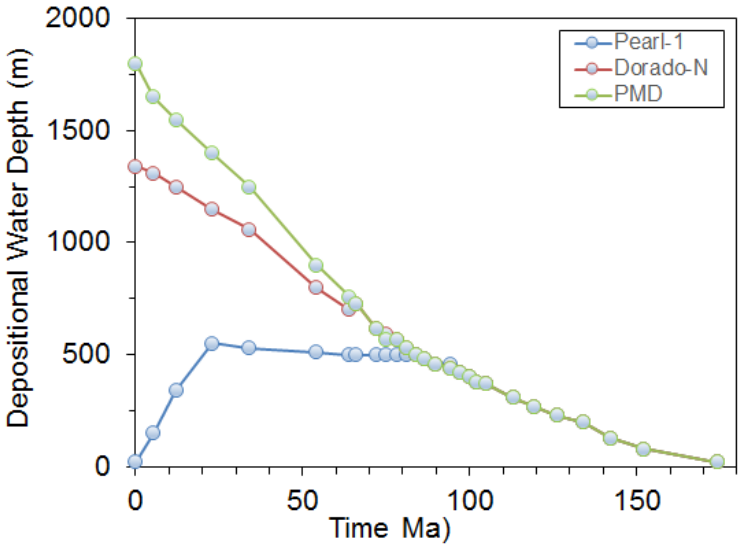

Fig. 3.12. Paleo depositional water depths assumed in the study for Pearl-1, Dorado-North, and Pseudo Mananr-Deep (PMD) well locations (see Fig 3.3. for well locations).

3.5.1.7. Optimization of heat flow

3.5.1.7.1. Optimization of present day heat flow

Bottom hole temperatures (BHT) at the depths of 1468 m and 2980 m in the Pearl-1 well were measured to be 64.4 °C and 98.3 °C, respectively. Assuming the OBT at the Pearl-1 well to be around 26 °C, the geothermal gradient (GTG) in the shallow water area of the Mannar Basin was determined to be 24.4 °C/km, and the GTG in the deep water area was tentatively assumed to be the same. Taking into account the deep water depths (> 1000 m),

the OBT at the Dorado-North well location was assumed to be 5 °C. Different present-day heat flow scenarios were applied to obtain the best fit for computed and observed GTG at the Pearl-1 and Dorado-North well locations (Figs. 3.13 & 3.14). The present-day heat flows at the Pearl-1 and Dorado-North locations were optimised at 39.8 and 33.5 mW/m^2, respectively.

The average surface heat flow in the Indian Ocean is 83.3 mW/m^2 (Sclater *et al*., 1980). The heat flow map of India (Shanker, 1988; Shanker *et al*., 2012) shows that the surface heat flow in the south and southwestern offshore areas of India is variable, ranging from 40 to 70 mW/m^2, and is also variable in the eastern and southeastern offshore areas, ranging from 40 to 100 mW/m^2. Compared to the available heat flow data, the Sri Lankan continental shelf seems to have relatively lower present-day heat flows.

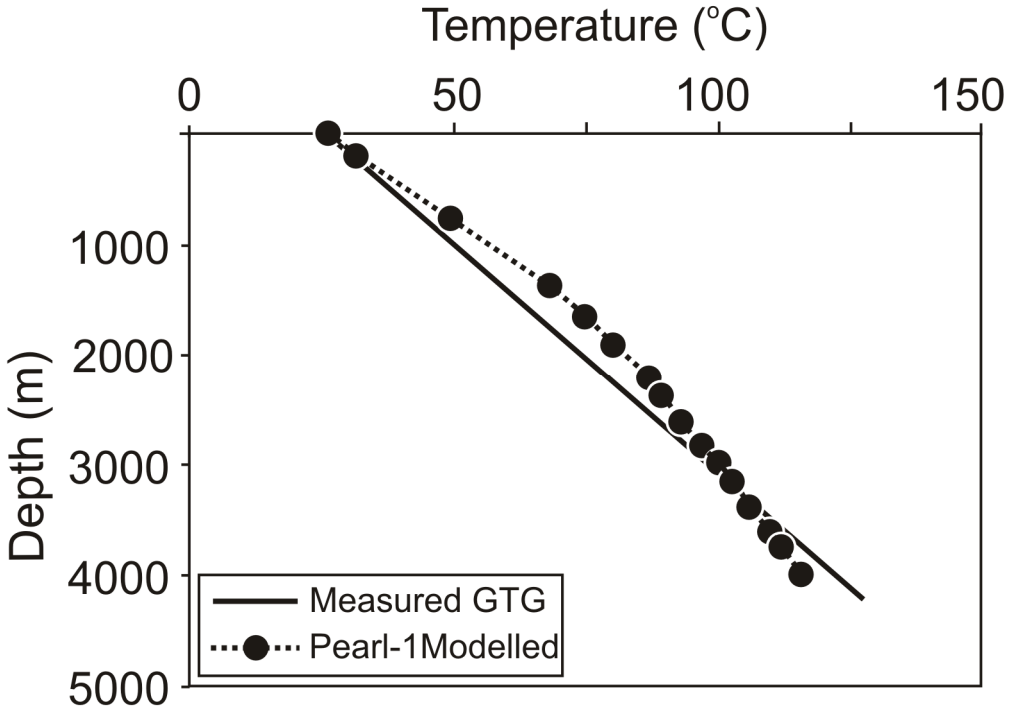

Fig. 3.13. Modeled geothermal gradient (GTG) for a stratigraphic column at the Pearl-1 well location. GTG calculated based on the bottom hole temperature data from the Pearl-1 well is also plotted for comparison.

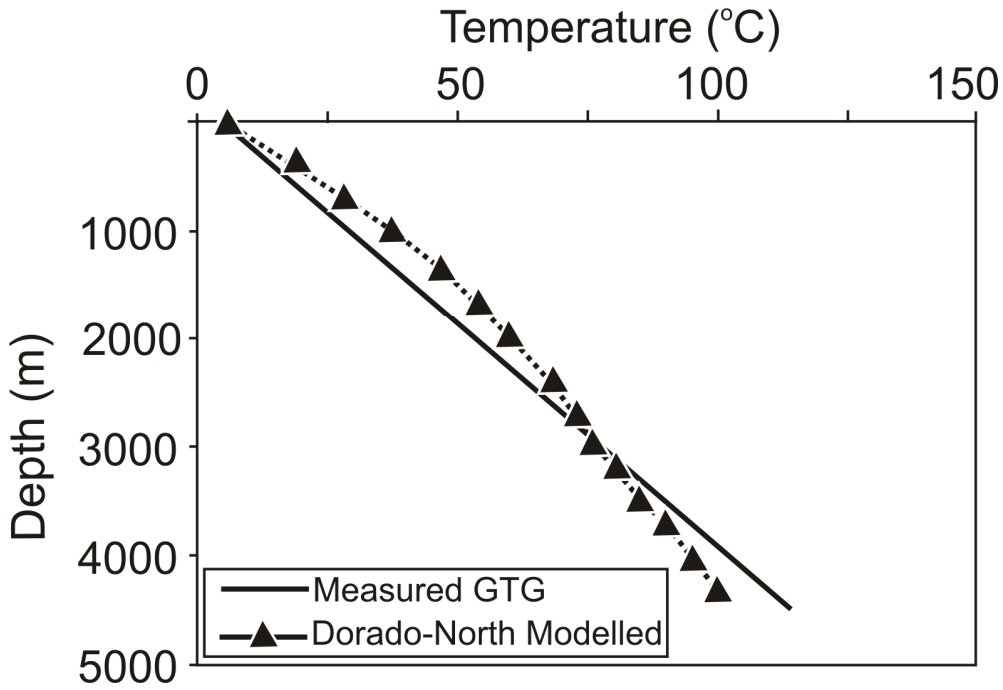

Fig. 3.14. Modeled geothermal gradient (GTG) for the Dorado-North well. Measured GTG is based on the bottom hole temperature (BHT) data from the Pearl-1 well. It was assumed that GTG in the Pearl-1 and Dorado-North wells are roughly similar.

3.5.1.7.2. Optimization of heat flow history

The Mannar Basin has a complex heat flow history due to multiple heating episodes related to lava flows, igneous intrusions, the juxtaposition of the Marion and Reunion hotspots (hotspot location: Fig. 1.3), and crustal thinning during rifting. Except for the heat increases during rifting, the impact of other heating events is relatively transient. According to Parsons and Sclater (1977), the heat flow of a rift basin increases during the syn-rift period, but decreases exponentially during the post-rift period after peaking at the end of rifting. The rate of increase of the heat flow during the syn-rift period is thought to be due to the upwelling of the asthenosphere with crustal extension. The decrease in the heat flow after rifting ceases, is due to crustal thickening resulting from solidification of the upwelled molten lava. McKenzie (1978) proposed a relationship to quantify the heat flow history of a rift basin (the McKenzie model). For calculation purposes McKenzie (1978) assumed instantaneous rifting, which is valid for rift basins with a < 20 Myr rifting period (Waples, 2001). However, the tectonic history described earlier suggests that the rifting period of the Mannar Basin was around 50 Ma. In addition, Baillie *et al.* (2003) suggested that the Mannar Basin underwent at

least two phases of rifting due to multiphase break up of Gondwana supercontinent. The McKenzie model, therefore, may not be directly applicable to quantify the heat flow history of the Mannar Basin. However, the typical pattern of heat flow change in a rift basin suggested by Parsons and Sclater (1977) and McKenzie (1978) is applicable for optimisation of the heat flow history of the Mannar Basin.

Seismic data suggest that the syn-rift period of the Mannar Basin has terminated at the end of the Cretaceous period. The palaeo-heat flow, therefore, was assumed to be the highest at the end of the Cretaceous (~66 Ma). Keeping the estimated present-day heat flows fixed, different scenarios were examined for optimisation of the heat flow history of the Mannar Basin. This was accomplished when the depth distribution of computed VR roughly matched that of measured VR. The heat flow history for the Dorado-North well location was optimised against the measured VR data for the Dorado and Dorado-North wells. However, the measured VR data for the Pearl-1 well in the shallow water depths are not available. The measured VR data from the Pesalai-1 & 2 wells reported by Cantwell *et al.* (1978) were used for optimisation of the heat flow history in the shallow water depths. These two wells are located in the Cauvery Basin close to the shallow water area on the northern boundary of the Mannar Basin (Fig. 3.3). The measured VR data for the Pesalai-1 & 2, Dorado, Dorado-North, and Barracuda wells were plotted in a linear trend on a log VR versus the depth diagram (Fig. 3.15 & 3.16). The pre-rift heat flow in the Gulf of Mannar Basin is poorly understood. As previously discussed, continental separation occurred simultaneously with or post-dated the onset of the separation of Antarctica from India, which is suggested to have occurred at around 130 Ma (Lal *et al*., 2009). Different scenarios for the timing of the onset of rifting such as 130, 120, and 113 Ma, and different scenarios for the pre-rift heat flow were examined in association with the optimisation of heat flow history.

The best fit of the computed and measured VR (Fig. 3.15 & 3.16) for the Pearl-1 and Dorado-North locations were achieved when the optimised heat flow history for each location was as shown in Fig. 3.18. At the end of the rifting period around 66 Ma, the maximum heat flows in the stratigraphic section at the Pearl-1 and Dorado-North locations were 68.2 and 71 mW/m^2, respectively. The increasing rate of heat flow in the Mannar Basin began at around 113 Ma, and the pre-rift heat flow was 50.2 mW/m^2. The heat flow in the Mannar Basin appears to have increased from the north of the basin towards the south.

The optimised heat flow history of the Mannar Basin follows the typical pattern of heat flow change in rift basins proposed by Parsons and Sclater (1977). It should be noted that the accuracy of the optimised heat flows in Fig. 3.18 depends on the accuracy of the assumed palaeo ocean bottom temperatures (Fig. 3.10) and the estimated thermal conductivity of the rocks. Relatively higher pre-rift heat flow in the Mannar Basin is due to the effect of the Marion hotspot, which was closer to Sri Lanka in Gondwana during the Early Cretaceous (e.g., Torsvik *et al*., 2002; Fig. 1.3). The heat flow during the pre-rift stage, however, does not seriously influence the maturity modeling. Palaeo-heat flows increasing from the north to the south of the Mannar Basin may be related to the extent of crustal extension during rifting of the Indo-Lanka landmasses. During rifting, Sri Lanka has rotated counter-clockwise direction, acting the northern part of the island as a pivot. Therefore, crustal extension toward the southern part of the Mannar Basin is expected to be greater than that toward the northern part of the basin. Similarly, the heat flow, which primarily increased due to crustal thinning, is also expected to be greater toward the south of the Mannar Basin.

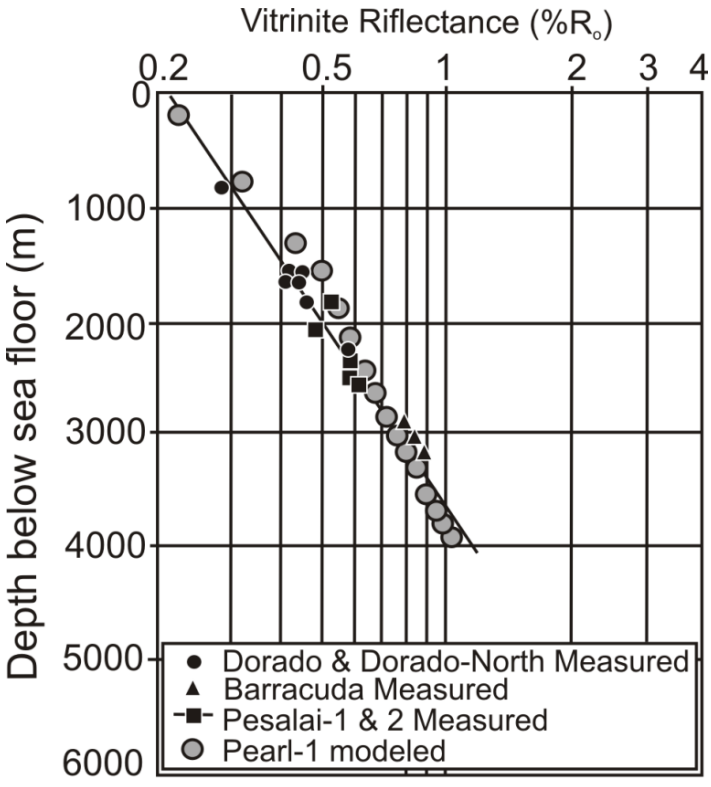

Fig. 3.15. The best fit of modelled and measured VR data for a stratigraphic column at the Pearl-1 well location. Since measured VR data is not available for the Pearl-1 well, optimisation was performed against the measured VR for the Pesalei-1 & 2 wells by Cantwell *et al.* (1978; Fig. 3.3). For comparison, VR data for the Dorado, Dorado north and Barracuda wells are also plotted.

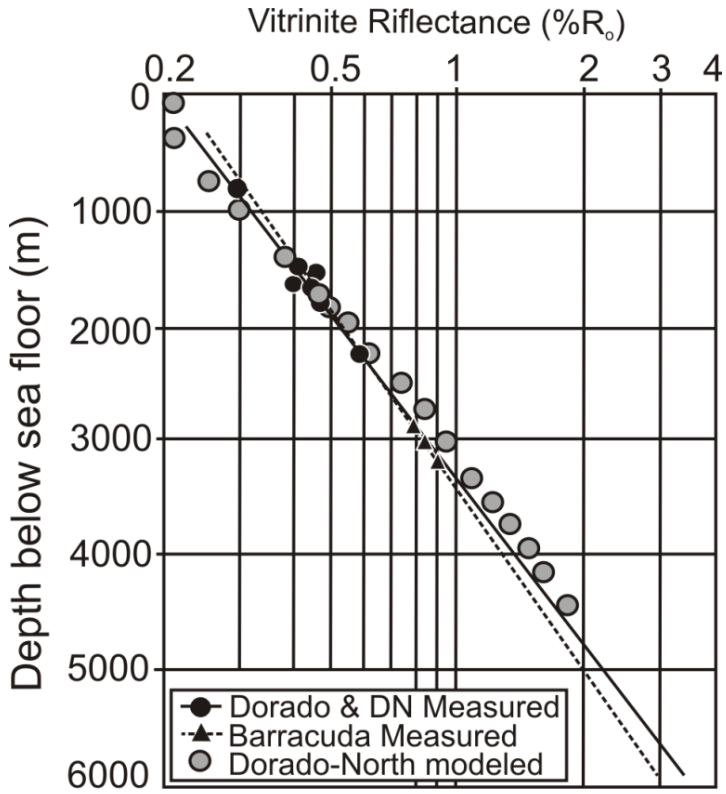

Fig. 3.16. The best fit of the modeled and measured VR data for a stratigraphic column at the Dorado-North well location. For comparison, VR data for the Dorado and Barracuda wells are also plotted.

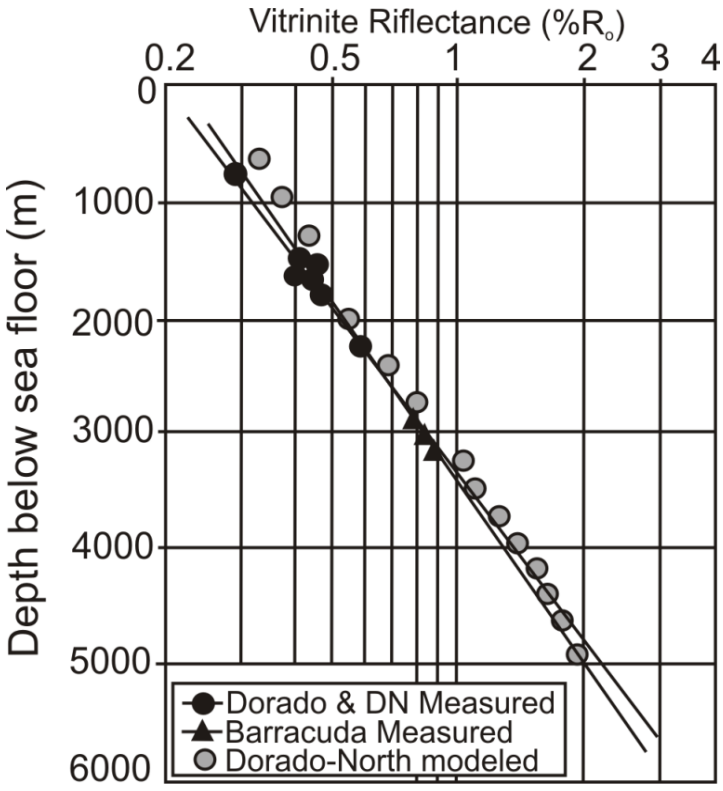

Fig. 3.17. Modeled VR data for the pseudo Mannar-Deep well. For comparison, VR data for the Dorado, Dorado-North and Barracuda wells are also plotted.

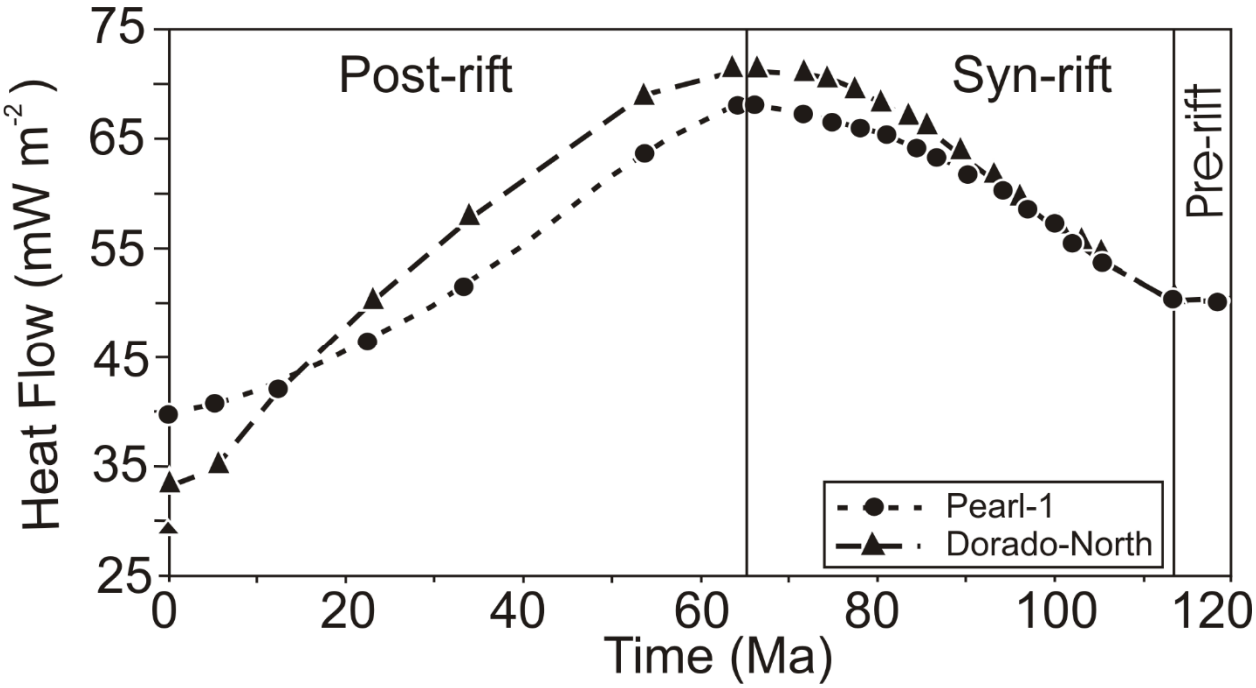

Fig. 3.18. Optimized heat flow history for stratigraphic columns at the Pearl-1 and Dorado-North well locations at different stages of basin development.

3.5.2. Burial and thermal history

The decompacted depth versus time relationships (burial history plot) for the complete stratigraphic section from the sea floor to the basement at the Pearl-1, Dorado-North, and pseudo Mannar-Deep well locations are shown in Figs. 3.19 to 3.21. These burial history plots are based on the assumption that the Mannar Basin had no major erosional episodes. Table 3.5 summarises the average rate of sedimentation at different time intervals during the development of the basin. The rate of sedimentation was calculated based on decompacted depths in the burial history plots. The data suggest a relatively higher rate of sedimentation in the Cenomanian and Turonian at the Dorado-North and pseudo Mannar-Deep well locations. A relatively higher rate of sedimentation in the Oligocene was observed in the Pearl-1 well compared with the Dorado-North and pseudo Mannar-Deep wells, showing that the rate of sedimentation in the Oligocene decreased from the north of the Mannar Basin to the south. The Dorado-North well showed a relatively lower rate of sedimentation in the Neogene than the Pearl-1 and pseudo Mannar-Deep wells. The rate of sedimentation the Mannar Basin has varied greatly throughout its geological history.

The absence of major erosional episodes in the Mannar Basin is due to either relatively smaller uplift or greater water depths. Sea levels were relatively high when the early Eocene, K-Pg, and Albian unconformities have been formed (see Fig. 3.11). The higher rate of sedimentation in the Dorado-North and pseudo Mannar-Deep wells during the Cenomanian and Turonian may be due to a high sediment supply from adjacent landmasses including India, Sri Lanka, and Madagascar (Fig. 1.3). Sediment supply decreased when India has separated from Madagascar and started moving northward. The separation of Madagascar is thought to have triggered a second phase of rifting between the Indo-Lanka landmasses (e.g., Baillie *et al*., 2003). Further rifting could have created more lateral accommodation space. This means that sediment dispersed over a wider area, resulting in a lower rate of sedimentation. The relatively higher rate of sedimentation during the Oligocene in the Pearl-1 well compared with the Dorado-North and the pseudo Mannar-Deep wells may be due to an ample supply of sediment from India, primarily terrigenous sediments generated by rapid erosion of the uplifting Himalayas. The low rate of sedimentation during the Neogene period in the Dorado-North well could be related to erosion or the non-deposition of sediments. The seismic data clearly show a relatively thin Neogene section in the vicinity of the Dorado-North well (Fig. 3.4a), which could be related to undersea currents. A larger lateral accommodation space and higher rate of subsidence due to greater crustal extension in the southern part of the Mannar Basin could account for the deep water depths in the Dorado-North and pseudo Mannar-Deep well locations. Decompacted depth versus time for the stratigraphy penetrated by the Conoco-15/30-1 well in the Central Graben of the North Sea was plotted by Allen and Allen (1990). The average rate of sedimentation calculated based on this burial history plot is around 0.041 mm/year from the Campanian to the present. This is roughly comparable with the rate of sedimentation observed in the Mannar Basin. The rate of sedimentation in the Surma Basin in Bangladesh, which is a sub basin of the Bengal Basin in northeast Bangladesh (Hossain, *et al*., 2014) mainly fed by sediments from the Himalayan orogeny, was calculated based on burial history plots reported by Ismail and Shamsuddin (1991). The average rate of sedimentation in this basin ranged from 0.18–0.4 mm/year during the Miocene. In comparison, the rate of sedimentation in the Mannar Basin is around 10 times lower.

Heat flow histories for the Pearl-1 and Dorado-North wells were applied to the burial histories in order to reconstruct the thermal history. The heat flow and OBT histories at the Dorado-North well were tentatively applied to the pseudo Mannar-Deep well in order to predict its thermal history. Dashed contour lines (isotherms) on the burial history diagrams in

Figures. 3.19 to 3.21 show the changes in the formation temperatures throughout the development of the basin. These isotherms indicate that GTG in the Mannar Basin was highest at the end of the Cretaceous. This is nearly consistent with the heat flow history in Figure 3.18; however, the isotherms at shallow burial depths (< 1000 m) are sub-parallel to the time axis of the burial history plot. Similar to the pattern of heat flow in the Mannar Basin, the maximum geothermal gradient for the Dorado-North and pseudo Mannar-Deep well locations in the deep water areas occurred at the end of syn-rift phase, around 66 Ma. However, the maximum geothermal gradient of the Pearl-1 well occurred around 35 Ma. The maximum temperatures recorded in the oldest sediments underlain by the basement in the Pearl-1, Dorado-North, and Mannar-Deep wells are 120, 180 and 220 °C, respectively. The low thermal conductivity of the sediments is responsible for sub-linear isotherms at the shallow burial depths. Sediments at shallow depths have a higher porosity because they are less compacted. A higher amount of pore water in sediment reduces its thermal conductivity. The maximum geothermal gradient in the Pearl-1 well around 34 Ma is related to the gradual increase of OBT with increasingly swallowing of the water depth from the Albian to the present. In contrast, the OBT in the deep water depths decreased from the Albian to the present due to increasing water depths (Fig. 3.12). The maximum temperatures from the Pearl-1 through the Dorado-North to the pseudo Mannar-Deep wells progressively increased primarily due to increase in stratigraphic thickness (Fig. 3.4b). In addition to crustal extension, radioactive elements in the basement rocks and in the sediments may have contributed to the overall heat flow history of the Mannar Basin. The thermal history of the Mannar Basin could have been temporarily perturbed by lava flows during the Maastrichtian. Based on depositional water depths (Fig. 3.12), the basin was submerged under seawater for most of the Maastrichtian. The heat given off by lava may not have significantly affected the overall thermal history of the Mannar Basin. The timing of the lava flows coincides with the timing of the maximum heat flow in the Mannar Basin (around 66 Ma), but the possible influence of the lava flows on the heat flow would be minimal or insignificant. The pattern of heat flow is of utmost importance in petroleum system modeling because it governs the timing of hydrocarbon generation and expulsion.

Table 3.5. Temporal variation of the sedimentation rate at the Pearl-1, Dorado-North, and pseudo Mannar-Deep (PMD) well locations.

Time (Ma)	Rate of sedimentation (mm/year)		
	Pearl-1	Dorado-N	PMD
0 - 23	0.051	0.027	0.054
20 - 34	0.056	0.035	0.024
40 - 66	0.031	0.037	0.041
80 - 90	0.044	0.084	0.072

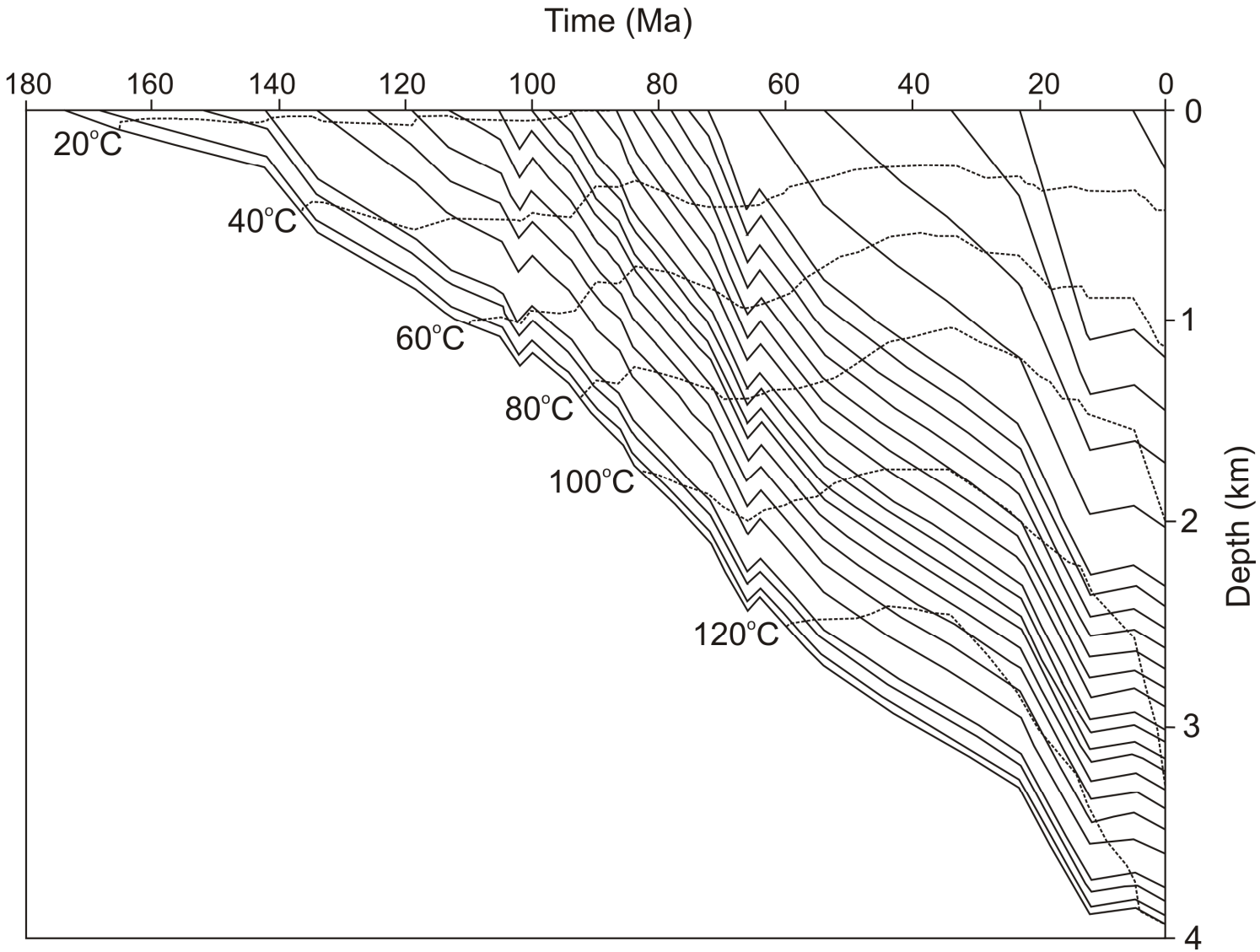

Fig. 3.19. Burial history plot for the stratigraphic column at the Pearl-1 well location. The depth is in meters below sea floor. Dashed contours indicate the changing formation temperatures with geological time.

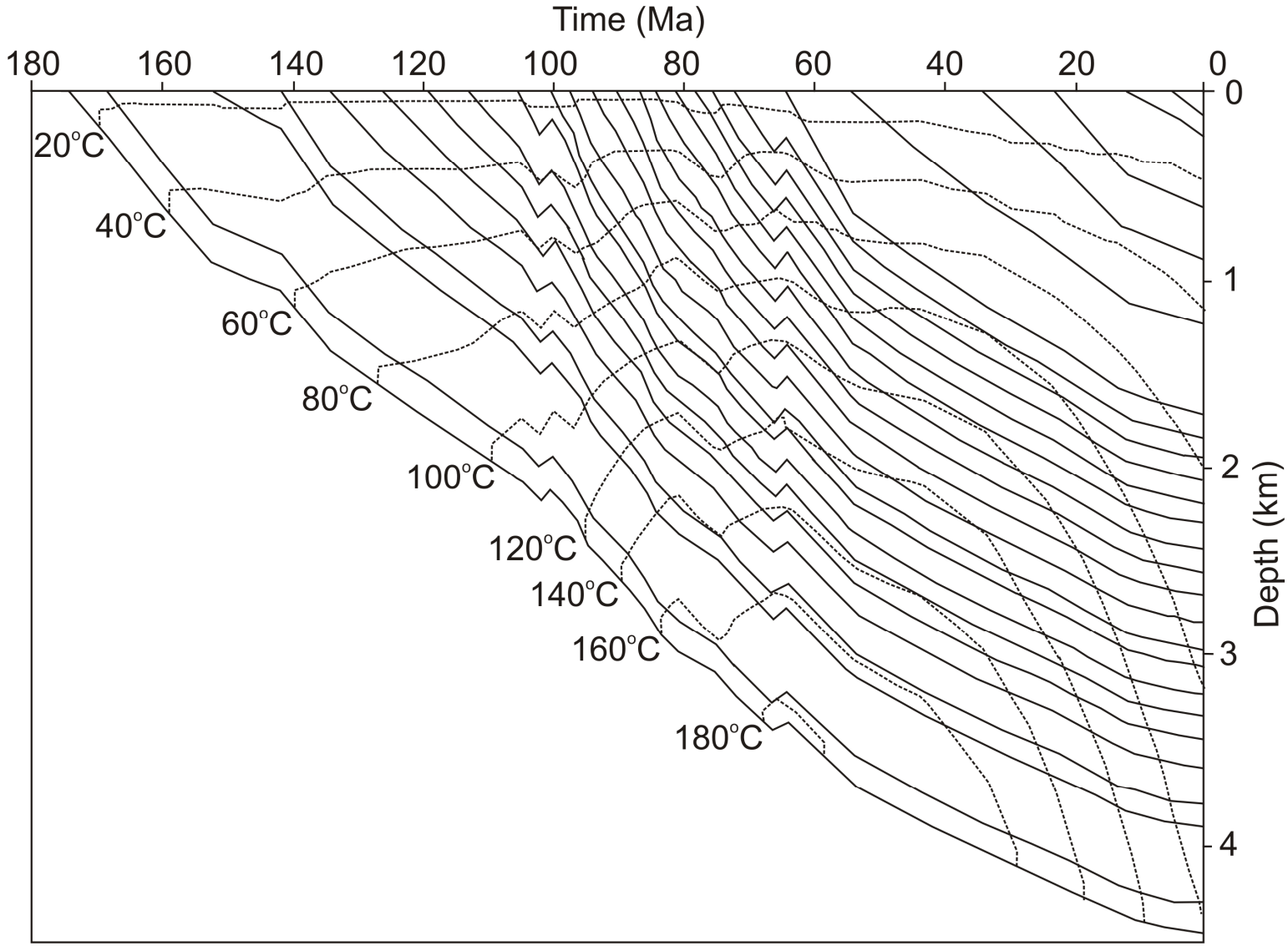

Fig. 3.20. Burial history plot for stratigraphic column at the Dorado-North well location. The depth is in meters below sea floor. Dashed contours indicate the changing formation temperatures with geological time.

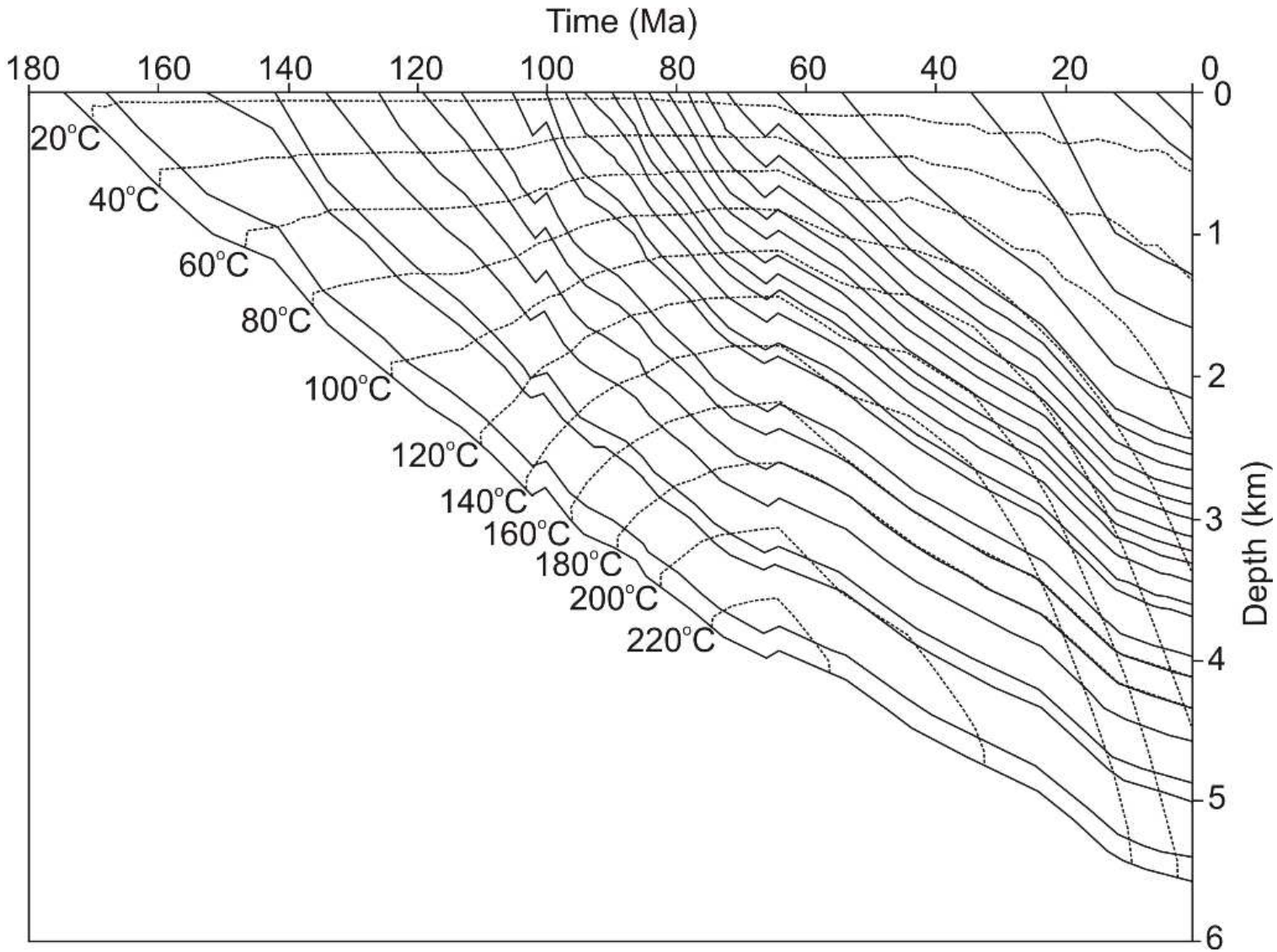

Fig. 3.21. Burial history plot for pseudo Mannar-Deep well. The depth is in meters below sea floor. Dashed contours indicate the changing formation temperatures with geological time.

3.5.3. Data required for generation and accumulation modeling

3.5.3.1. TOC and kerogen composition

Figures 2.7 and 2.9 show the TOC content of the sediment penetrated by the Pearl-1, Dorado and Barracuda wells. The data show that a majority of sediment from the Pearl-1 well has around 0.5% TOC. Claystones penetrated by the Dorado well and calcareous claystones between the depths of 3500 and 4260 m in the Barracuda have relatively higher organic carbon content (1.0 - 2.5%). Rao *et al*. (2010) reported that Albian sediments penetrated by the GMS1 well in Indian shallow waters (Location: Fig. 3.3) have low TOC content (~0.5%) and higher contribution from Type III kerogen. Plot of hydrogen index (HI) against the oxygen index (OI) shows that the sediments penetrated by the Pearl-1 well are rich in Types III and IV kerogen (Fig. 2.8). Marceral composition analysis shows that sediment from the Dorado, Dorado-North and Barracuda wells are also rich in Types III kerogen (Fig. 2.11 and 2.12). Particularly, the calcareous claystone between the depths of 4260 to 4740 m in the Barracuda well is rich in fusinite but poor in petroleum generative kerogen (Fig. 2.11C).

The data show that Holocene to Albian sediments in shallow water depths in the Mannar Basin have poor hydrocarbon source potential. Though, the Campanian and younger claystone penetrated by the Dorado well have higher TOC content, neither this well nor the Dorado-North well have entered the oil window (Premarathne *et al*., 2015). On the contrary, sediments in the Pearl-1 and Barracuda wells have entered the oil window (VR = 0.6-1.3 $\%R_o$; Peters and Cassa, 1994; Petersen, 2002) at the depths of 3500 and 4260 m respectively. However, thermally matured sediment penetrated by the Pearl-1 well is mostly sandstone, while the thermally matured calcareous claystone in the Barracuda well have poor hydrocarbon source character. Therefore, the wells drilled in the Mannar Basin may not have penetrated potential source rocks in the basin.

Chandra *et al*. (1991) reported that Albian and earlier sediment in the Indian sector of the Cauvery Basin have a TOC content varying from 0.34% to 2.49% and around 20% contribution from Type II kerogen and the remainder being Type III kerogen. Cantwell *et al*. (1978) reported the Albian mudstone penetrated by the Pesalai-1 well (Location: Fig. 3.3) to have a TOC content varying from 2.8% to 6.9% and a significant contribution from Type II kerogen. Ratnayake and Sampei (2015) reported that brown to black coloured Jurassic mudstone in the Aadigama graben (Location: Fig. 3.3) has relatively high TOC content (3.05-5.10%). Based on these observations, it was thought that Early Cretaceous and older sediment could be the most significant hydrocarbon source in the Mannar Basin. Due to no well

penetration, the exact source character of this older sediment is not known. Therefore, different scenario modeling was performed on hydrocarbon source character. 0.5% of TOC and 100% contribution from Type III kerogen were assumed as the pessimistic source character scenario, while 2.5% of TOC and 50% contribution from Types II kerogen (the remainder being III kerogen) were assumed as the optimistic source character scenario. In addition, a moderate source character scenario of 1.5% of TOC and 20% contribution from Type II kerogen (the remainder being Type III kerogen) was performed.

3.5.3.2. Kinetic model for hydrocarbon generation

Like in the case of source character, kinetic models for kerogen conversion into hydrocarbons are not available for Early Cretaceous and older sediment in the Mannar Basin. Nevertheless, many kinetic models, which are based on laboratory pyrolysis of sediment from petroliferous basins in various parts of the world, are available in the public domain (eg. Tissot *et al*., 1987; Burnham, 1989; Suzuki and Matsubayashi, 1995; Pepper and Corvi, 1995a). The two most commonly used kinetic models are those derived by French Petroleum Institute (eg. Tissot *et al*., 1987) and Laurence Livermore National Laboratory (eg. Burnham, 1989). They described Types I, II and III kerogen in shales from the Green River in the US, the Paris Basin in France and the Mahakam delta in Malaysia. Waples (1994) compared the two models and found that the kinetic model of the French Petroleum Institute (IFP) proposed by Tissot *et al*. (1987) does not produce natural gas directly from kerogen.

Pepper and Corvi (1995a) proposed an alternative approach to select a kinetic model especially for basins with limited knowledge such as the Mannar Basin. This approach is based on the depositional environment of potential source rocks, which is thought to determine the oreganofacies in sedimentary rocks. Kinetic model proposed by Pepper and Corvi (1995a) for marine silisiclastic rocks, the possible lithofacies of potential source rocks in the Mannar Basin, agrees well with the Laurence Livermore National Laboratory (LLNL; Burnham, 1989) kinetic model. Therefore, the LLNL kinetic model for types II and III kerogen was used in this study (Fig. 3.22). In addition, kinetics for oil and coke cracking into natural gas were adopted from the same model.

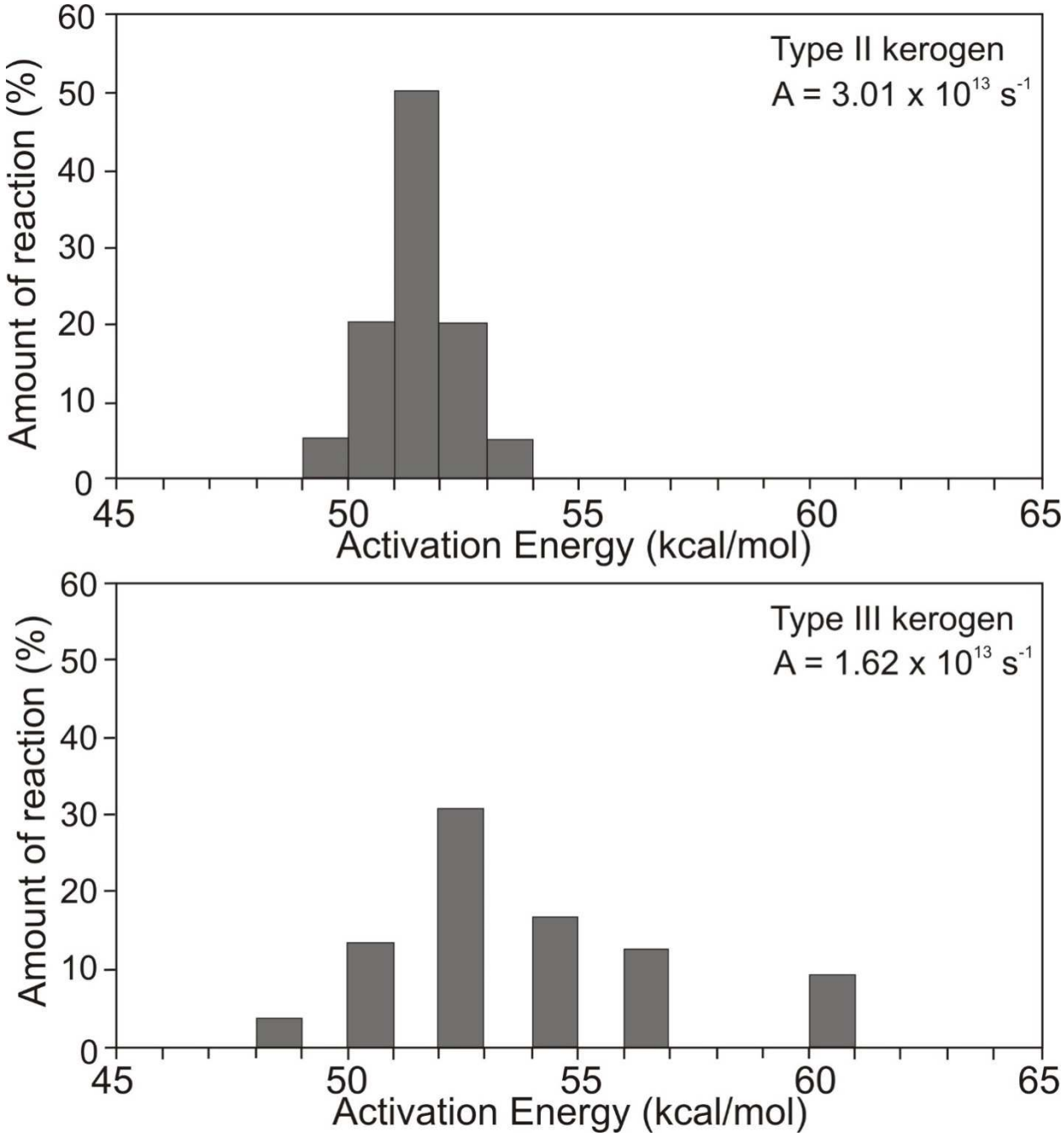

Fig. 3. 22. Laurence Livermore National Laboratory (LLNL) kinetic model for Types II and III kerogen (after Burnham, 1989).

3.5.3.3. Hydrocarbon expulsion threshold.

Fluid flow in a sedimentary rock is controlled by buoyancy, capillary attraction and the wettability of fluid (England and Fleet, 1991). The concept of relative permeability, which is an adoption of the Darcy's law, is used to explain multiphase fluid flow in a non-mixing mixture. It is the ratio between the effective permeability of a phase of the mixture to the absolute permeability of the phase in a rock. The SIGMA-2D software simulates the hydrocarbon expulsion threshold based on the relative permeability of fluids (oil, gas and water) in shale.

Discussions on relative permeability of mudstones are uncommon compared to those on sandstones (Aplin and Larter, 2005). However, Ungerer *et al.* (1987); Pepper (1991); Okui and Waples (1993); Pepper and Corvi (1995b) explained relative permeability of oil-water system in mudstones. Relative permeability is an experimentally derived property lacking profound theoretical foundation (Ungerer *et al*., 1984). Pepper and Corvi (1995b) thought that laboratory measurement of relative permeability in compacted fine grained rocks is difficult, and therefore a simple analogy has to be guessed, assumed with reservoir rocks or extrapolate from other data sets. Okui and Waples (1993) based on a computer simulation estimated the relative permeability of oil-water system in shale source rocks (Fig. 3.23). According to this model, irreducible water saturation in mudstones is relatively high (~80%). The crossover point, beyond which oil relative permeability exceeds the water relative permeability, achieves at relatively low oil saturations. As a result, oil expulsion readily takes place at low oil situations. The model proposed by Okui and Waples (1993) for oil-water system in shale was used in this study for shale source rocks. Discussions on relative permeability of gas-water and gas-oil systems are also rare. Pepper and Corvi (1995b) reported the relative permeability of gas-water system in fractured coal. According to this model, gas is readily movable at low saturations. Based on the discussions of relative permeability in Ungerer *et al.* (1987); Pepper (1991); Okui and Waples (1993); Pepper and Corvi (1995b), the relative permeability of gas-water and gas-oil systems in shale were assumed as shown in Figs. 3.24 & 3.25, respectively.

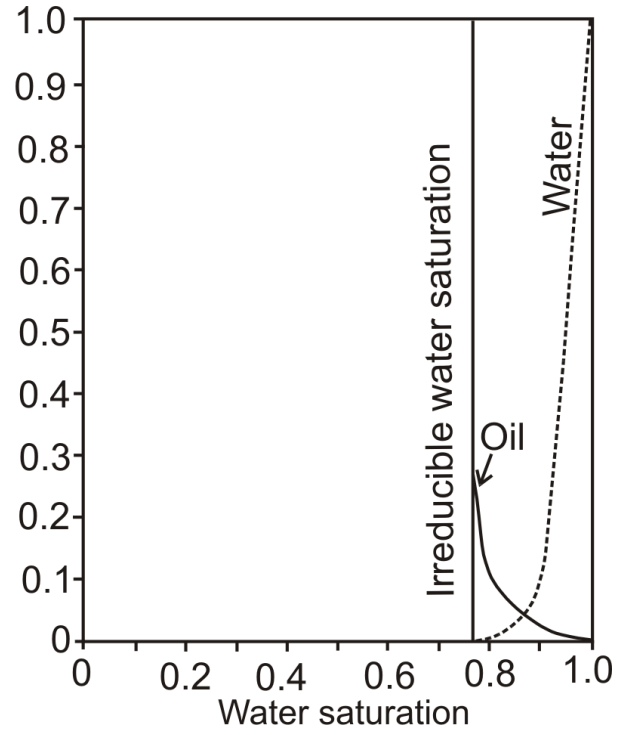

Fig. 3.23. Oil-water relative permeability in shale rocks (After Okui and Waples, 1993)

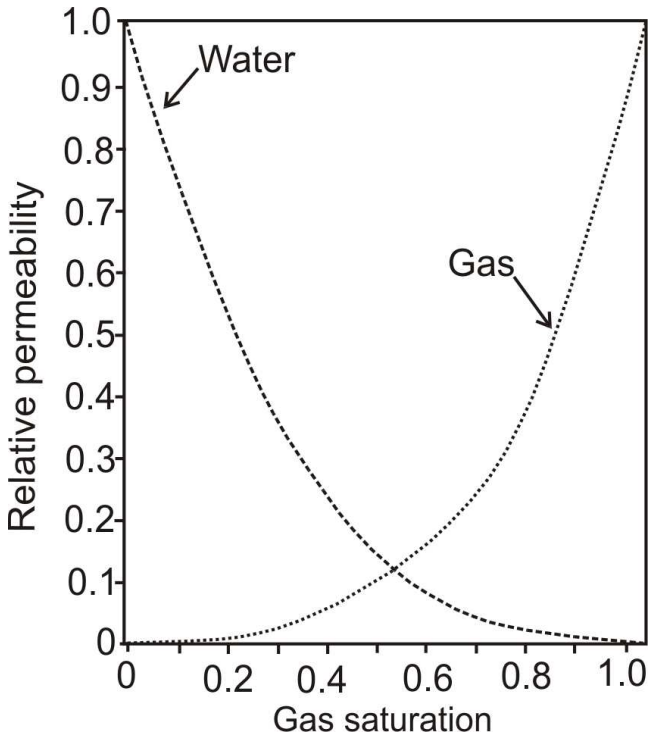

Fig. 3.24. Gas-water relative permeability in shale rocks assumed for modeling in this study.

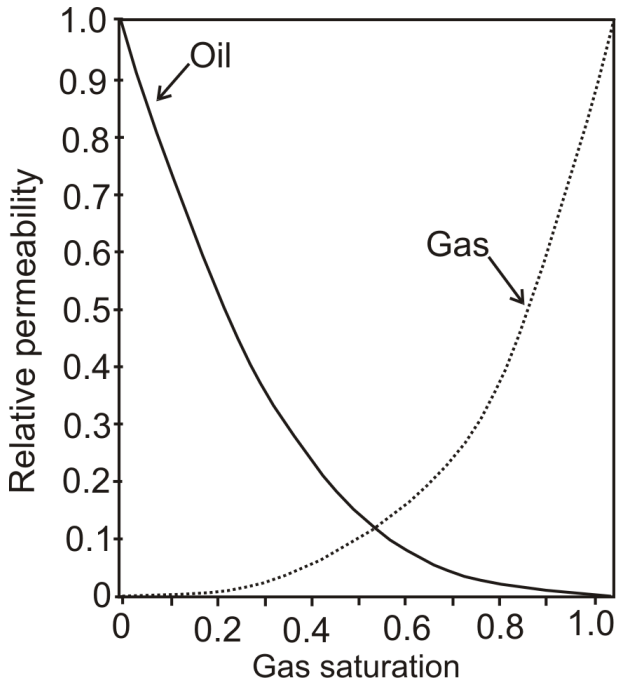

Fig. 3.25. Gas-oil relative permeability in shale rocks assumed for modeling in this study.

3.5.3.4. Secondary hydrocarbon migration

Discussions on relative permeability of the oil-water system are common (eg. Ungerer *et al.* 1987; England and Fleet, 1991; Dandeker, 2013; Pepper and Corvi, 1995b). Dandeker (2013) reported typical oil-water relative permeability curves (Fig. 3.26). This was adopted for relative permeability of oil-water system in sandstone and limestone. The similar relative permeability curves shown in Figs. 3.24 and 3.25 for gas-water and gas-oil systems, respectively were assumed for sandstone and limestone as well.

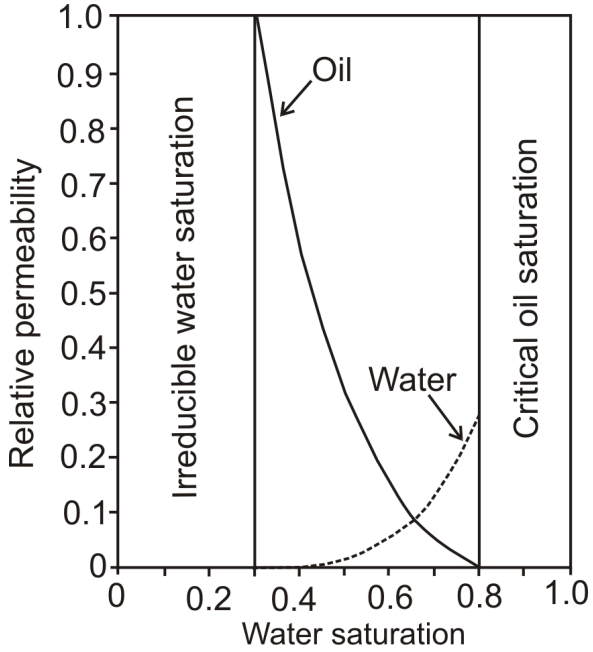

Fig. 3.26. Typical oil-water relative permeability in reservoir rocks (After Dandeker, 2013).

3.5.4. Modeled hydrocarbon generation and expulsion timing

Timing of hydrocarbon generation and expulsion in three stratigraphic columns at the Pearl-1, Dorado-North and pseudo Mannar-Deep well locations under optimistic and pessimistic source character scenarios are discussed below. Though Pearl-1 and Dorado-North wells penetrated only a part of the total stratigraphic column, their names in the discussion refer to the total stratigraphic column at the respective well locations. Table 3.6 summaries the duration of the peak oil generation and cracking and the amount of oil generation in kilogram per unit volume of rock (kg/m^3) under the optimistic scenario. Appendices C and D show the quantity and timing of hydrocarbon generation and the expulsion, respectively in the three stratigraphic columns at above mentioned well location under the optimistic and pessimistic scenarios.

3.5.4.1. Pearl-1 well

Peak hydrocarbon generation in Berriasian and older sediment under the optimistic scenario (TOC = 2.5% and Type II kerogen = 50%) takes place during Campanian to Eocene (78-35 Ma). Peak oil generation in the Aptian, Turonian and Santonian sediments take place during 60-10 Ma, 45-5 Ma and 30-5 Ma, respectively. No hydrocarbon is generated in sediments younger than the Santonian. Amount of hydrocarbon generated in the Santonian and Turonian sediment is lesser than that in older sediment. Hydrocarbon generation timing in both optimistic and pessimistic scenarios is more or less the same. Under the pessimistic source character scenario, the maximum oil generation in Bathonian to Kimmeridgian sediment is less than 1 kg/m^3, which is a much less quantity compared to 15 kg/m^3 observed in the same section under the optimistic scenario (App. C1 & C4). Sediments younger than the Kimmeridgian produce even a lesser amount of hydrocarbon under the pessimistic scenario.

Under the optimistic scenario, peak hydrocarbon expulsion from the Late Jurassic sediment takes place from the middle Campanian to Oligocene. However, there is a minor gas expulsion phase in this section during the Neogene. Peak hydrocarbon expulsion from the Valanginian to Berriasian and the Aptian sediment takes place from the Maastrichtian to Pliocene and from the middle Palaeocene to the Pliocene, respectively. Hydrocarbon expulsion from these two stratigraphic intervals during the Neogene period seems to be a second expulsion phase. A smaller phase of hydrocarbon expulsion could be seen in the Turonian and Santonian sediment during the Neogene period. Timing of hydrocarbon expulsion from a particular stratigraphic interval, both under optimistic and pessimistic scenarios, is roughly the same.

Table 3.6. Summary of oil generation timing for different stratigraphic intervals in the Pearl-1, Dorado-North and pseudo Mannar-Deep wells under the optimistic source character scenario. Oil generation is in kilograms per unit volume of rock (kg/ m^3). Timing of oil cracking is also listed. Gen. = generation.

Stratigraphic interval		Pearl-1			Dorado-North			Pseudo Mannar-Deep		
		Gen. timing (Ma)	Oil Cracking (Ma)	Oil Gen. (kg/m^3)	Gen. timing (Ma)	Oil Gen. (kg/m^3)	Oil Cracking (Ma)	Gen. timing (Ma)	Oil Cracking (Ma)	Oil Gen. (kg/m^3)
Late Cretaceous	Campanian	-	-	-	-	-	-	40-30	-	3
	Santonian	30-5	-	2	45-35	2	-	65-30	-	9
	Coniacian	-	-	-	55-25	4	-	70-30	-	12
	Turonian	45-5	-	4	65-35	10	-	77-30	-	15
	Cenomanian	-	-	-	70-35	15	-	80-70	-	15
Early Cretaceous	Albian	-	-	-	80-45	15	-	85-75	75-40	15
	Aptian	60-10	-	10	85-65	15	-	95-80	80-75	15
	Hauterivian -Barremian	-	-	-	85-75	15	-	100-90	90-70	15
	Berriasian to Valanginian	70-35	-	15	90-75	15	-	105-90	90-72	15
Late Jurassic	Tithonian	-	-	-	95-85	15	75-40	110 90	90- 77	15
	Bathonian -Kimmeridgian	78-35	-	12	100-85	12	70-35	120-95	95-80	15

However, amount of hydrocarbon expulsion under the pessimistic scenario is more than 100 times lesser than that under the optimistic scenario. Accuracy of modeling is confirmed by the fact that the production index for the Coniacian to Turonian (?) sediment at the depths of 2920 m in the Pearl-1 well yields 0.43 (Table 2). Oil generation at this depth agrees with source maturity suggested by greater than 435 ^{o}C of Rock Eval T_{max} (Table 2.1), which indicate the onset of the oil window (Peters and Cassa, 1994). Reason for not generating hydrocarbon in some stratigraphic intervals in the Pearl-1 well, such as the Albian, Hauterivian, Barremian and the Tithonian is due to the assumption of 100% sandstone and zero percent TOC content in these stratigraphic intervals. It is possible to have thin layers of claystone interbedded with sandstone. However, it is difficult to distinguish such interbeddings in seismic profiles due to the level of seismic resolution used in this study. In addition, there are software limitations on the maximum number of horizons/ formations that could be used for modeling. The reason for a minor hydrocarbon generation and expulsion during the Neogene could be related to temperature elevation due to rapid burial during this period.

3.5.4.2. Dorado-North well

Hydrocarbon generation in Late Jurassic sentiment under the optimistic scenario takes place from the Cenomanian to Santonian (100-85 Ma). Peak hydrocarbon generation in the Early Cretaceous sediment mainly takes place during the late Cretaceous, excluding the Albian sediment that continued to generate hydrocarbon up to the middle Eocene (~45 Ma). Peak hydrocarbon generation in the Cenomanian and Turonian sediment, takes place during the Maastrichtian to late Eocene, while in the Santonian and Coniacian sediment during the Eocene. Less hydrocarbon generation (2-4 kg/m^3) takes place in the Santonian and Coniacian sediment compared to that (~15 kg/m^3) in older sediment. It is seen that oil generated in the Late Cretaceous sediment thermally cracks into natural gas from the Maastrichtian to the late Eocene. No significant hydrocarbon generation could be seen in the Campanian and younger sediment under the optimistic scenario. Like in the case of the Pearl-1 well, oil generation in the Late Jurassic and younger sediment is less than 1.0% kg/m^3 under the pessimistic scenario. This is a much less quantity compared to oil generation under the optimistic scenario.

Oil expulsion from the Late Jurassic sediment takes place from the Cenomanian to early Campanian (~95-80 Ma). However, gas expulsion from this sediment takes place from

the Campanian to the middle Palaeocene, an extended period compared to the duration of oil expulsion (App. D4). Peak oil expulsion from the Valanginian to Berriasian sediment takes place from the Turonian to middle Campanian (~90-80 Ma), while peak gas expulsion from the same stratigraphic interval takes place from the Coniacian to the end of the Maastrichtian. Oil and gas expulsion from the Hauterivian to Barremian, Aptian and Albian sediments takes place from the Santonian to late Palaeocene, Santonian to middle Eocene and the Maastrichtian to middle Eocene, respectively. Though hydrocarbon generation in the Cenomanian and Turonian sediment is roughly the same as that in earlier sediments (Table 3.6), relatively lesser amount of hydrocarbon is expelled from the Turonian to Cenomanian sediment. Though hydrocarbon is generated in Santonian sediment, expulsion does not take place. Timing of oil and gas expulsion in both optimistic and pessimistic scenarios is more or less the same. Nevertheless, amount of hydrocarbon expulsion under optimistic scenario is more than 100 times higher than that under the pessimistic scenario.

The Cenomanian, Turonian and earlier sediment can produce roughly the same amount of hydrocarbon per unit volume of rock (Table 3.6). However, relatively the thinner Cenomanian and Turonian sections generate and expel relatively smaller amount of total hydrocarbon than relatively thicker older sections. Oil produced in the Late Jurassic sediment thermally cracks into natural gas due to high formation temperatures. The maximum temperatures recorded in the Dorado-North well has been around 180 ^{o}C (Premarathne *et al*., 2015). It is because of oil cracking into gas that oil expulsion stops earlier than the stopping of gas expulsion. Reduction of hydrocarbon expulsion from the Late Jurassic and Early Cretaceous sediment around 70 Ma could be due to reduction of formation temperature related to upliftment close to that time, which has given rise to the Cretaceous-Palaeogene (K-Pg) unconformity.

3.5.4.3. Pseudo Mannar-Deep well

Hydrocarbon generation in the Late Jurassic sediment under optimistic scenario takes place from the Aptian to Turonian (App. D5 & D6). In the Early Cretaceous sediment hydrocarbon generation takes place from the late Albian to Campanian. The Cenomanian to Campanian sediment generates hydrocarbon from the Campanian to middle Oligocene. Oil generated in the Late Jurassic and Early Cretaceous sediment thermal cracks into natural gas from the Cenomanian to middle Eocene. Almost all oil generated in the Kimmeridgian to Bathonian sediment, which reached a maximum temperature of around 220 ^{o}C towards the

latter part of the late Cretaceous cracks into natural gas. Hydrocarbon generation in Campanian sediment is lesser (~3 kg/m^3) compared to that in the older sediment. Sediments younger than the Campanian do not generate a significant quantity of hydrocarbon. Oil generation in the Late Jurassic and younger sediment under the pessimistic scenario is around 1.0% kg/m^3, which is much less than oil generation in the same stratigraphic intervals under the optimistic scenario.

Timing of hydrocarbon expulsion from the Late Jurassic and Early Cretaceous sediment in pseudo Mannar-Deep well is roughly similar to hydrocarbon expulsion from the same aged sediments in the Dorado-North well. However, duration and quantity of oil expel from each stratigraphic interval in the pseudo Mannar-Deep well is smaller compared to that in respective stratigraphic intervals in the Dorado-North well. A smaller quantity of oil and gas expels from the Cenomanian to Santonian sediment. Timing of oil and gas expulsion in both the optimistic and pessimistic scenarios is more or less the same. However, amount of hydrocarbon expulsion under optimistic scenario is more than 100 times greater than that under the pessimistic scenario (App. D5 & D6). There is always a time lag of about 5 Ma between hydrocarbon generation and expulsion.

Oil produced in the Albian and older stratigraphic intervals in the pseudo Mannar-Deep well cracks into natural gas due to high formation temperatures (Table 3.6). Integrated burial and thermal history plot show that thermal cracking of oil starts at around 120-140 ^oC (Fig. 3.21). The increasing formation temperature from the Pearl-1 well towards the pseudo Mannar-Deep well is due to increasing stratigraphic thickness and heat flow from north to south of the Mannar Basin (Fig. 3.4b). The timing and quantity of oil expulsion in the Late Jurassic and Early Cretaceous sediment are smaller because of oil cracking into natural gas. Gas expulsion from the Late Jurassic and Early Cretaceous sediment take place for a longer period due to continuous production of gas through oil cracking**.**

3.5.5. Modelled hydrocarbon accumulation

Modeling results under the optimistic scenario show oil deposits with close to 100% oil saturation mainly in the Late Cretaceous sandstone (Fig. 3.27). In addition, a few oil accumulations with low oil saturation (~20%) is seen in the Early Cretaceous and Palaeogene sections. A couple of gas accumulations with close to 100% gas saturation could be seen in the Albian and Cretaceous sandstone under the optimistic source character scenario (Fig. 3.29). In addition, oil and gas accumulation can take place in the Cretaceous sandstone under

moderate source character scenario (TOC = 1.5% and Type II kerogen 20% and the remainder being type III kerogen; Figs. 3.30 & 3.31). Though, no significant oil accumulation could be seen under the pessimistic scenario (Fig. 3.28), a gas accumulation with close to 100% gas saturation could be seen in the Albian sandstone (Fig. 3.30). Pink coloured arrows in Figs. 3.27 to 3.31 show lateral hydrocarbon migration, while purple coloured counters in Figs. 3.27 and 3.29 show the vitrinite reflectance (VR) calculated using the SIMPLE-R_o (Suzuki *et al*., 1993). The data show that VR of the Late Jurassic sediment in the pseudo Mannar-Deep well enters 3 $\%R_o$.

Modeling results suggest that the optimistic source character scenario of 2.5% TOC and Types II and III kerogen 50% each has potential to generate oil and gas deposits in the Mannar Basin. On the other hand, the pessimistic source character scenario of 0.5% TOC and presence of only Type III kerogen in claystone is not good enough to produce economically viable oil deposits, yet may give rise to natural gas deposits. Since some sandstone layers extend almost across the entire length of the stratigraphic section, hydrocarbon migration seems to take place from southern part of the Mannar Basin in deep water depths towards shallow water depths towards the south of the basin. Accumulation modeling shows that the probability of occurring hydrocarbon deposits in the Late Cretaceous sandstone could be higher. Modeling results further suggest that the majority of hydrocarbon expelled from source rocks could have leaked into the ocean. VR more than 2 $\%R_o$ shows over maturity, in which case oil and gas generation stop (Petersen, 2002). The Late Jurassic and Early Cretaceous (Berriasian to Barremian) sediment in the pseudo Mannar-Deep well is over matured. The over maturity (VR = 2 $\%R_o$) line (eg. Fig. 3.27) could be expected to enter into sediment younger than the Berriasian age further towards the south of the pseudo Mannar-Deep well.

.

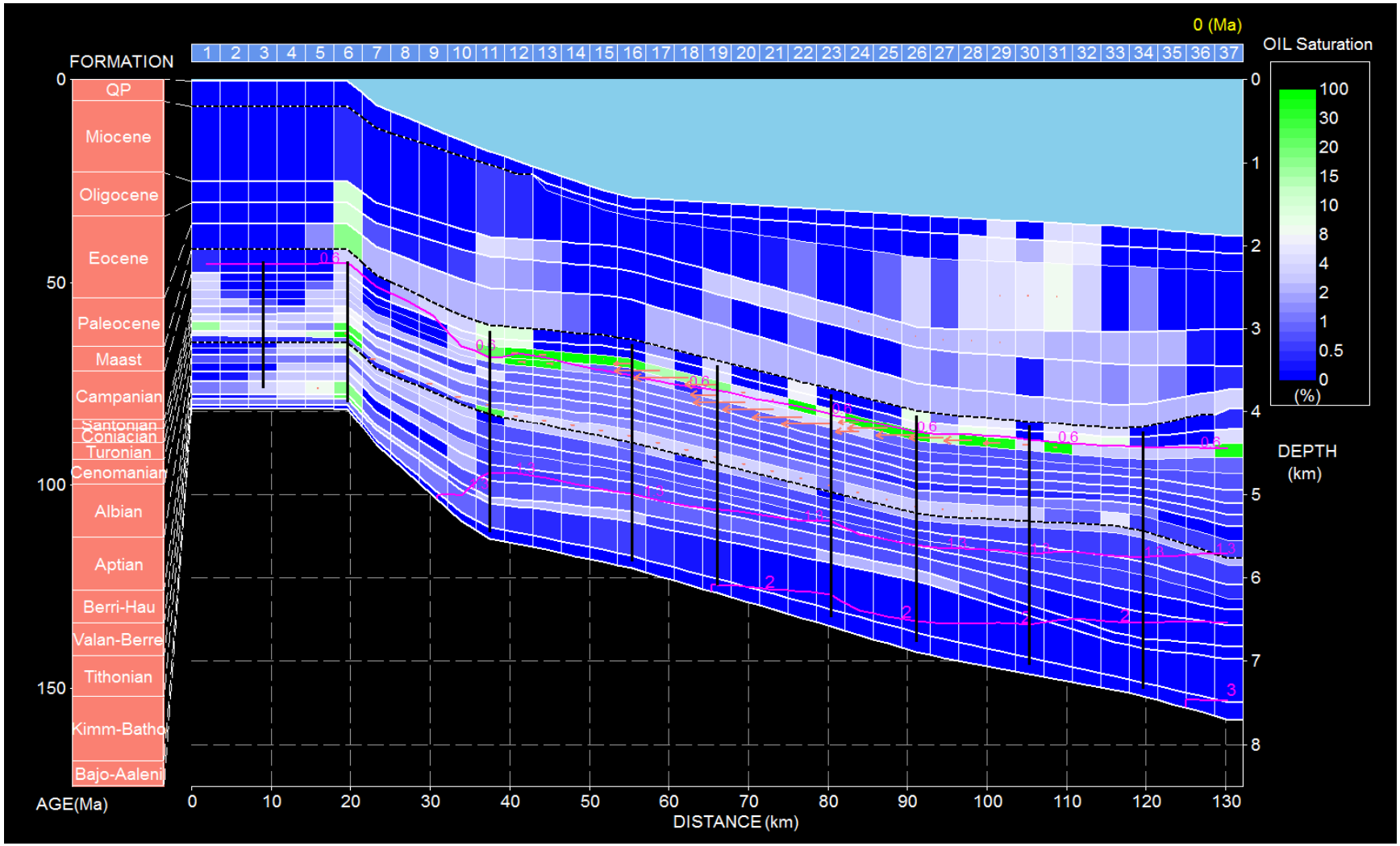

Fig. 3.27. Modelled oil accumulation under the optimistic source character scenario (TOC = 2.5% and Types II & III kerogen 50% each) Pink coloured arrows show lateral hydrocarbon migration, while purple coloured contours show vitrinite reflectance in R_o%.

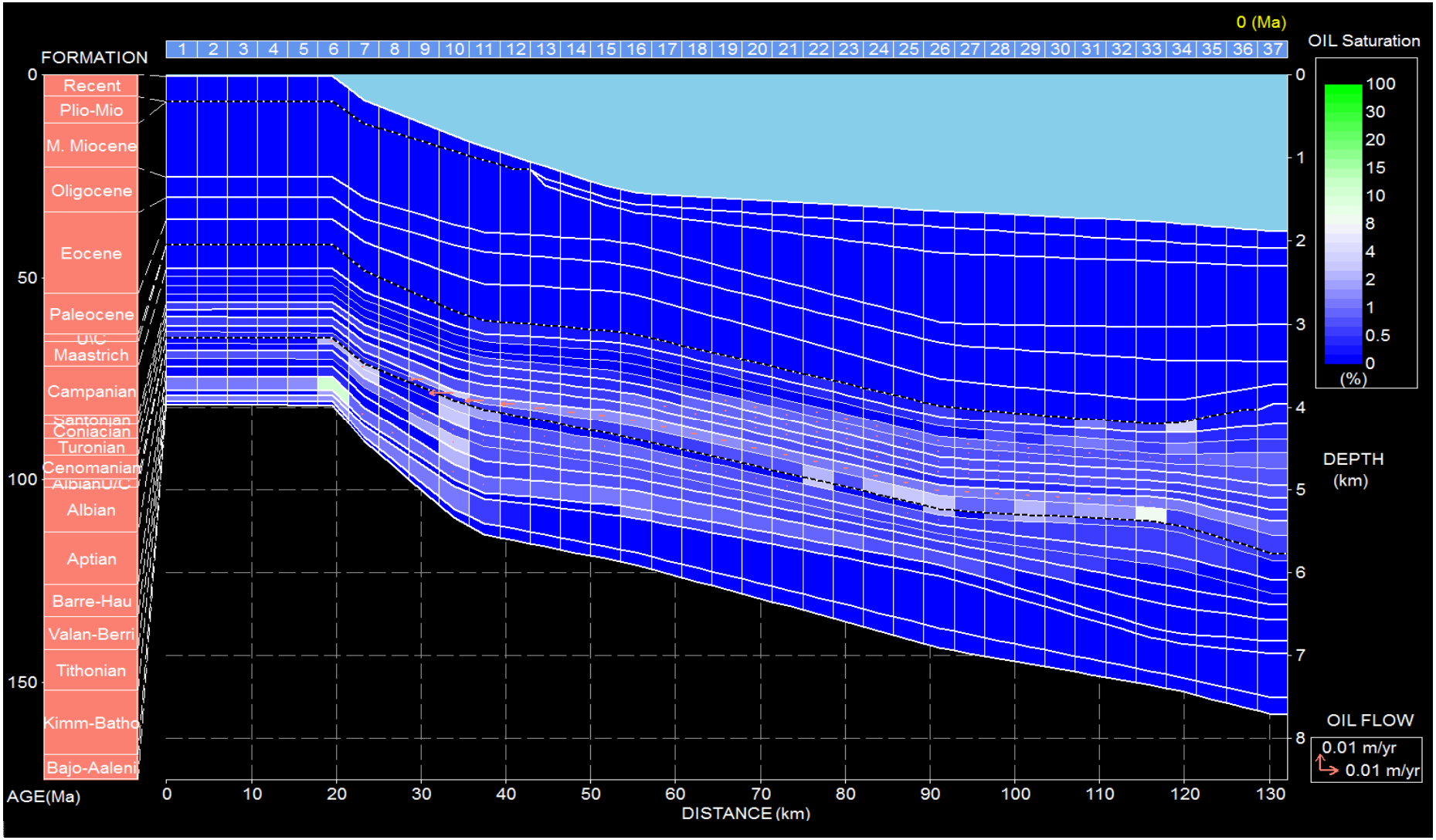

Fig. 3.28. Modelled oil accumulation under the pessimistic source character scenario (TOC = 0.5% and Type III kerogen 100%). Pink coloured arrows show lateral hydrocarbon migration.

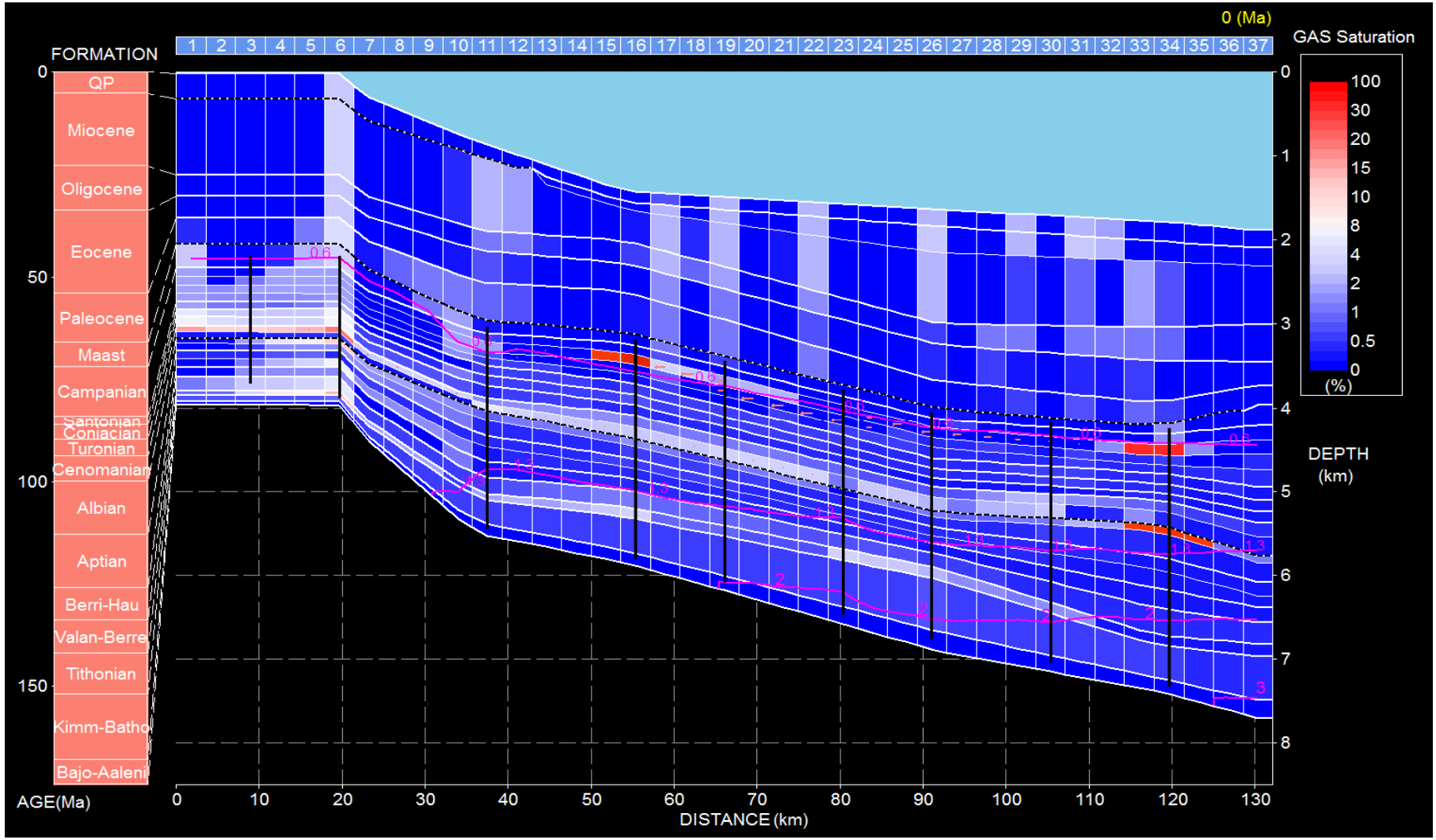

Fig. 3.29. Modelled gas accumulation under the optimistic source character scenario (TOC = 2.5% and Type II kerogen 50%. Pink coloured arrows show lateral hydrocarbon migration, while purple coloured contours show vitrinite reflectance in R_o%.

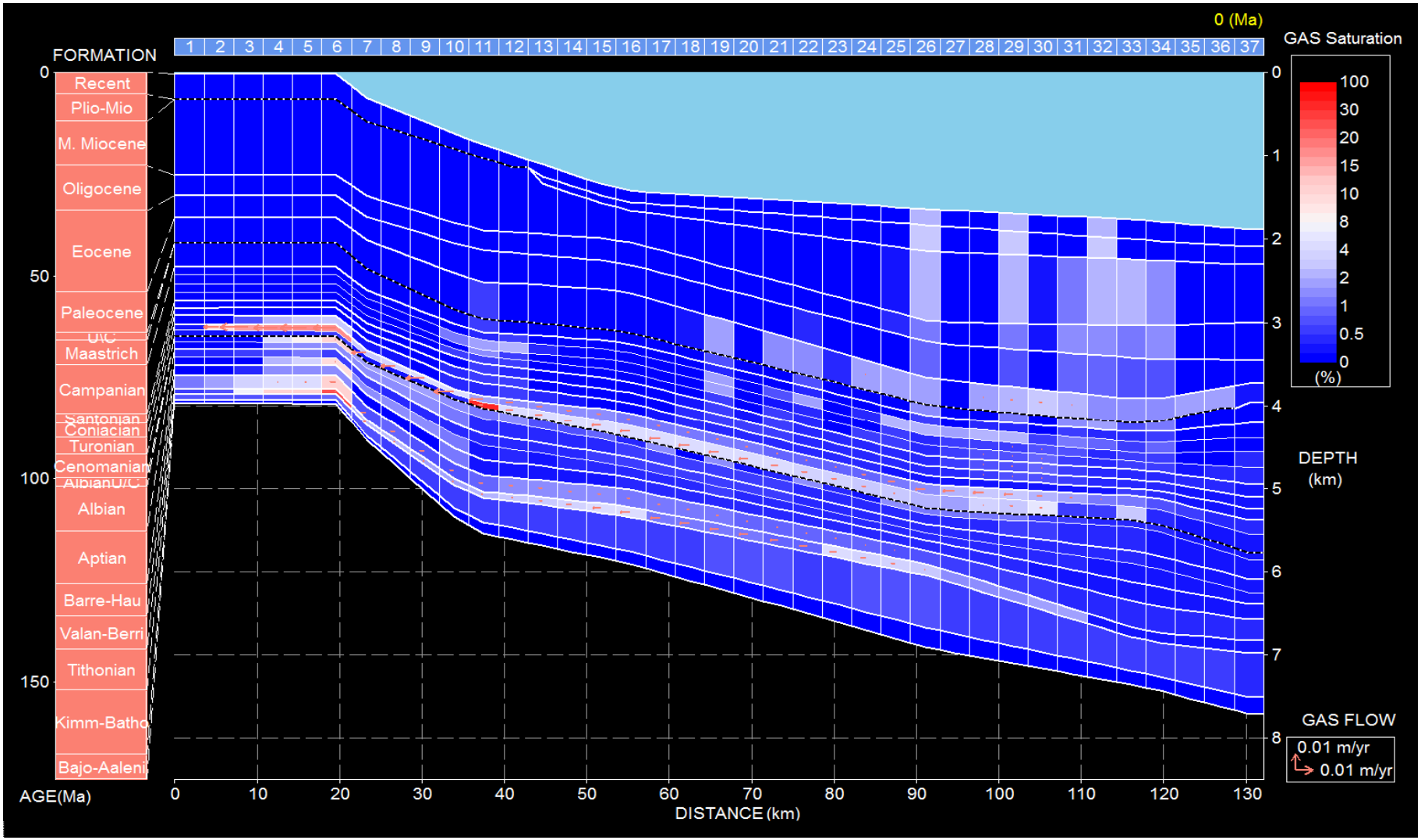

Fig. 3.30. Modelled gas accumulation under pessimistic source character scenario (TOC = 0.5% and Type III kerogen 100%. Pink coloured arrows show lateral hydrocarbon migration.

3.5.6. Petroleum system in Mannar Basin

3.5.6.1. Source rocks

If the Mannar Basin is to produce economically viable oil deposits its Early Cretaceous and older sediments should have good hydrocarbon source character. The Aptian and Turonian–Cenomanian ages experienced well-known global oceanic anoxic events (e.g., Schlanger and Jenkyns, 1976; Arthur *et al*., 1987). These anoxic events (OAE) might have given rise to good hydrocarbon source rocks in the Mannar Basin. Fine grained sedimentary rocks with 1% or higher TOC could be considered as having good hydrocarbon source potential (Peters and Cassa, 1994). Based on previously mentioned discussion on source potential of the Cauvery Basin by Cantwell *et al*. (1978); Chandra *et al*. (1991) and on Late Jurassic mudstone in the Aadigama graben by Ratnayake and Sampei (2015), it could be thought that Early Cretaceous and older sediment in the Mannar Basin might have at least 1.0% of average TOC and at least 10-15% contribution from Type II kerogen. Based on hydrocarbon accumulation under the moderate source character scenario (Figs. 3.31 and 3.32), it could be thought that the Mannar Basin might accommodate economically viable oil and gas deposits. Due to increasing formation temperatures towards the southern part of the Mannar Basin, the potential for having natural gas deposits could be higher towards the southern part of the basin. Source of thermogenic gas encountered in the Dorado and Barracuda wells in 2011 could be the Early Cretaceous and/or older claystone.

3.5.6.2. Reservoir rocks

Stratigraphy of wells (Fig. 1.4) indicates the occurrence of clastic and carbonate potential reservoir rocks in the Late Cretaceous, Palaeogene and Neogene sections. The Pearl-1 well penetrated more than 900 m thick reservoir quality sandstone of the Late Cretaceous age (Fig. 1.4A). The Dorado-North and Dorado wells also penetrated reservoir quality sandstones, particularly in the Palaeogene and Late Cretaceous stratigraphic sections (Fig. 1.4B & C). The Cretaceous and Paleogene sandstone and sometimes carbonate rocks could be the potential hydrocarbon plays in the Mannar Basin. Natural gas discovered in the Late Cretaceous sandstone in the Dorado and Barracuda wells supports the modeling results in this study. However, no oil deposits have been discovered in the Mannar Basin to date.

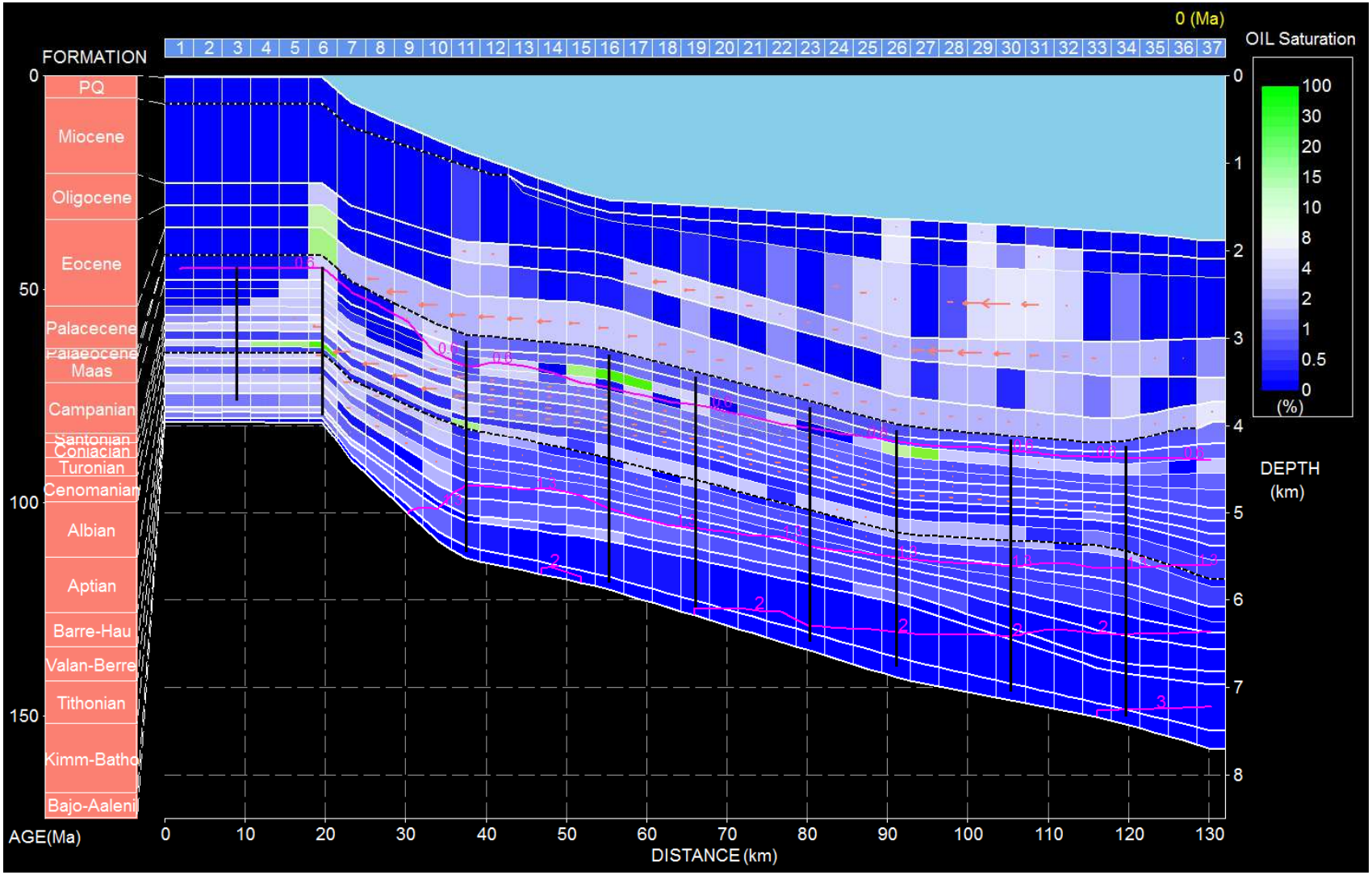

Fig. 3.31. Modelled oil accumulation under moderate source character scenario (TOC = 1.5% and Types II kerogen 20%, remaining 80% being Type III kerogen). Pink coloured arrows show lateral hydrocarbon migration, while purple coloured contours show vitrinite reflectance in R_o%.

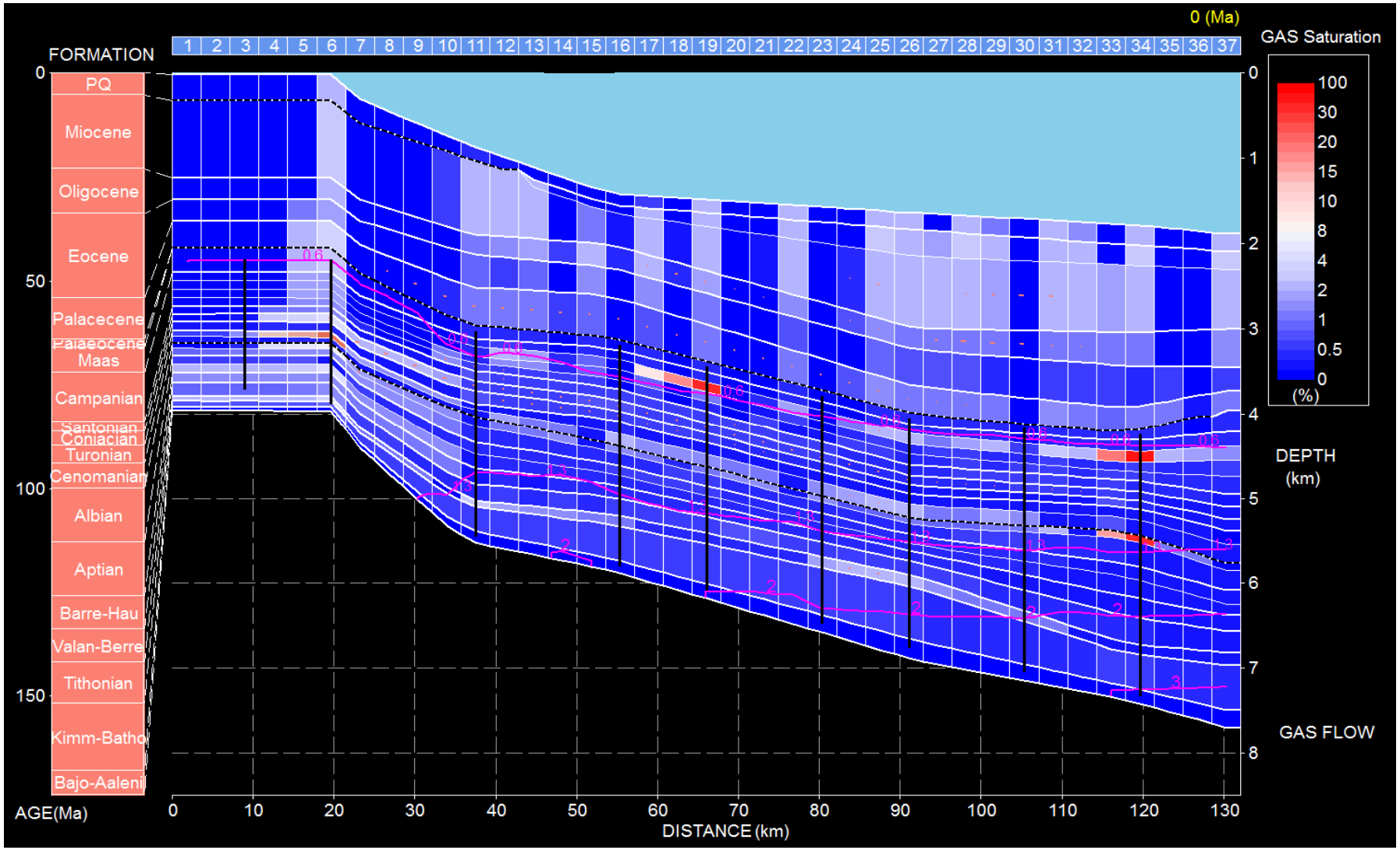

Fig. 3.32. Modelled gas accumulation under moderate source character scenario (TOC = 1.5% and Types II kerogen 20%, remaining 80% being Type III kerogen). Pink coloured arrows show lateral hydrocarbon migration, while purple coloured contours show vitrinite reflectance in R_o%.

3.5.6.3. Traps, seals and migration path ways

Seismic data show the occurrence of structural and stratigraphic traps in the Mannar Basin (Fig. 3.4a). Structural traps may include tilted/rotated fault blocks and anticlinal closures. The compressional tectonics in the Gulf of Mannar might have been instrumental in formation of anticlinal traps. Stratigraphic traps include pinch-outs and channel fills.

Stratigraphy of the Pearl-1, Dorado, and Dorado-North wells (Fig. 1.4) shows the occurrence of fine-grained sediments that can act as potential seals overlain by clastic and carbonate potential reservoir rocks, especially in the Late Cretaceous and Palaeogene sections. Pearl-1 well encountered approximately 250 m thick Palaeogene claystone (Fig. 1.4A). Similar strata, though in lesser thickness, are encountered in the Palaeogene section in the Dorado-North and Dorado wells (Figs. 1.4B & C and Fig. 3.4). Igneous rocks interbedded with sedimentary rocks in the Mannar Basin (Fig. 1.4D) may also act as traps and seals.

Seismic data show many faults terminating at the top of the Cretaceous (Fig. 3.4a). These faults may provide ample pathways for vertical hydrocarbon migration from source rocks in the deeper part of the basin to shallower traps creating a vertical drainage system in the Mannar Basin. However, the simulated hydrocarbon accumulation indicates the predominance of lateral hydrocarbon migration (pink coloured arrows in Figs. 3.27 to 3.31).

4. CONCLUSIONS

The Mannar Basin is filled with present to Late Jurassic or older sedimentary rocks. The sediment thickness ranges from 4 km in the north to more than 6 km towards the southern part of the basin. The Mannar Basin has a rift structure. Rifting likely began in the late Aptian and ceased at the end of the Cretaceous. Several episodes of basin wide basaltic lava flows have occurred in the Gulf of Mannar during the Maastrichtian. The present-day geothermal gradient in the basin is around 24.4 °C/km. The present-day heat flows in the shallow and deep water depths are around 40 and 33 mW/m^2, respectively. The present-day heat flows in the northern Mannar Basin are relatively lower than that in the adjacent Indian waters. The Mannar Basin has the heat flow history of a typical rift basin. The maximum heat flows at the end of rifting in the Pearl-1 and Dorado-North well locations are around 68.2 and 71.1 mW/m^2, respectively.

The Campanian to present sedimentary rocks in the northern Mannar Basin, which has been derived from vascular land plants, is rich in type III and IV kerogen and has poor hydrocarbon source potential. If the Santonian to Cenomanian sediment has good source potential it could have expelled relatively a small quantity of oil and natural gas. The productivity of this stratigraphic interval increases from north to south of the Mannar Basin. The Early Cretaceous to older sediment, which could be the potential hydrocarbon source rocks in the Mannar Basin, has not been penetrated by exploration wells. Source character of this deeply buried sediment is uncertain. In the event of the Early Cretaceous to older sedimentary rocks having good hydrocarbon source potential, oil and gas could have been expelled mainly during the Late Cretaceous, which is followed by a couple of minor expulsion phases in the Palaeogene and Neogene. The time lag between oil generation and expulsion is around 5 Ma. Oil cracking starts at 120-140 ^oC. The probability of occurring natural gas deposits increases towards the southern part of the Mannar Basin. Even if the deeply buried sediment has poor hydrocarbon source potential of around 0.5% of TOC content and only Type III kerogen they may still give rise to economically viable gas deposits. The potential source rocks in the Mannar Basin could be expected to have an average TOC content of at least 1% and 10-15% contribution from Type II kerogen, in which case economically feasible oil and gas deposits may occur mainly in the Cretaceous sandstone. Potential hydrocarbon traps in the Mannar Basin include tilted/rotated fault blocks, anticlinal closures, channel fills and stratigraphic pitchouts. Igneous rocks interbedded with sandstone may also act as hydrocarbon traps and seals. Both vertical and lateral drainage system might have occurred in the Mannar Basin. An active petroleum system exists in the Mannar Basin**.**

5. SUMMARY

The Gulf of Mannar is located between the southeastern coast of India and the western coastline of Sri Lanka. The Sri Lankan sector of the gulf is called the Mannar Basin. It extends over around 45000 km^2 in 20 m to more than 3000 m water depths. The basin has the Holocene to probably Late Jurassic or earlier sedimentary rocks. The sediment thickness ranges from 4 km in shallow water depths in the northern part of the Mannar Basin to more than 6 km in the deep water areas towards the south. The basin has rift structure. The rifting has started probably in the late Aptian and has ended at the end of the Cretaceous. The rifting period has been about 50 Ma. There have been a several episodes of massive basaltic lava flows in the Mannar Basin during the Maastrichtian. This event seems to be synchronous with the Deccan eruptions in India. The basin has entered a thermal sag phase in early Palaeocene. During rifting, the Sri Lankan landmass has undergone a counterclockwise rotation, acting the northern part of the island as a pivot. Therefore, the crustal extension in the southern part of the Gulf of Mannar has been higher than that in the northern part. Pop up structures appear in the seismic data suggests the Mannar Basin to have experienced compressional tectonics in the latter part of the basin development.

The Mannar Basin has been an exploration frontier with only Pearl-1 well drilled in shallow water depths in 1981. In 2011, Cairn Lanka Private Limited (CLPL), having received an exploration license from the Sri Lankan Government for an exploration block in the northern part of the Mannar Basin, drilled three exploration wells. Two of these wells, the Dorado and Barracuda, encountered natural gas bearing sandstones. This was the first time that hydrocarbon was discovered in Sri Lanka an in the Gulf of Mannar. The discovery confirmed the occurrence of an active petroleum system in the gulf. However, geology, geological history and petroleum system of this exploration frontier is poorly understood. The objective of this research is to understand these aspects of the Mannar Basin. Drill cutting samples from the Dorado, Dorado-North and Barracuda wells, the well completion report for the Pearl-1 well and the seismic data acquired by TGS in 2001 were collected for this study.

The results of the initial study show that drill cutting samples from the Dorado, Dorado-North and Barracuda wells have contaminated with diesel based drilling fluid. Therefore, the cutting samples are not suitable for biomarker studies and Rock Eval pyrolysis. Pulverised cutting samples used for elemental analysis to determine total organic carbon (TOC) were washed with methanol and dichloromethane in 2:1, 1:1 and 0:1 volume ratio three times in an ultra-sonication bath each time for 15 minutes to remove drilling oil. This seems a successful method to remove drilling oil contamination in cutting samples, used for elemental analysis. Maturity and source character data indicate that none of the wells drilled in the Mannar Basin

have penetrated potential source rocks, which could be Early Cretaceous and older sedimentary rocks. Therefore, further study of drill cuttings will not give an insight into the petroleum system of the Mannar Basin. As a result, the focus of the study was shifted to two dimensional (2D) basin and petroleum system modeling. The SIGMA-2D basin modeling software of Japanese Oil, Gas and Metals National Corporation (JOGMEC) was used in this study.

Modeling results suggest that the geothermal gradient in the northern Mannar Basin is 24.4^{o}C/km. The present day heat flows in the Mannar Basin vary from 33 to 40 mW/m^2. The present-day heat flows in the northern Mannar Basin are relatively lower than that in the adjacent Indian waters. The heat flow history of the Mannar Basin was predicted, assuming that it has a heat flow history of a typical rift basin. The maximum heat flows at the end of rifting in the Pearl-1 and Dorado-North well locations are around 68.2 and 71.1 mW/m^2, respectively. The Campanian to present sediment in the northern Mannar Basin, which has been derived from vascular land plants, is rich in type III and IV kerogen and has poor hydrocarbon source potential. If the Santonian to Cenomanian sediment has good source potential it could have expelled relatively smaller quantity of oil and natural gas. The productivity of this stratigraphic interval increases from north to south of the Mannar Basin. Due to no well penetration, the source character of the Early Cretaceous to older sediment, the potential hydrocarbon source rocks in the Mannar Basin, is unknown. In the event of the Early Cretaceous to older sediment having good hydrocarbon source potential, oil and gas could have been expelled mainly during the Late Cretaceous, which is followed by a couple of minor expulsion phases in the Palaeogene and in the Neogene. The time lag between oil generation and expulsion is around 5 Ma. Oil cracking starts at 120-140 ^{o}C. Even if the deeply buried sediment has poor hydrocarbon source potential of around 0.5% TOC content and only Type III kerogen they may still give rise to economically viable gas deposits. Potential source rocks in the Mannar Basin could have an average TOC content of at least 1% and 10-15% contribution from Type II kerogen. In this case, economically feasible oil and gas deposits could occur mainly in the Cretaceous sandstone. Potential hydrocarbon traps in the Mannar Basin include tilted/rotated fault blocks, anticlinal closures, channel fills and stratigraphic pitchouts. Igneous rocks interbedded with sandstone may also act as hydrocarbon traps and seals. Both vertical and lateral drainage system might have occurred in the Mannar Basin.

ACKNOWLEDGEMENT

I am thankful to;

1. Prof. Noriyuki Suzuki for accepting me as one of his Ph.D students, sound guidance, words of encouragement and support provided throughout the degree course,
2. Other academic staff members of the Division of Earth and Planetary System Sciences for their valuable review comments, words of encouragement and support,
3. Prof. Nalin Rathnayake for introducing and recommending me to Prof. Suzuki, words of encouragement and support,
4. staff of the Office of International Academic Support (OIAS), the Educational Affairs Section and the Dean's Office at the Graduate School of Science and the Office of International Affairs (OIA) in the Hokkaido University for their support,
5. Dr. Kenta Asahina and Dr. Hiroyuki Saito, present and former project assistant professors, respectively at Creative Research Institution (CRIS) in the Hokkaido University for their support,
6. Ms. Naoko Kanou and Ms. Mizue Asarashi current and former secretaries, respectively to Prof. Suzuki for their support,
7. Mr. Saliya Wickramasooriya, the Director General of the Petroleum Resources Development Secretariat (PRDS) in Sri Lanka for providing samples and data for this research and granting permission to publish manuscripts,
8. Ms. Preeni Vithanage, Mr. Chaminda Kularathne and Mr. Damsith Weerasinghe of PRDS for their support,
9. Mr. Kosuke Nakamura of Hokkaido University for preparing thin sections of igneous rock cuttings,
10. my colleagues in the Division of Earth and Planetary System Sciences for their words of encouragement and support,
11. Hokkaido University Special Grant Program for Young Foreign Scientists for providing financial support for this research,
12. Japan Petroleum Exploration Co., Ltd. (JAPEX). A part of this research was funded by a donation from JAPEX,
13. Michiko Seki International student's Support Fund of the Hokkaido University for covering out of pocket expenses of a surgery that I had to undergo during my stay in Japan,
14. Sapporo English Medical Interpreters (SEMI) for their voluntary interpreter service and other valuable information provided during my wife's pregnancy and postnatal period,
15. my beloved wife for I could not have reached this milestone without her words of encouragement and support.

REFEENCES

AL-HAJERI, M.M., AL SAEED, M., DERKS, J., FUCHS, T., HANTSCHEL, T., KAUERAUF, A.,…. PETERS, K., 2009. Basin and Petroleum System Modeling. Oil Field Review, **21**(2), 14-29.

ALLEN, P.A., and ALLEN, R.A., 1990. Basin Analysis: Principles and Applications. Blackwell Publishing, Oxford. Second Edition, 549 pp.

APLIN, A.C., and LARTER, S.R., 2005. Fluid flow, pore pressure, wettability, and leakage in mudstone cap rocks. In: BOULT, P. and KALDI, J. (Eds.) Evaluating fault and cap rock seals, AAPG Hedberg Series **2**, 1– 12.

ARTHUR, M.A., SCHLANGER, S.O., and JENKYNS, H.C., 1987. The Cenomanian-Turonian Oceanic Anoxic Event, II. Palaeoceanographic controls on organic-matter production and preservation. Geological Society, London, Special Publications, **26**, 401-420.

ATHY L.F., 1930. Density, porosity and compaction of sedimentary rocks, AAPG Bulletin., **14**, 1-24.

BAILLIE, P.W., SHAW, R.D., LIYANAARACHCHI, D.T.P., and JAYARATNE, M.G., 2003. A New Mesozoic sedimentary basin, offshore Sri Lanka. Proceedings of EAGA 64th Conference & Exhibition, Florence, Italy. 4pp.

BLACKWELL, D.D., and STEELE, J.L., 1989, Heat flow and geothermal potential of Kansas: Kansas Geological Survey Bulletin **226**, 267–295.

BURNHAM, A.K., 1989. A simple kinetic model of petroleum formation and cracking, Lawrence Livermore Laboratory Report UCID-21665.

CHAPMAN, D.S., H.KEHO, T., BAUER, M.S., and PICARD, M.D., 1984. Heat flow in the Uinta Basin determined from bottom hole temperature (BHT) data, Geophysics, **49,** 453-466.

CHANDRA, K., PHILIP, P.C., SRIDHARAN, P., CHOPRA, V.S., RAO, B., and SAHA, P.K., 1991. Petroleum source-rock potentials of the Cretaceous transgressive-regressive sedimentary sequences of the Cauvery Basin. Journal of Southeast Asian Earth Sciences, **5** (1-4), 367-371.

CANTWELL, T., BROWN, T.E., and MATHEWS, D.G., 1978. Petroleum Geology of the Northwest Offshore Area of Sri Lanka. Proceedings of South Asian Petroleum Society Session, Singapore.

CHARI, N.M.V., SAHU, J.N., BNERJEE, B., ZUTSHI, P.L., and KULDEEP, C., 1995. Evolution of the Cauvery basin, India from subsidence modeling. Marine and Petroleum Geology, **12** (6), 667-675.

COLLINS, C., 2007. Implementing Phytoremediation of Petroleum Hydrocarbons, Methods in Biotechnology., **23,** 99–108.

COORAY, P.G., 1984. An introduction to geology of Sri Lanka (Ceylon). National Museum of Ceylon, 340 p.

COORAY, P.G., 1994. The Precambrian of Sri Lanka: a historical review. Precambrian Research, **66**, 3–18.

CURRAY, J.R., 1984. Sri Lanka: is it a mid-plate platelet? Journal of NARA **31**, 30-50.

DANDEKER, A.Y., 2013. Petroleum reservoir rock and fluid properties. CRC Press, Taylor and Francis Group, 544p.

DARANIYAGALA, P.E.P., 1939. A carbonaceous Jurassic shale from Ceylon. Ceylon Journal of Science, **B21** (3), 193-194.

DE SILVA, N.R., 2006. Compressional tectonics and oil fields offshore Sri Lanka. Proceedings of AAPG International Conference & Exhibition, Perth Western Australia.

DIEDERIX, K.M., 1982. Anomalous relationships between resistivity index and water saturations in the Rotliegend sandstone (the Netherlands) In: NELSON P.H., 1994. Permeability porosity relationships in sedimentary rocks. The log Analyst, **35,** 38-62.

DOYEN, P.M., 1988. Permeability, conductivity, and pore geometry of sandstone. Journal of Geophysical Research, **93**, 7729–7740

EDIRISOORIYA, G., and DHARMAGUNAWARDHANE, H.A., 2013. Plant Insect-Interactions in Jurassic Fossil Flora from Sri Lanka. International Journal of Scientific and Research Publications, **3** (1), 1-13.

ENGLAND, W.A., and FLEET, A.J., 1991. Petroleum migration: The Geological Society Special Publication, **59**: London.

EPPELBAUM**,** L., KUTASOV, I., and PILCHIN**,** A., 2014. Applied Geothermics. Springer, 783p.

ESPITALIÉ, J., MADEC, M., TISSOT, B., MENNIG, J.J., and LEPLAT, P., 1977. Source rock characterization method for petroleum exploration. Proceedings of the 9th Annual Offshore Technology Conference, **3**, 439-448.

FUNNELL, R., CHAPMAN, D., ALLIS, R., and AMSTRONG, P., 1996. Thermal state of the Taranaki Basin, New Zealand, Journal of Geophysical Research, **101**, 25197-25215.

FUTALAN, K., MITCHELL1, A., AMOS, K., and BACKE, G., 2012. Seismic Facies Analysis and Structural Interpretation of the Sandakan Sub-basin, Sulu Sea, Philippines. AAPG Search and Discovery Article #30254.

HANTSCHEL, T., and KAUERAUF, A.I., 2009. Fundamentals of Basin and Petroleum Systems Modeling, Springer-Verlag Berlin Heidelberg, 469p.

HOSSAIN, MD. A., SUZUKI, N., MATSUMOTO, K., SAKAMOTO, R. and TAKEDA, N., 2014. In-reservoir fractionation and the accumulation of oil and condensates in the Surma Basin, NE Bangladesh. Journal of Petroleum Geology, **37(3)**, 269-286.

HORAI, K., 1971. Thermal conductivity of rock-forming minerals, Journal of Geophysical Research**, 76,** 1278-1308.

ISMAIL, M., and SHAMSUDDIN, A.H.M., 1991. Organic matter maturity and its relation to time, temperature and depth in the Bengal Fore deep, Bangladesh, of Southeast Asian Earth Sciences, **5(1-4)**, 381-390.

JASPER, J., and GAGOSIAN, R.B., 1990. The sources and deposition of organic matter in the Late Quaternary Pigmy Basin. Gulf of Mexico Geochimica et Cosmochimica Acta **54**, 1117-l 132.

KRÖNER, A., WILLIAMS, I.S., COMPSTON, W., BAUR, N., VITANAGE, P.W., and PERERA, L.R.K., 1987. Zircon ion microprobe dating of Precambrian high-grade rocks in Sri Lanka. Journal of Geology, **95**, 775-791.

KRÖNER, A., KEHELPANNALA, K.V.W., and HEGNER, E., 2003. Ca. 750-1100 Ma magmatic events and Grenville - age deformation in Sri Lanka: relevance for Rodinia supercontinent formation and dispersal, and Gondwana amalgamation. Journal of Asian Earth Sciences, **22**, 279-300

LAL, N.K., SIAWAL, A., and KAUL, A.K., 2009. Evolution of east coast of India-A plate tectonic reconstruction. Journal Geological Society of India, **73**, 249-260.

LEE, Y., and DEMING, D., 1998. Evaluation of Thermal conductivity temperature corrections applied in terrestrial heat flow studies. Journal of Geophysical Research, **103** (B2), 2447-2454.

LINDGREEN, H., FALLICK, A.E., JAKOBSEN, F., and SPRINGER, N., 2012. The tight Danian Ekofisk chalk reservoir formation in the south Arne field, North Sea: mineralogy and porosity properties. Journal of Petroleum Geology, **35(3)**, 291–309.

LUCIA, P.J., 1983, Petrophysical parameters estimated from visual descriptions of carbonate rocks a field classification of carbonate pore space. In: NELSON, P.H., 1994.

Permeability-Porosity Relationships in Sedimentary Rocks. The log analysis, **35**, 38-62.

MAKHOUS, M., and GALUSHKIN, Y., 2005. Basin analysis and modeling of the burial, thermal and maturation histories in sedimentary basins. Paris, Editions TECHNIP, 380p.

MCKENZIE, D., 1978. Some remarks on the development of sedimentary basins. Earth and Planetary Science Letters, **40**, 25-32.

MILES, J.A., 1994. Illustrated Glossary of Petroleum Geochemistry. Oxford University Press, 146pp.

MITCHUM JR., R.M., 1977. Seismic stratigraphy and global changes of sea level, part 11: glossary of terms used in seismic stratigraphy. In: PAYTON, C.E. (Ed.), Seismic Stratigraphy – Applications to Hydrocarbon Exploration. AAPG Memoir, **26**, 205-212.

MOHAPATRA, P., SRINIVAS, M., KUMAR, N., ROUTRAY, P., ADHIKARI, S., and DALY, C., 2012. The geology and petroleum systems of the Mannar Basin, Sri Lanka. Proceedings of AAPG International Conference & Exhibition, Singapore.

MONEY, N.J., and COORAY, P.G., 1966. Sedimentation in the Tabbowa beds of Ceylon. Journal of the Geological Society of India **7**, 134-141.

OKUI, A., and WAPLES, D.W., 1993. Relative permeabilities and hydrocarbon expulsion from source rocks. In: DARE, A.G., AUGUSTON, J.H. HERMANRUD, C., STEWART D.J., and SYLTA, Ø. (Eds.), Basin Modelling, Advances and Applications (Norw. Petrol. Sot. Pub/. No. 3, Elsevier, Amsterdam, 293-301.

OKUI, A., HARA, M., FU, H., and TAKAYAMA, K., 1996. SIGMA-2D: A simulator for the integration of generation, migration, and accumulation of oil and gas. In: OKUI, A. 1998. Petroleum system evaluation by basin modeling. Journal of the Japanese Association for Petroleum Technology, **63**(1), 78-91.

OKUI, A., 1998. Petroleum system evaluation by basin modeling. Journal of the Japanese Association for Petroleum Technology, **63**(1), 78-91.

PARSONS, B., and SCLATER, J.G., 1977. An analysis of the variation of ocean floor bathymetry and heat flows with age. Journal of Geophysical Research, **82** (5), 803-827.

PAYTON, C.E., 1977. Seismic Stratigraphy-Applications to hydrocarbon exploration. AAPG Memoir **26**,

PELLERIN, F.M., and ZINSZNER, B., 2007. Geoscientist's guide to petrophysics, Editions Technip, 381p.

PEPPER, A.S., and CORVI, P.J., 1995a. Simple kinetic models of petroleum formation. Part I: oil and gas generation from kerogen. Marine and Petroleum Geology, **12**, (3), 291-319.

PEPPER, A.S., and CORVI, P.J., 1995b. Simple kinetic models of petroleum formation. Part III: Modeling an open system. Marine and Petroleum Geology, **12**, (4), 417-452.

PEPPER, A.S., 1991. Estimating the petroleum expulsion behavior of source rocks: a novel quantitative. The Geological Society Special Publication, **59**, 9-31.

PETERS, K.E., 1986. Guidelines for evaluating petroleum source rock using programmed pyrolysis. In: SYKES, R. and SNOWDON, L.R., 2002. Guidelines for assessing the petroleum potential of coaly source rocks using Rock-Eval pyrolysis. Organic Geochemistry **33**, 1441–1455.

PETERS, K.E., and CASSA., M.R., 1994. Applied source rock geochemistry. In MAGROON, L.B., and DOW, W.G., (Eds.) The petroleum system- from source to trap: AAPG Memoir **60**. 93-120.

PETERS, K.E., WALTERS, C.C., and MOLDOWAN, J.M., 2007. The biomarker guide: biomarkers and isotopes in the environment and human history, Cambridge University Press, **1**, 471 p.

PETERSEN H.I., 2002. A reconsideration of the "oil window" for humic coal and kerogen type III source rocks. Journal of Petrol Geology **25**(4), 407–432.

PITMAN, W.C., 1978. The relationship between eustacy and stratigraphic sequences of passive margins. Geological Society of America Bull., 89 **(9)**, 1389-1403.

PREMARATHNE, D.M.U.A.K., 2008. Petroleum Potential of Sri Lankan Cauvery Basin. Proceedings of 24th Annual technical sessions of the Geological Society of Sri Lanka, 7.

PREMARATHNE, D.M.U.A.K., Suzuki, N., Rathnayake, N.P., and Kularathne, E.K.C.W., 2013. A petroleum System in the Gulf of Mannar Basin, Offshore Sri Lanka. Proceedings of 29th annual technical sessions of Geological Society of Sri Lanka, 9-12.

PREMARATHNE, U., SUZUKI, N, RATHNAYAKE, N., and KULARATHNE, C., 2015. Burial and thermal history of the Mannar Basin, offshore Sri Lanka (in review).

PROSELKOV, Y.M., 1975. Heat transfer in wells. In: EPPELBAUM**,** L., KUTASOV, I., and PILCHIN, A., (Eds.): Applied Geothermics. Springer, 783p.

RAJU, D.S.N., JAIPRAKASH, B.C., RAVINDRAN, C.N., KALYANSUNDAR, R., and RAMESH, P., 1994. The magnitude of hiatuses and sea level changes across K/T

boundary in Cauvery and Krishna-Godavari basins. Journal of Geological Society of India, **44**, 301-315.

RAMKUMA, M., STÜBEN, D., and BERNER, Z., 2011. Barremian-Danian chemostratigraphic sequences of the Cauvery Basin, India: Implications on scales of stratigraphic correlation. Gondwana Research, **19**, 291-309.

RANA, M.S., CHAKRABORTY, C., SHARMA, R., and GIRIDHAR, M., 2008. Mannar Volcanics- implications for Madagascar Breakup. Proceedings of 7th International Conference and Exposition on Petroleum Geophysics, Hyderabad, 358.

RAO, M.V., CHIDAMBARAM, L., BHARKTYA, D., and JANARDHANAN, M., 2010. Integrated Analysis of Late Albian to Middle Miocene Sediments in Gulf of Mannar Shallow Waters of the Cauvery Basin, India: A Sequence Stratigraphic Approach. Proceedings of 8th biennial international conference and exposition on petroleum geophysics, 9p

RATNAYAKE, A.S., SAMPEI, Y., and KULARATHNE, C.W., 2014. Stratigraphic responses to major depositional events from the Late Cretaceous to Miocene in the Mannar Basin, Sri Lanka. Journal of Geological Society of Sri Lanka, **16**, 5-18.

RATNAYAKE, A.S., and SAMPEI, Y., 2015. Characterization of organic matter and depositional environment of the Jurassic small sedimentary basins exposed in the northwest onshore area of Sri Lanka. Research Organic Geochemistry, **31**, 1-14.

RAVEENDRASINGHE, S.V.T.D., DHARMAGUNAWARDHANE, H.A., and DAHANAYAKE, K., 2013. Coal Potential in Jurassic Sediments, Aadigama, Sri Lanka. Proceedings of 29th Technical Sessions of Geological Society of Sri Lanka, 83-86

ROBERTSON, E. C., 1988. Thermal properties of rocks. U.S. Geological Survey, open-file report 88-441, 109p.

SANER, S., HASSAN, H.M., AL-RAMADAN, K.A., and ABDULGHANI, W.M., 2006. Mineralogical, pore and petrophysical characteristics of the Devonian Jauf sandstone reservoir, Hawiyah field, eastern Saudi Arabia. Journal of Petroleum Geology, **29(3)**, 257-272.

SASS, J.H., LACHENBRUCH, A.H., MOSES T.H. JR., and MORGAN, P., 1992. Heat flow from a scientific research well at Cajon Pass, California, Journal of Geophysical research, **97**, 5017-5030.

SASTRI, V.V., SINHA, R.N., SINGH G., and MURTHY, K.V.S., 1973. Stratigraphy and tectonics of sedimentary basins on east coast of peninsular India, AAPG Bulletin, **57**, 655- 678.

SCHLANGER, S.O., and JENKYNS, H.C., 1976. Cretaceous anoxic events: causes and consequences. In: CHANDRA, K., PHILIP, C., SRIDHARAN, P.C., CHOPRA, P., BRAHMAJI RAO, V.S., and SAHA, P.K., 199. Petroleum source-rock potentials of the Cretaceous transgressive-regressive sedimentary sequences of the Cauvery Basin. Journal of Southeast Asian Earth Sciences, **5** (1-4), pp. 367-371

SCLATER, J.G. and CHRISTIE, P.A.F., 1980. Continental Stretching: An Explanation of Post Mid-Cretaceous Subsidence of the Central North Sea," Journal of Geophysical Re-search, 85 (B7), 3711-3739.

SCLATER, J.G., JAUPART, C., and GALSON, D., 1980. The heat flow through oceanic and continental crust and the heat loss of the earth. In: ALLEN, P.A., and ALLEN, R.A., (Eds.): Basin analysis: principles and applications. Blackwell Science Ltd, 451p.

SEKIGUCHI, K., 1984. A model for determining terrestrial heat flow in oil basinal areas. Tectonophysics, **103**, 67-79.

SHANKER, R., 1988. Heat flow map of India and its geological and economic significance. Indian Minerals, **42**, 89-110.

SHANKER, R., ABSAR, A., and BAJPAI, P., 2012. Heat flow map of India – update. 21st New Zealand Geothermal Workshop, 157-162.

SHENHAV, H., 1971. Lower Cretaceous sandstone reservoirs, Israel: Petrography, Porosity and permeability. AAPG Bulletin **55 (12**), 2194-2224.

SITHOLEY, R.V., 1942. Jurassic Plants from the Tabbowa series in Ceylon Journal of Indian Botanical Society, **24**, 3-17.

SITHOLEY, R.V., 1944. Jurassic Plants from the Tabbowa series in Ceylon, Spolia Zeylanicav. **24**, 577-602

SLOSS, L.L., 1963. Sequences in the cratonic interior of North America. Geological Society of America Bulletin **74**, 93-114.

SOMERTON, W.H., 1992. Thermal properties and temperature-related behavior of rock/fluid systems. Elsevier, New York, 257 pp.

STOKER, M.S., PHEASANT, J.B., and JOSENHANS, H., 1997. Seismic Methods and Interpretation. In: DAVIES, T.A., BELL, T., COOPER, A.K., JOSENHANS, H., POLYAK, L., SOLHEIM, A., STOKER, M.S., and STRAVERS, J.A., (Eds):

Glaciated Continental Margins; An Atlas of Acoustic Images, Springer, Netherlands, 315p.

SUZUKI, N., MATSUBAYASHI, H., and WAPLES, D.W., 1993. A simpler kinetic model of vitrinite reflectance. AAPG Bulletin, **77**, 1502-1508.

SUSUKI, N., and MATSUBAYASHI, H., 1995. Kinetic models of petroleum generation and vitrinite reflectance-predicting the evolution of macro-molecular organic matter in the sedimentary basin. Chishitsu News, **487**, 52-62.

TANTRIGODA, D.A., and GEEKIYANAGE, P., 1991. An interpretation of gravity anomalies over the Adigama and Tabbowa sedimentary Basins in Northwest of Sri Lanka. Journal of National Science Foundation, Sri Lanka **19**(I), 39-51.

THOMPSON, T.L., 1976. Plate tectonics in oil and gas exploration of continental margin. In: CANTWELL, T., BROWN, T.E., and MATHEWS, D.G., 1978. Petroleum Geology of the Northwest Offshore Area of Sri Lanka, Proceedings of South Asian Petroleum Society Session.

TISSOT, B.P., WELET, R., and UNGERER, P., 1987. Thermal history of sedimentary basins, maturation indices, and kinetics of oil and gas generation. AAPG Bulletin **71**, 1445–1466.

TORSVIK, T.H., CARLOS, D., MOSAR, M., COCKS, L.R.M. and MALME, T., 2002. Global reconstructions and North Atlantic paleogeography 440 Ma to Recent In: EIDE, E.A., (Eds.): BATLAS-Mid Norway plate reconstruction atlas with global and Atlantic perspective. Geological survey of Norway, 18-39.

TURNER, J.B., 1983. Problematical petrophysical characteristics of the Smackover at Bayyou Middel Fork field ClaiborneParish, Louisiana. In: NELSON, P.H., 1994. Permeability porosity relationships in sedimentary rocks. The log Analyst, **35**, 38-62.

UNGERER, P., BESSIS, F., CHENET, P. Y., DURAND, B., NOGARET, E., CHIARELLI, A., OUDIN, J. L. and PERRIN, J.F., 1984. Geological and geochemical models in oil exploration: principles and practical examples. In: DEMAISON, G., and MURRIS, R.J., (Eds.): AAPG Memoir **35**, 53-57

UNGERER, P., DOLIGEZ, B., CHENET, P.Y., BURRUS, J., BESSIS, F., LAFARGUE, E., GIROIR, G., HEUM, S., and EGGEN, S., 1987. A 2D model of basin-scale petroleum migration by two-phase fluid flow: application to some case studies. In: Migration of Hydrocarbons in Sedimentary Basins (Ed. B. Doligez), Proceedings of the 2nd IFP Exploration Research Conference, Carcans, 15-19 June 1987, Editions Technip, Paris, 415-424

UNGERER P., BURRUS, J., DOLIGEZ, B., CHENET, P.Y., and BESSIS, F., 1990. Basin Evaluation by integrated two-dimensional modelling of heat transfer, fluid flow, hydrocarbon generation and migrated. AAPG Bulletin, **74**, 309-335.

VAIL, P.R., MITCHUM, R.M., JR, TODD, R.G., WIDMIER, J.M., THOMPSON, S III., SANGREE, J.B., BUBB, J.N., and HATLELID, W.G., 1977. Seismic stratigraphy and global changes of sea level. In: PAYTON, C.E, (Ed.) Seismic stratigraphy-application to hydrocarbon exploration. AAPG Memoir, **26**, 49-212.

WAPLES, D.W., 1994. Maturity Modeling : Thermal Indicators, Hydrocarbon Generation, and Oil Cracking. In: MAGOON, L.B, and DOW, W.G., (Eds.): the petroleum system-from source to trap: AAPG Memoir **60**.

WAPLES, D.W., 2001. A new model for heat flow in extensional basins: radiogenic heat, asthenospheric heat, and the McKenzie model. Natural Resources Research, **10** (3), 227-238.

WATTS, A.B., and STECKLER, M.S., 1979. Subsidence and eustasy at the continental margin of eastern North America. 3rd series of Moris Edwads symposium, American Geological Union, 218-234.

WAYLAND, E.J., 1920. Preliminary note on some fossiliferrous beds in Ceylon. Spolia Zeylanica, **11**, 191-197.

WENDT, W.A., SAKURAI, S., and NELSON P.H., 1986. Permeability prediction from well logs using multiple regression In: NELSON, P.H., 1994. Permeability porosity relationships in sedimentary rocks. The log Analyst, **35**, 38-62.

WOODSIDE, W., and MESSMER, J.H., 1961. Thermal conductivity of porous media: I. Unconsolidated sands, Journal of Applied Physics, **32**, 1688–1699.

YANG, Y., and APLIN, A.C., 2010. A permeability–porosity relationship for mudstones Marine and Petroleum Geology **27**, 1692-1697.

YOSHIDA, M., FUNAKI, M., and VITANAGE, P.W., 1992. Proterozoic to Mesozoic east Gondwana: the juxtaposition of India, Sri Lanka, and Antarctica. Tectonics, **11**(2), 381-391.

ZAKHAROV, Y.D., SHIGETA, Y., NAGENDRA, R., SAFRONOV, P.P., SMYSHLYAEVA, O.P., POPOV, A.M., VELIVETSKAYA, T.A. and AFANASYEVA, T.B., 2009. Cretaceous climatic oscillations in the southern palaeolatitudes: new stable isotope evidence from India and Madagascar. In: Hart, M.B. (Ed.), 8th International Symposium on the Cretaceous System, University of Plymouth, p 3.

ZENG, H., 2013. Frequency dependant seismic stratigraphic-stratigraphic and facies interpretation. AAPG Bulletin, **97**(2), 201-221.

Appendices

Appendix A: Details of cutting samples collected for this study from PRDS

Well Name	Depth Interval (m)	Total No. of Samples
Dorado	2150-2400	25
	2400-2645	25
	Side Tracking	
		48
	2620-2780	32
	2780-2940	32
	2940-3100	32
	3100-3260	32
	3260-3288	6
	TOTAL	**232**
Barracuda	2139-2300	16
	2300-2460	16
	2460-2620	16
	2620-2780	16
	2780-2940	16
	2940-3100	16
	3100-3260	16
	3260-3420	16
	3420-3570	16
	3570-3730	16
	3730-3890	16
	3890-4050	16
	4050-4210	16
	4210-4370	16
	4370-4530	16
	4530-4690	16
	4690-4740	5
	TOTAL	**261**
Dorado-North	2200-2400	20
	2400-2600	20
	2600-2800	20
	2800-3000	20
	3000-3200	20
	3200-3400	20
	3400-3560	16
	3560-3622	6
	TOTAL	**142**

Appendix B: Total organic carbon (TOC) data for Pearl-1 (from unpublished reports held at PRDS), Dorado, and Barracuda wells. Depth is in meters (m) blow mean sea level (MSL)

Pearl-1				Dorado				Barracuda	
Depth (m)	TOC (wt.%)		Depth (m)		TOC (wt.%)		Depth (m)		TOC (wt.%)
345	0.04	2170	–	2180	1.85	4300	–	4310	1.30
586	0.26	2220	–	2230	2.03	4310	–	4320	1.63
673	0.07	2240	–	2250	2.52	4340	–	4350	0.96
761	0.07	2260	–	2270	1.95	4370	–	4380	0.70
808	0.13	2330	–	2340	1.41	4390	–	4400	0.72
847	0.04	2380	–	2390	1.61	4410	–	4420	2.44
895	0.36	2420	–	2430	1.19	4440	–	4450	0.90
1042	0.37	2430	–	2440	1.17	4450	–	4460	1.21
1156	0.69	2470	–	2480	0.89	4460	–	4470	1.04
1210	0.58	2480	–	2490	1.13	4480	–	4490	2.18
1222	0.88	2520	–	2530	0.59	4500	–	4510	0.89
1234	1.00	2530	–	2540	1.02	4520	–	4530	1.57
1282	0.32	2550	–	2560	1.70	4540	–	4550	0.44
1334	0.08	2560	–	2570	1.33	4550	–	4560	1.47
1342	0.58	2570	–	2580	0.99	4590	–	4600	0.76
1361	0.98	2590	–	2600	1.11	4600	–	4610	0.77
1380	0.48	2620	–	2630	1.16	4620	–	4630	1.83
1393	0.17	2640	–	2650	1.19	4640	–	4650	0.68
1404	0.46	2660	–	2670	2.36	4650	–	4660	0.86
1411	0.68	2690	–	2700	0.59	4670	–	4680	2.13
1419	0.58	2730	–	2740	0.65	4690	–	4700	1.39
1426	1.05	2760	–	2770	1.12	4710	–	4720	0.64
1434	0.39	2770	–	2780	1.22	4720	–	4730	0.82
1441	0.66	2790	–	2800	0.85	4730	–	4740	1.26
1449	2.36	2810	–	2820	0.53				
1456	0.37	2860	–	2870	0.92				
1461	0.23	2880	–	2890	0.88				
1468	0.24	2930	–	2940	1.16				
1601	0.62	2960	–	2970	1.04				
1763	0.06	3000	–	3010	1.32				
1892	0.01	3010	–	3020	1.32				
1994	0.17	3030	–	3040	0.92				
2028	0.58	3100	–	3110	0.66				
2305	0.08	3110	–	3120	0.44				
2378	0.19	3120	–	3130	0.93				
2615	0.79	3130	–	3140	0.87				
2674	0.54	3140	–	3150	0.93				
2765	2.55	3150	–	3160	0.84				

2844	0.18	3160	–	3170	0.64
2866	0.32	3170	–	3180	0.71
2871	0.19	3190	–	3200	1.82
2907	0.37	3240	–	3250	0.30
2915	0.56				
2920	0.48				
2928	0.23				
2933	0.69				
2942	0.45				
2945	0.78				
2947	0.21				
2948	0.44				

Appendix C

Timing and quantity of hydrocarbon generation

App. C1. Hydrocarbon generation in Pearl-1 well under pessimistic scenario (TOC = 0.5% and Type III kerogen = 100%)

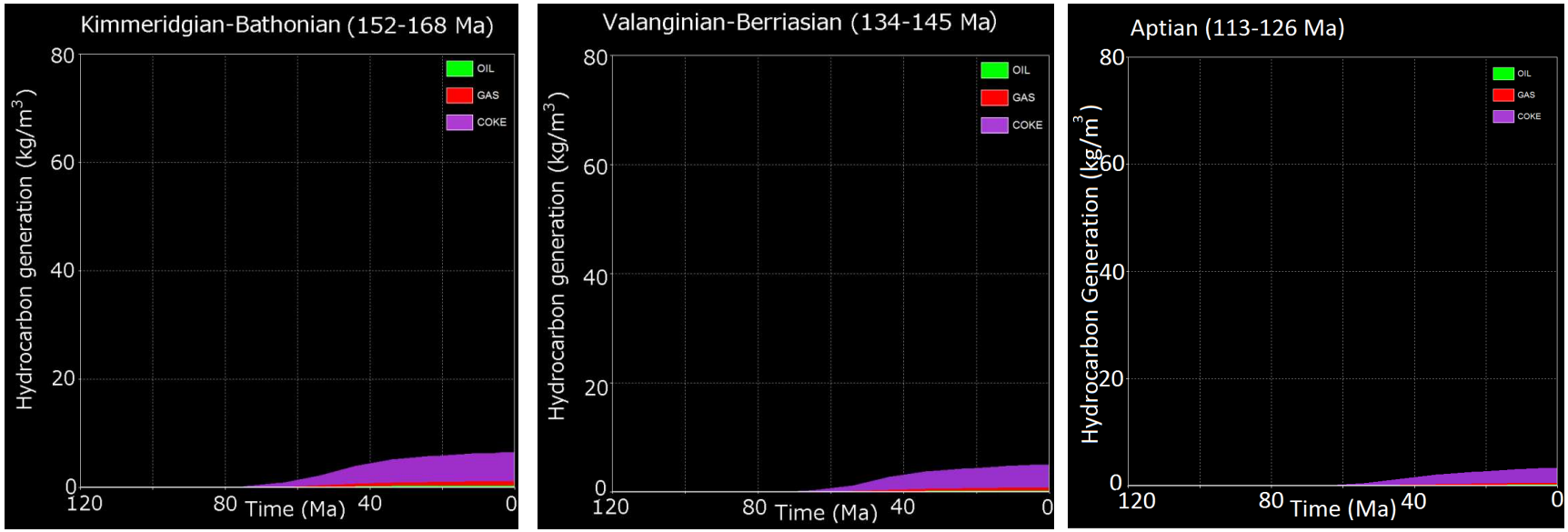

App. C2. Hydrocarbon generation in the Dorado-North well under pessimistic scenario (TOC = 0.5% and Type III kerogen = 100).

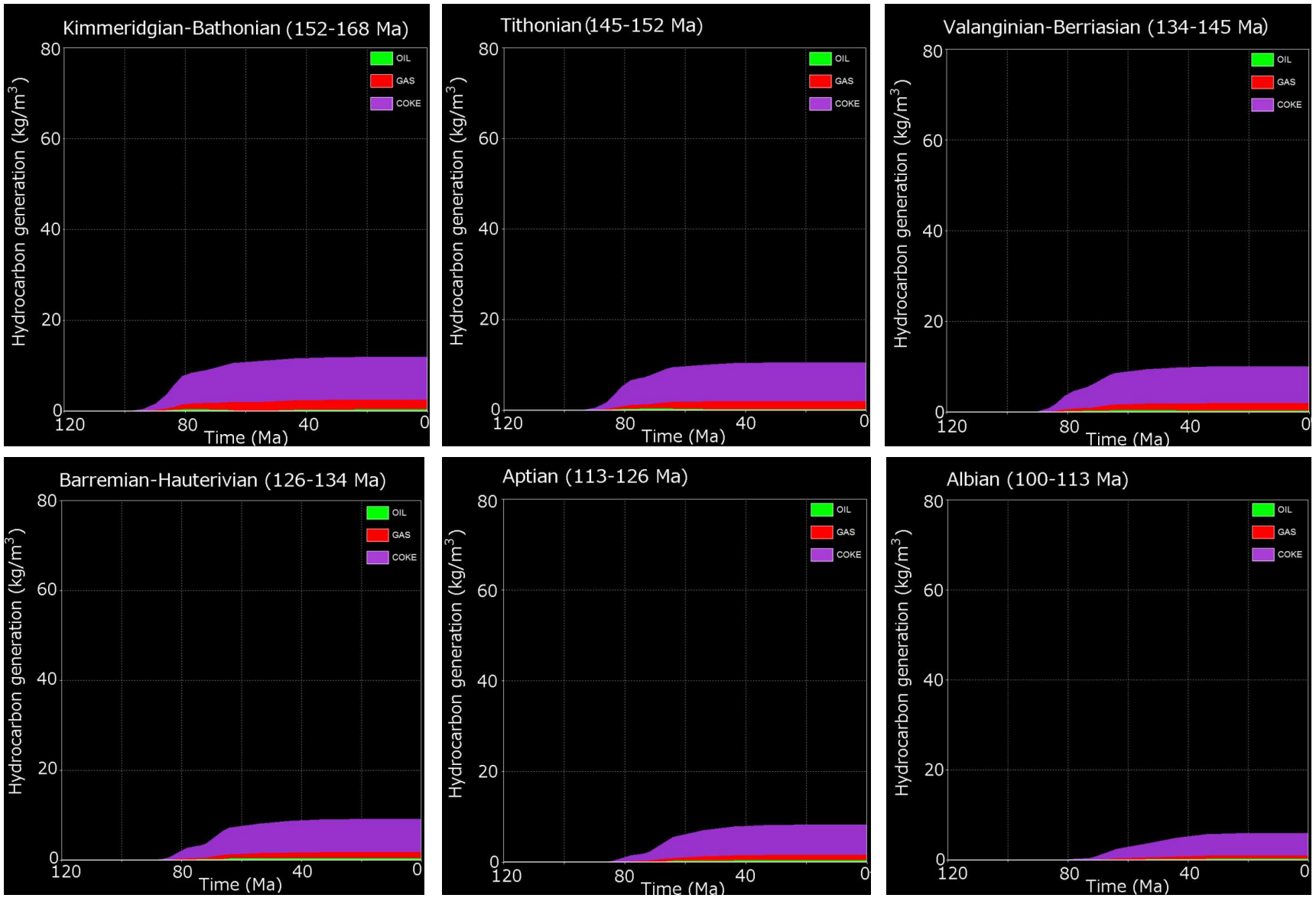

Hydrocarbon generation in Dorado-North well cont……..

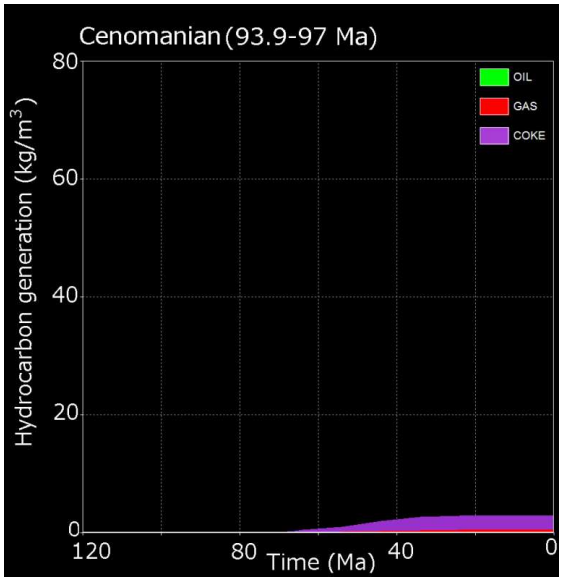

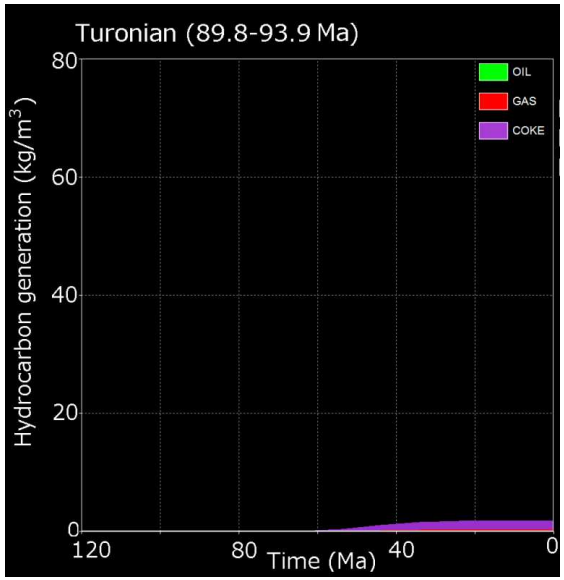

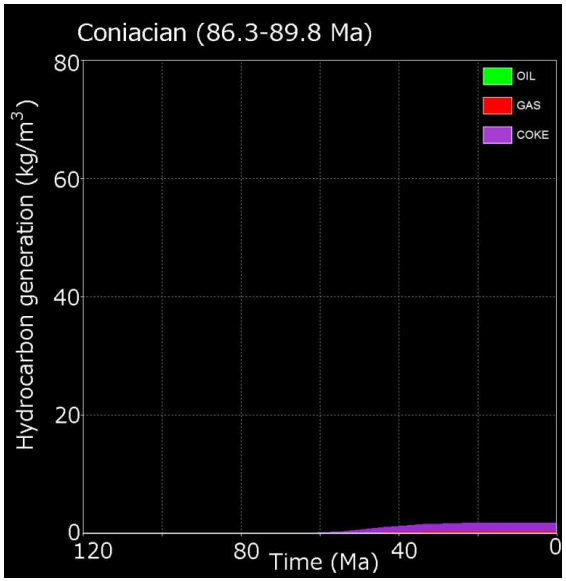

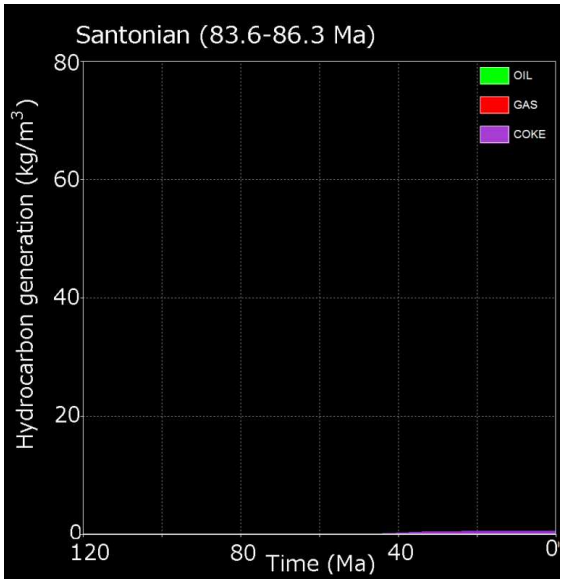

App. C3. Hydrocarbon generation in Pseudo Mannar Deep well under pessimistic scenario (TOC = 0.5% and Type III kerogen = 100).

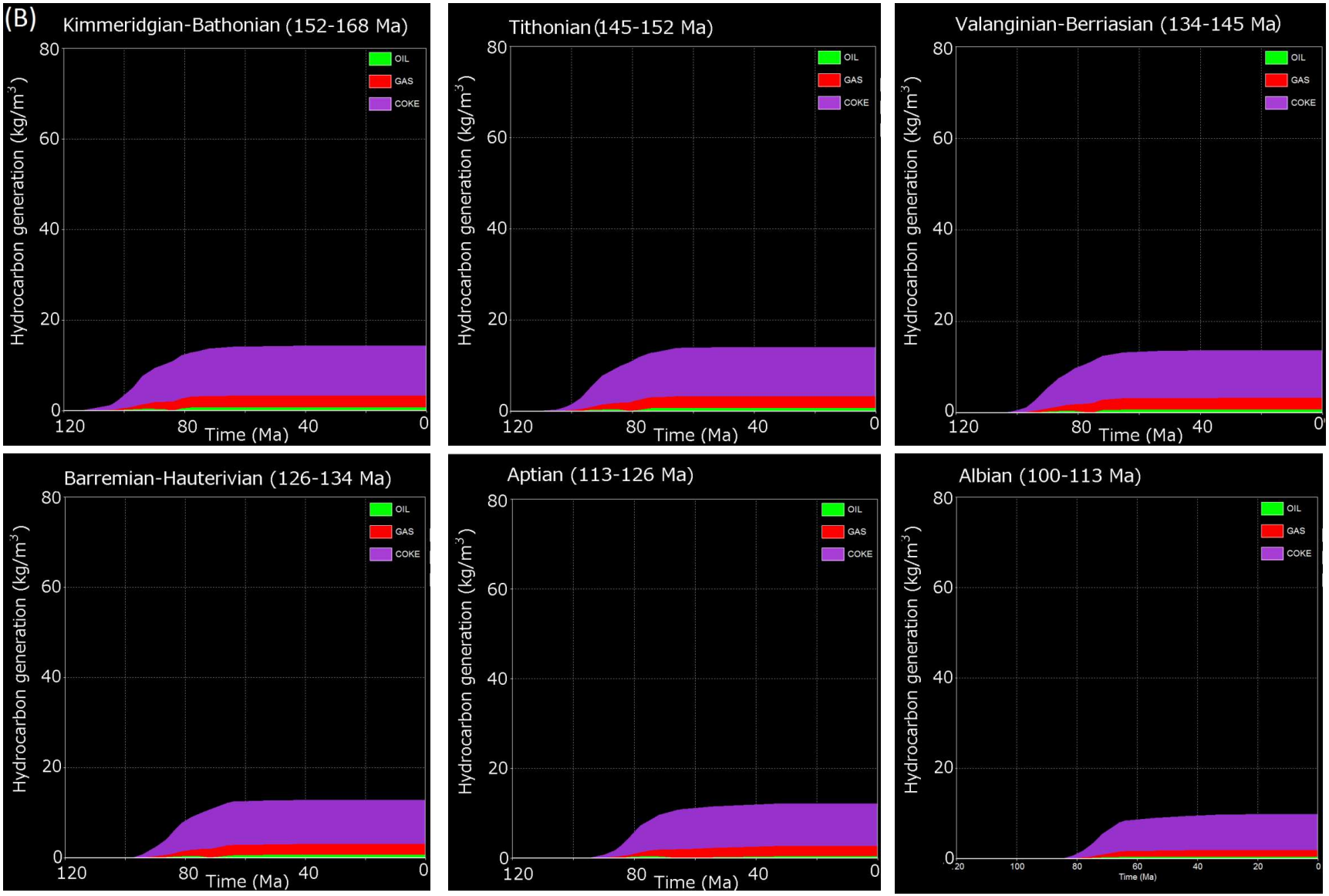

Hydrocarbon generation in Pseudo Mannar Deep well cont……..

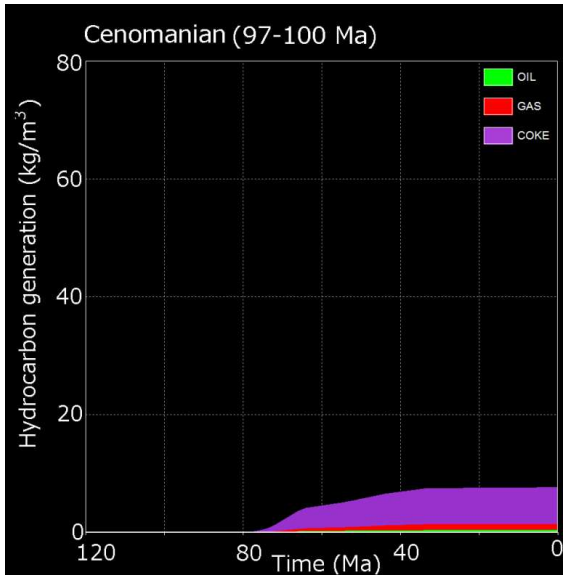

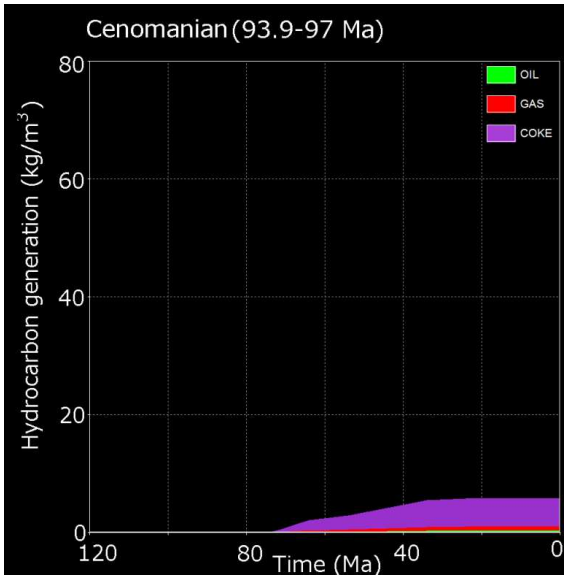

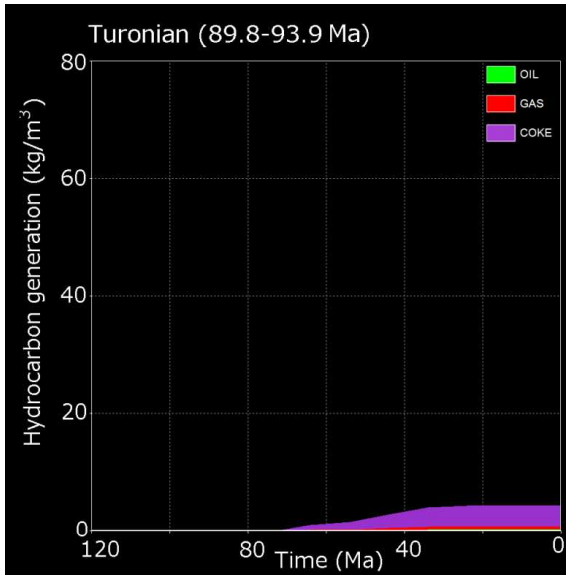

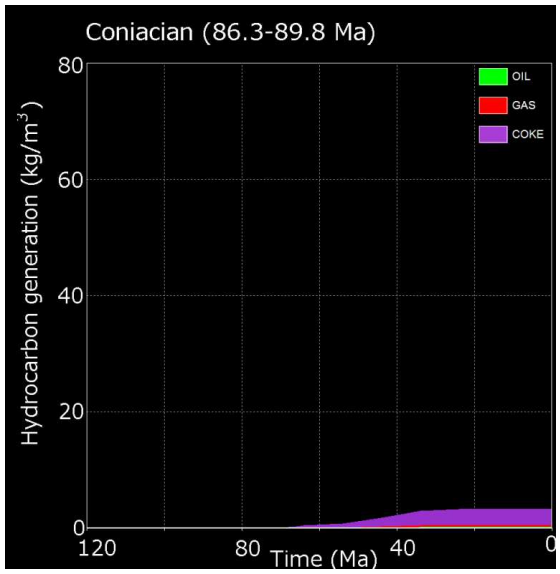

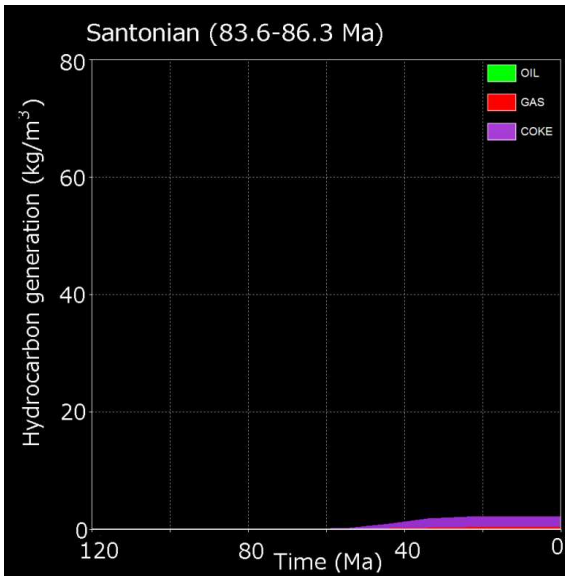

App. C4. Hydrocarbon generation in Pearl-1 well under optimistic scenario (TOC = 2.5% and Types II and III kerogen = 50% each).

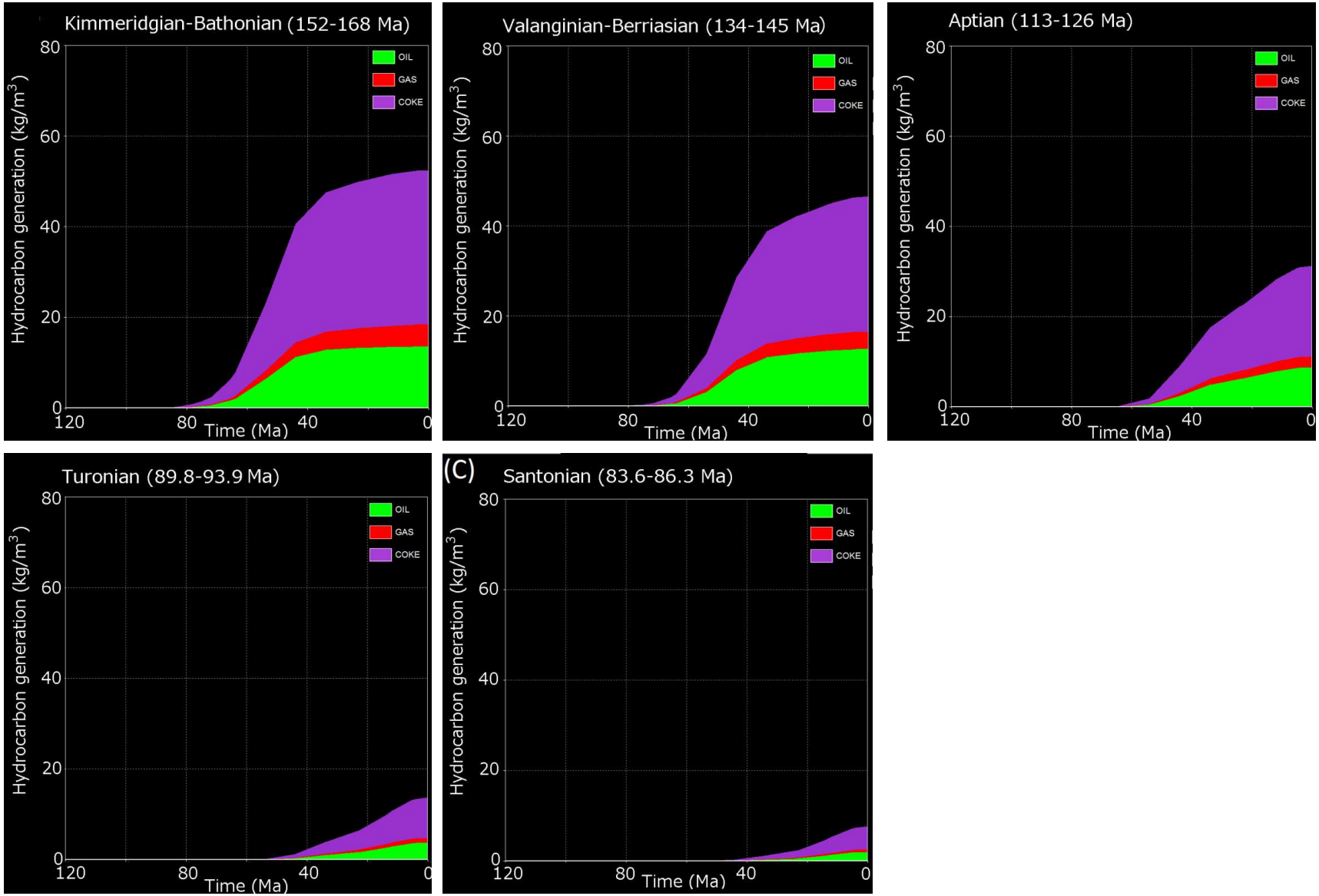

App. C5. Hydrocarbon generation in Dorado-North well under optimistic scenario (TOC = 2.5% and Types II and III kerogen = 50% each).

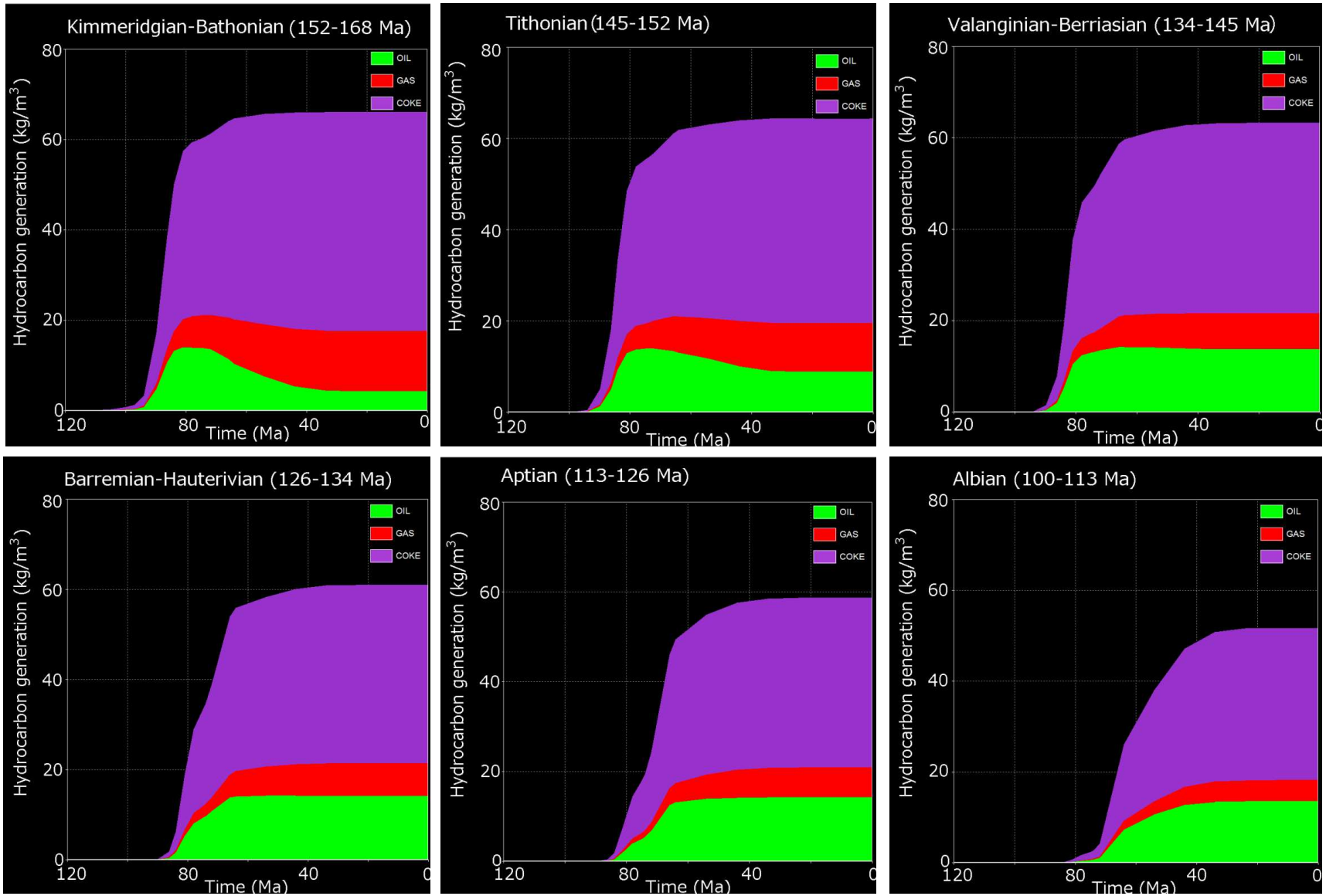

Hydrocarbon generation in Dorado-North well cont…..

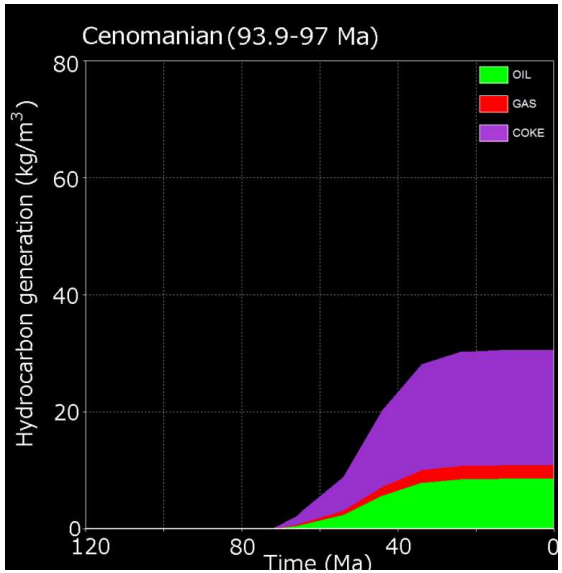

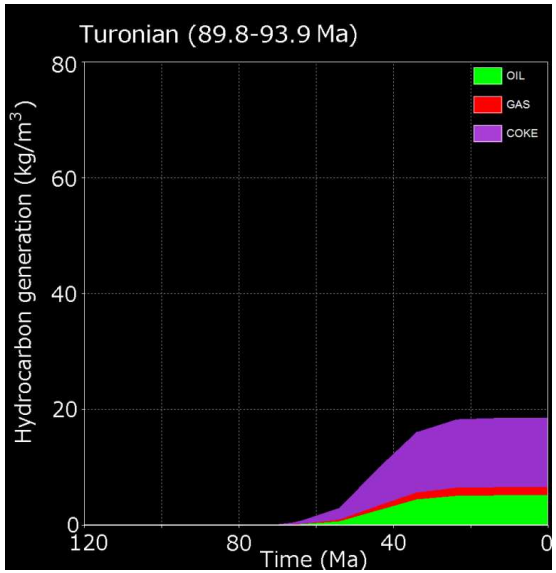

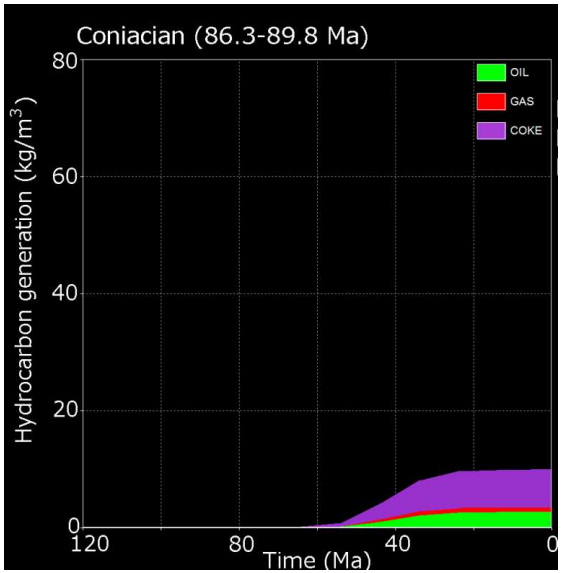

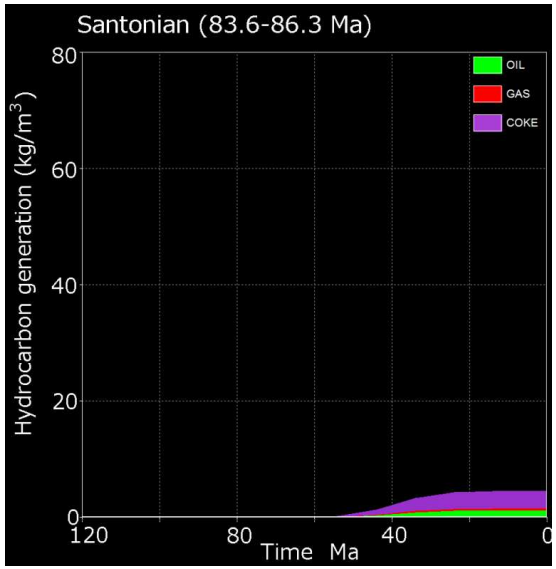

App. C6. Hydrocarbon generation in Pseudo Mannar Deep well under optimistic scenario (TOC = 2.5% and Types II and III kerogen = 50% each).

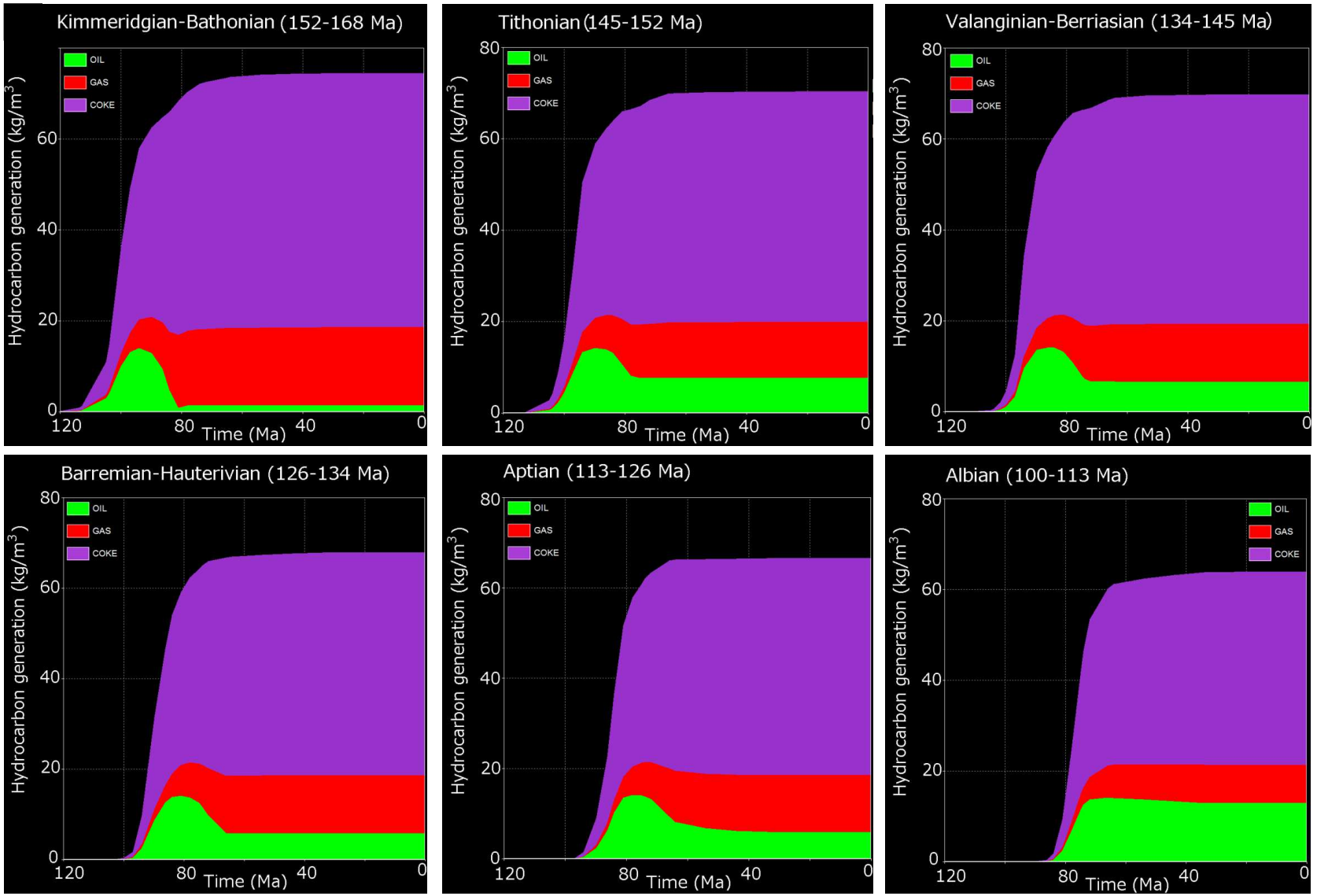

Hydrocarbon generation in Pseudo Mannar Deep well cont……..

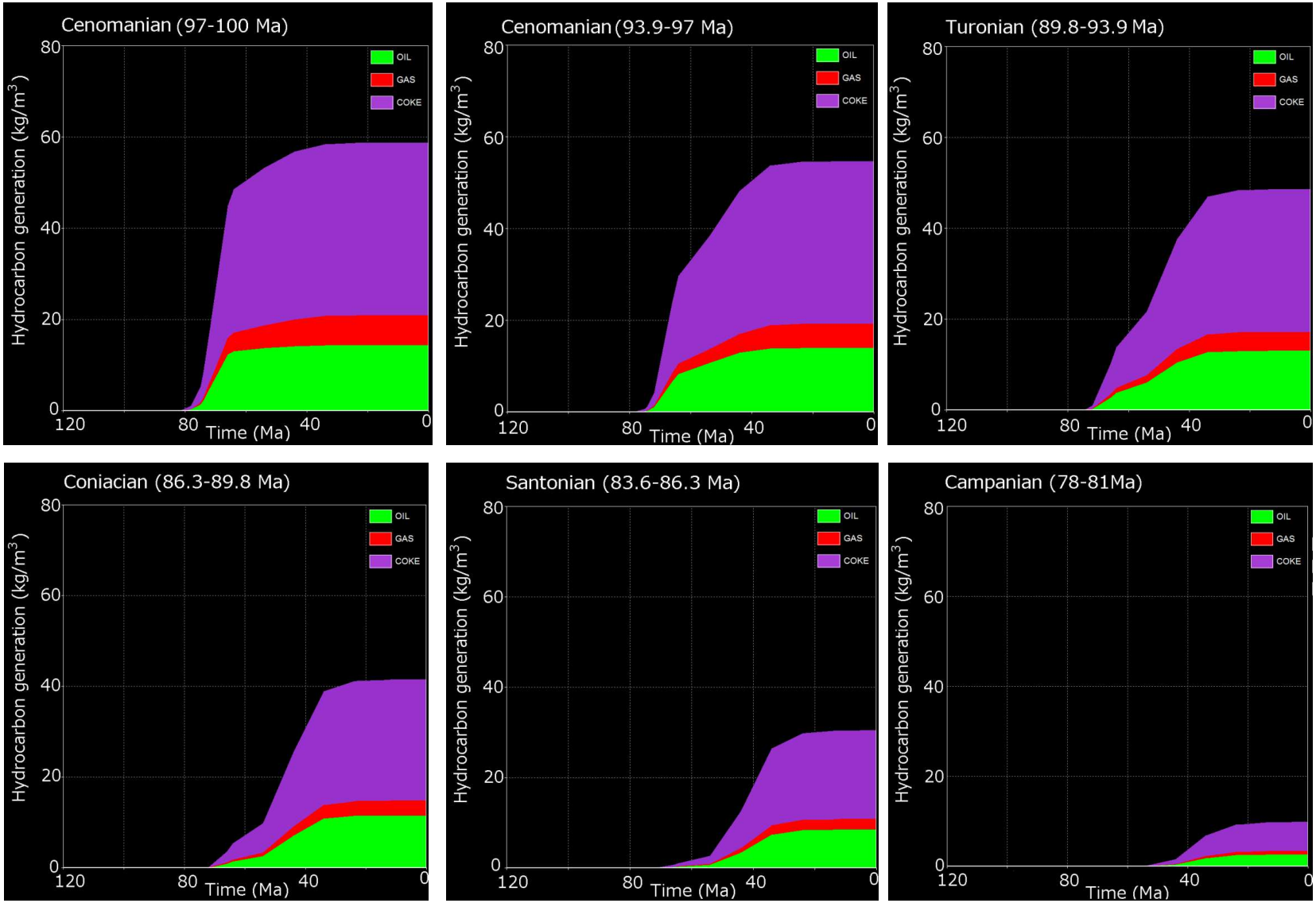

Hydrocarbon generation in Pseudo Mannar Deep well cont……..

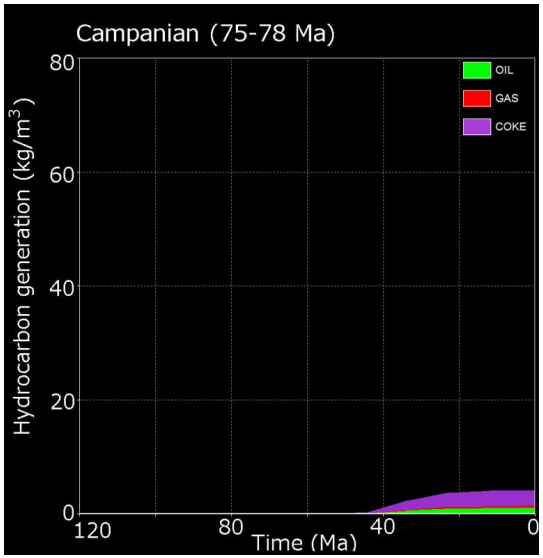

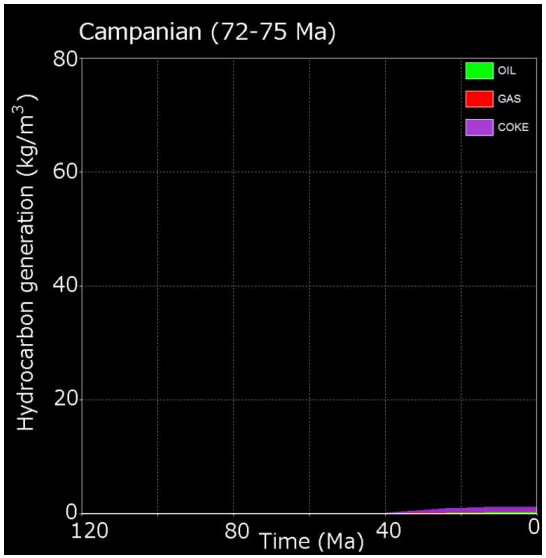

Appendix D

Timing and quantity of hydrocarbon expulsion

App. D1. Hydrocarbon expulsion timing for the Pearl-1 well under pessimistic scenario (TOC = 0.5% & Type III kerogen = 100%).

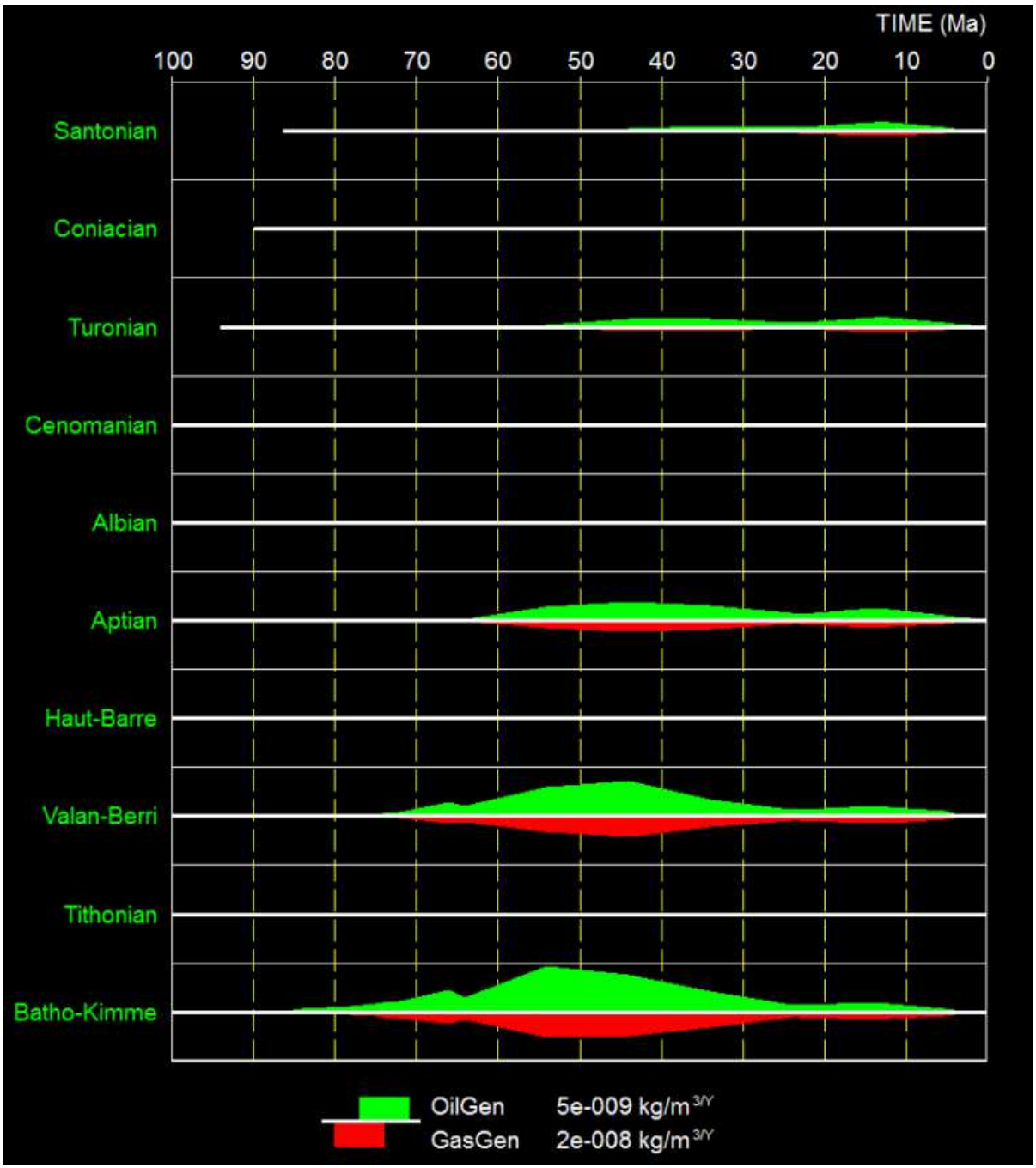

App. D2. Hydrocarbon expulsion timing for the Pearl-1 well under optimistic scenario (TOC = 2.5% and Type II kerogen = 50%).

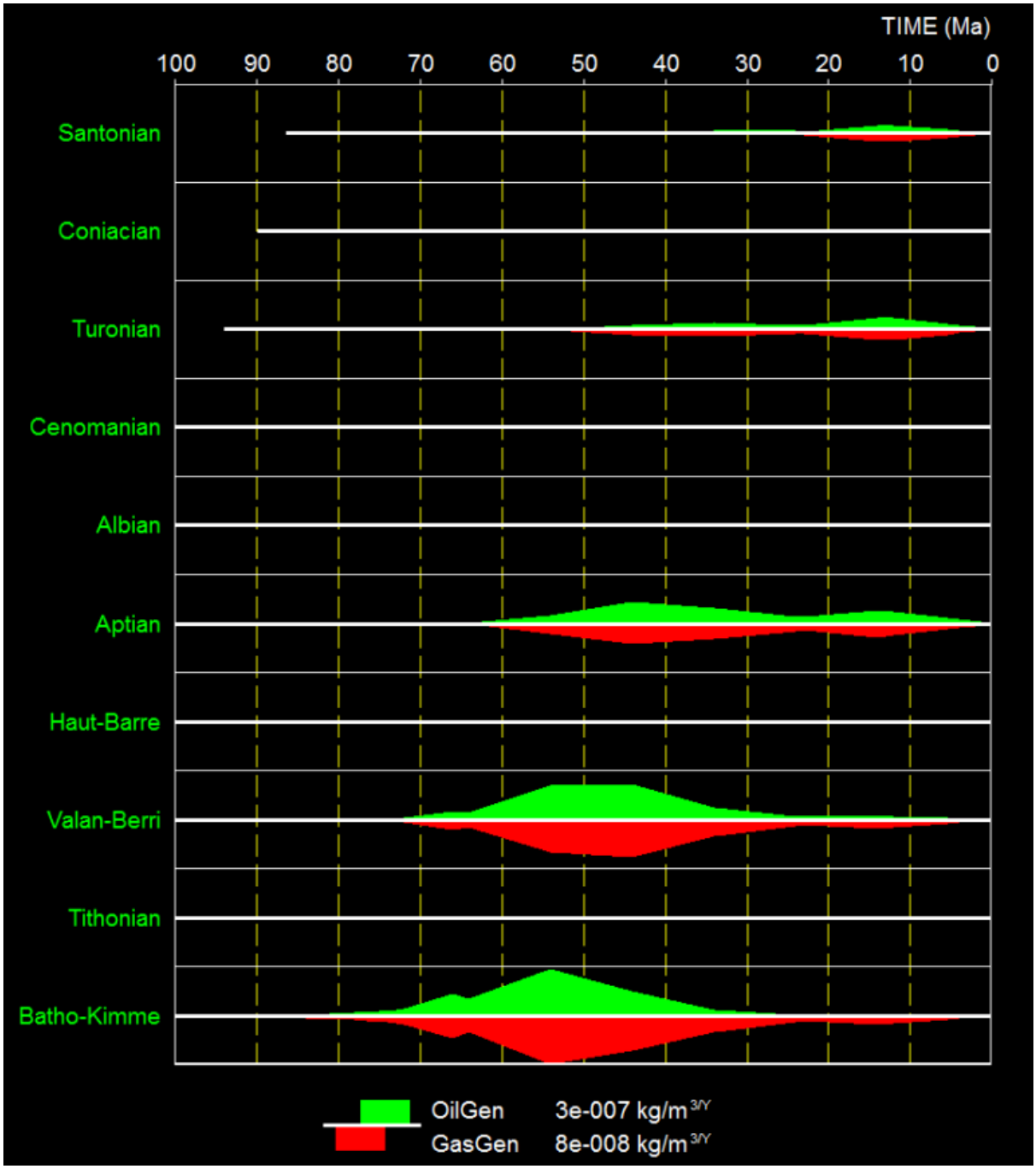

App. D3. Hydrocarbon expulsion timing for the Dorado-North well under pessimistic scenario (TOC = 0.5% and Type III kerogen = 100%).

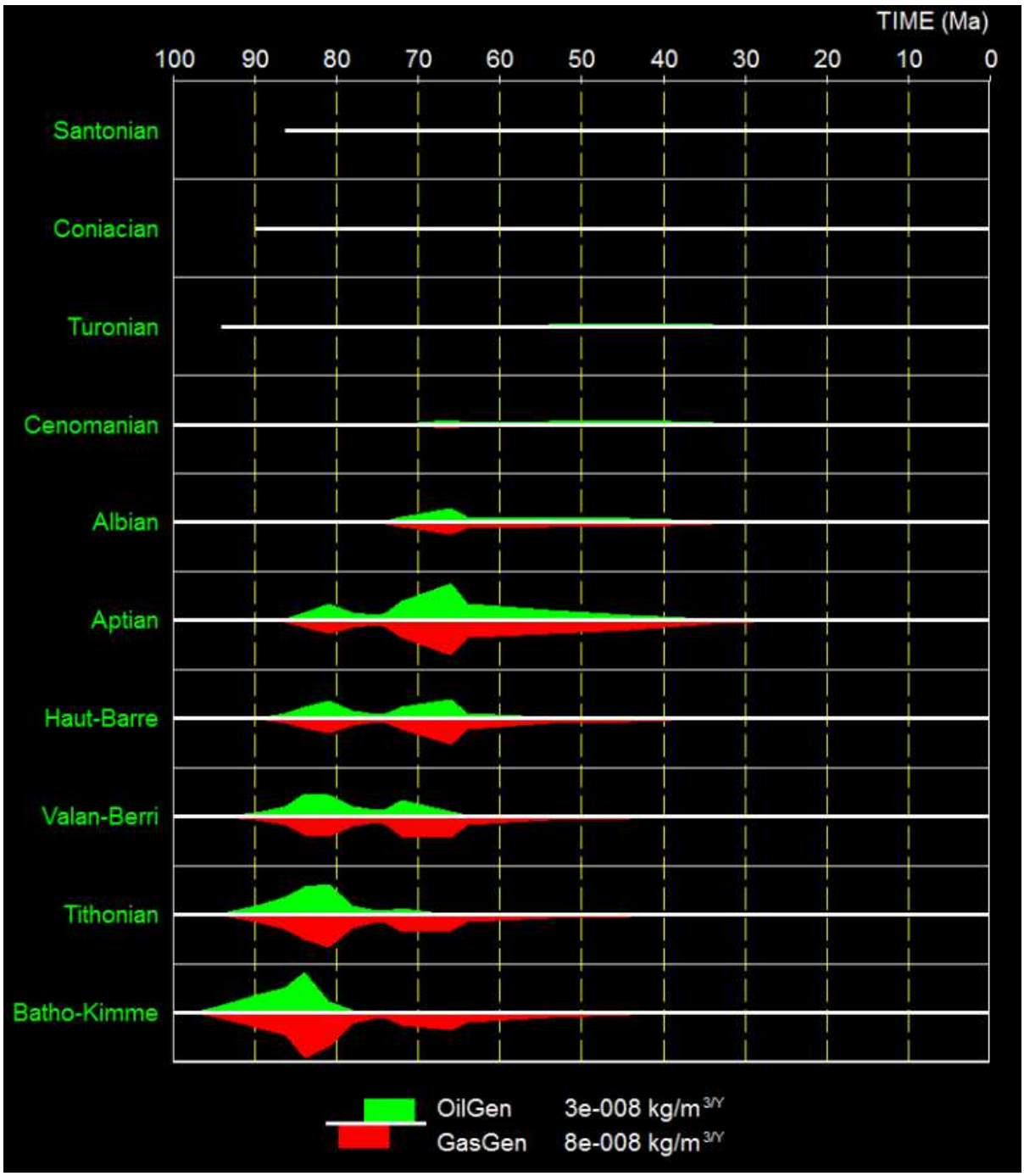

App. D4. Hydrocarbon expulsion timing for the Dorado-North well under optimistic scenario (TOC = 2.5% and Type II kerogen = 50%).

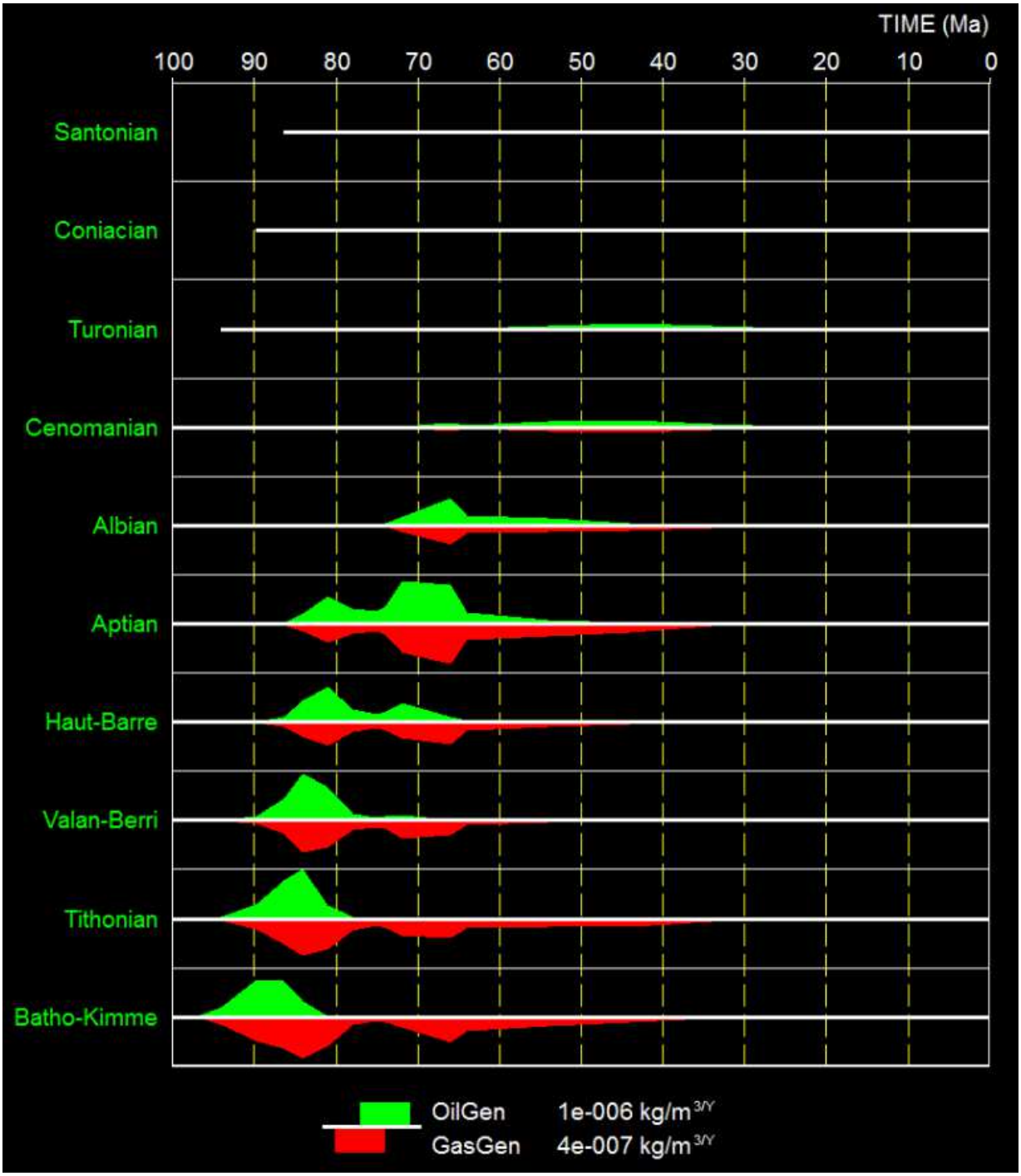

App. D5. Hydrocarbon expulsion timing for the pseudo Mannar-Deep well under pessimistic scenario (TOC = 0.5% and Type III kerogen = 100%).

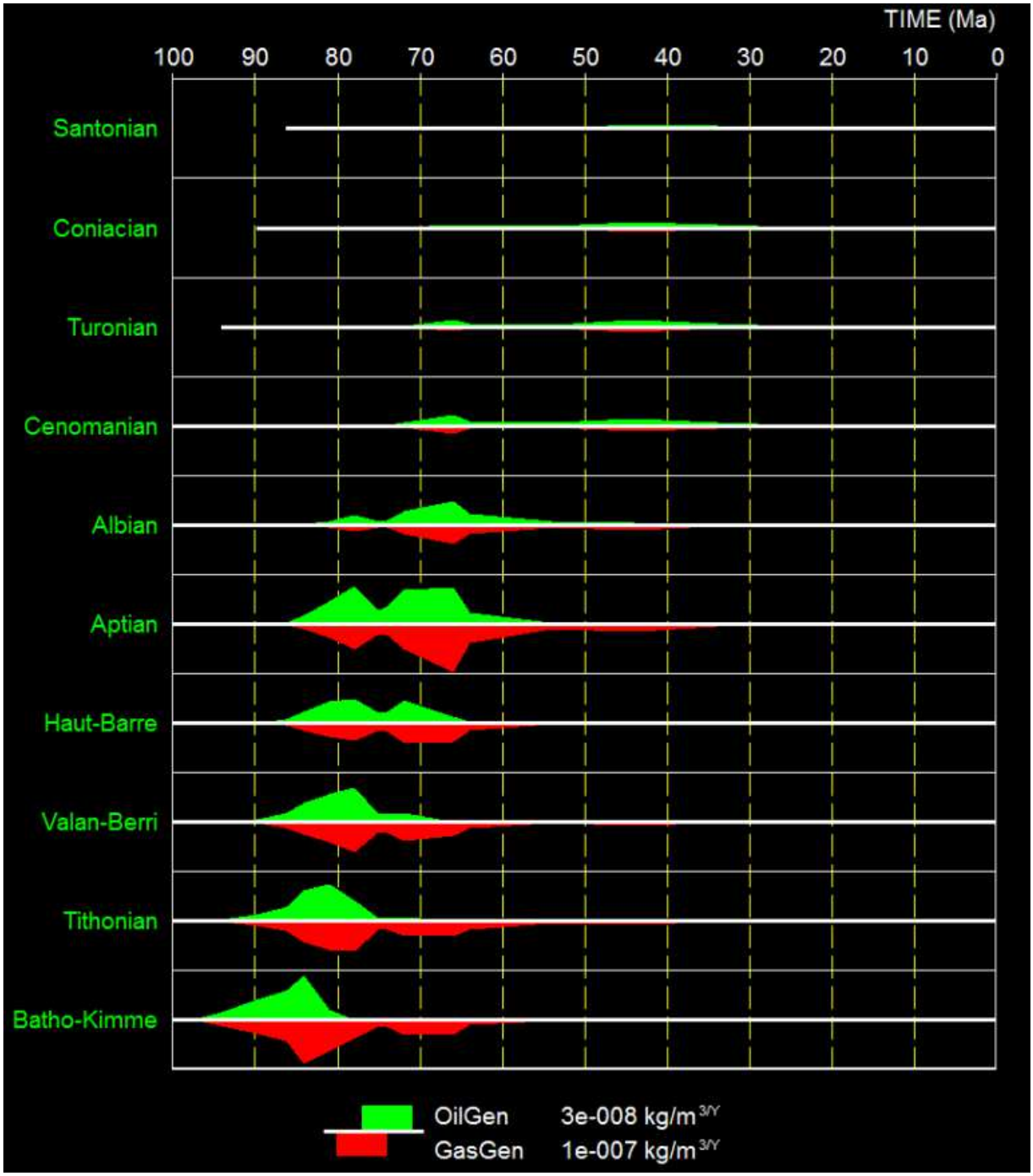

App. D6. Hydrocarbon expulsion timing for the pseudo Mannar-Deep well under optimistic scenario (TOC = 2.5% and Type II kerogen = 50%).